Investigation of Small Molecule Inhibitors Targeting β-Catenin/TCF4 Interaction in Ovarian Cancer Cell Lines

RUFEI YAN

A THESIS SUBMITTED TO THE FACULTY OF GRADUATE STUDIES IN PARTIAL FULFILLMENT OF THE REQUIREMENTS FOR THE DEGREE OF

MASTER OF SCIENCE

GRADUATE PROGRAM IN BIOLOGY YORK UNIVERSITY
TORONTO, ONTARIO

June 2026

Abstract

Epithelial ovarian cancer (EOC) is the deadliest gynecological malignancy. The development of chemoresistance and relapse is a major challenge in treating ovarian cancer. The Wnt/β-catenin pathway plays critical roles in embryonic development and adult homeostasis. The aberrant activation of β-catenin and its interaction with its co-activator TCF4 is implicated in the progression of EOC; therefore, targeting and inhibiting this interaction is desirable for the development of targeted therapies. Previous studies have identified a small molecule inhibitor of β-catenin known as C10, and novel analogues of C10, C45-C62 have been synthesized in-house. In this study, C45-C62 have been characterized through structure-activity relationship analyses and functional assays to determine their direct binding to β-catenin and antitumour effects. Optimization of C10 and its analogues could lead to potential development of a novel β-catenin/TCF4 inhibitor for ovarian cancer treatment.

Acknowledgements

Firstly, I would like to thank my primary supervisor, Dr. Yi Sheng. Thank you for granting me the opportunity to join your lab, and thank you for your patient guidance and mentorship throughout my time here. Your support has been invaluable to my growth as a scientist and overall.

I would also like to thank my co-supervisor, Dr. Chun Peng, for entrusting me with this research project. I am grateful for all your support and guidance in shaping this project.

Additionally, I am grateful to Dr. Vivian Saridakis for being part of my supervisory committee. Thank you for your critiques and advice throughout this project.

I am also grateful to the members of both the Sheng and Peng labs, for all their unwavering support and encouragement.

To Nour, Vanessa, Daniel, Angelo and Gaby: thank you for training and teaching me lab techniques and protocols. Your assistance and support helped form the foundation for my skills today. To Erica and Romina: thank you for all the support and encouragement while we worked together.

To Tobi, Riddhi, Gagan, Sajid, Asghar, Farzaneh, Yumin, Yanan, Yan, Shero, Atara, Shaina, Dr. Jiang, Kadin, and Mu Ran: thank you for all the advice, expertise, and support, and help with my experiments when needed.

I also want to specially thank Sihat, Kanwar, and Jatin for all the coffee runs, advice, and laughs over the years, as well as all the other friends I have made at the LSB and on campus. All of you have helped me grow as a person.

I would like to thank my friends who have constantly supported me throughout my time on this project, especially Li Qi, Yolanda, Victor, and Siyuan. Thank you for the late-night messages, life advice, and encouragement.

Last, but not least, I would like to thank my family. Without your love and unwavering support, I would not be who I am today, nor would this research have been possible. Mom and Dad, thank you for believing in me and for all the late-night pickups from the lab. Cindy, thank you for always cheering me up and being the best older sister I could ask for. Grandma and Grandpa, thank you for your endless support and belief in me.

Table of Contents

List of Tables

Chapter 1

Chapter 3

Chapter 4

Supplementary Data

List of Figures

Chapter 1

Chapter 3

Supplementary Data

List of Abbreviations

- ABC: ATP-binding cassette
- ADME: Absorption, distribution, metabolism, excretion
- ALDH: aldehyde dehydrogenase
- ALDH1A1: Aldehyde dehydrogenase 1 family member A1
- APC: Adenomatous polyposis coli
- ATP: Adenosine triphosphate
- BCL9: B cell CELL/lymphoma 9
- BLI: Biolayer interferometry
- BME: β-mercaptoethanol
- BRAF: B-Raf proto-oncogene
- BSA: Bovine serum albumin
- βTrCP: β-transducin repeat-containing protein
- CBD: Catenin-binding domain
- CBP: CREB-binding protein
- CKI: Casein kinase 1
- CKII: Casein kinase 2
- CSC: Cancer stem cell
- CSNK1A1: Casein kinase 1 alpha 1
- CTNNB1: β-catenin gene
- DMSO: Dimethyl sulfoxide
- Dvl: Disheveled
- EC: Endometrioid carcinoma
- EMT: Epithelial-to-mesenchymal transition
- EOC: Epithelial ovarian cancer
- Fzd: Frizzled
- GSK3β: Glycogen synthase kinase 3β
- HGSC: High-grade serous carcinoma
- hTCF4: human TCF4
- ICAT: Inhibitor of β-catenin and TCF
- IPTG: Isopropyl β-d-1-thiogalactopyranoside
- ITC: isothermal titration calorimetry
- LB: Lysogeny broth
- Log Po/w: Octanol-water partition coefficient
- LRP: Lipoprotein receptor-related protein
- MDR1: Multidrug resistance 1 gene
- OC: Ovarian cancer
- OCSC: Ovarian cancer stem cells
- PARP: Poly (ADP-ribose) polymerase

- P-gp: P-glycoprotein
- PMSF: Phenylmethanesulfonyl fluoride
- PORCN: Porcupine O-Acyltransferase
- SALI: Structure-activity landscape index
- SAR: Structure-activity relationship
- TCF/LEF: T cell factor/lymphoid enhancer factor
- TG2: Tissue transglutaminase 2
- xTCF3: *Xenopus* TCF3
- VEGF: Vascular endothelial growth factor

Chapter 1: Literature Review

Introduction

β-Catenin is an evolutionary-conserved protein which plays critical roles throughout the entire lifespan of animals. It is part of the canonical Wnt signalling pathway and is involved in tissue and organ development during embryonic growth and tissue homeostasis in adult organs (Logan & Nusse, 2004). A β-catenin homolog encoded by the *armadillo* gene was initially characterized in *Drosophila* as a protein contributing to morphogenesis (Wieschaus et al., 1984). Additionally, analysis of conditional β-catenin loss and gain-of-function mutant mice also demonstrated that it controls progenitor cell expansion and lineage decisions in both the early embryo and adult organs (Zechner et al., 2003; Miyoshi & Hennighausen, 2003). Importantly, aberrant activation of β-catenin signalling is now recognized as a hallmark of numerous human cancers, making this pathway an attractive target for therapeutic intervention (F. Yu et al., 2021). To better understand the structure and function of this molecule, the following sections review the discovery of β-catenin, the components of the Wnt/β-catenin signalling pathway, the structural basis of β-catenin's molecular interactions, and emerging strategies and challenges targeting β-catenin as a drug target.

1. Wnt/β-Catenin Signalling

1.1: Overview of the Wnt/β-Catenin Signalling Pathway

The discovery of the canonical Wnt signalling pathway dates back to the 20th century, when studies in mice first linked tumour growth to the overexpression of an unknown gene, later named Wnt (Nusse & Varmus, 1982; Nusse et al., 1984). Interestingly, loss-of-function mutations of Wnt were shown to cause severe embryonic developmental defects in both mice and *Drosophila* (Miyoshi & Hennighausen, 2003; Nüsslein-Volhard et al., 1984). Further genetic

screening in *Drosophila* identified additional mutants with similar impaired developmental phenotypes as Wnt, including mutations in the *armadillo* (known as β-catenin in vertebrates), *dishevelled* (Dvl) and *porcupine* (PORCN) genes (Klingensmith et al., 1994; Noordermeer et al., 1994; Riggleman et al., 1990). At the same time, discoveries of other major components of the Wnt pathway were made, including adenomatous polyposis coli (APC), Axin, Frizzled (Fzd), and lipoprotein receptor-related protein (LRP) – mutations of which were identified in carcinogenesis and their interactions with Wnt confirmed through biochemical analyses (Munemitsu et al., 1995; Pinson et al., 2000; Su et al., 1993; Tamai et al., 2000; Y. Wang et al., 1996). Together, these studies established the genetic and molecular framework of the initial canonical Wnt pathway.

The mechanism by which Wnt signalling influences gene expression was elucidated. The signal starts from the family of Wnt proteins, which are highly conserved across species (Nusse, 2001). Wnt proteins are lipid-modified glycoproteins that participate in either autocrine or paracrine signalling. During development, Wnt secretion is triggered by developmental transcriptional programs and mediated by PORCN dependent lipidation (Miranda et al., 2014). Wnt proteins contain a conserved serine residue, which is lipidated by PORCN to serve two crucial functions: secretion to the plasma membrane and binding to the cysteine-rich domain of the G-coupled protein receptor Fzd. The binding of Wnt to Fzd activates the cellular signaling pathway leading to the effector β-catenin stabilization and translocation (Dann et al., 2001).

In the absence of Wnt, β-catenin resides in the cytoplasm and is maintained at very low levels through proteasomal degradation. This process is mediated by the destruction complex, which consists of scaffold proteins Axin and APC as well as serine/threonine protein kinases casein kinase 1 (CKI), and glycogen synthase kinase 3β (GSK3β) (Clevers, 2006). CKI and

GSK3β phosphorylate β-catenin at its N-terminus Ser 45 residue and Thr 41, Ser 37, and Ser 33 residues respectively (C. Liu et al., 2002). GSK3β also phosphorylates Axin to stabilize it and enhance its interaction with β-catenin. Once phosphorylated, β-catenin is recognized by the ubiquitin E3 ligase β-transducin repeat-containing protein (βTrCP), which modifies β-catenin by ubiquitination and targets it for proteasomal degradation (C. Liu et al., 1999).

In the presence of a secreted Wnt ligand, its interaction with Fzd promotes the dimerization of Fzd and the co-receptor LRP5/6. This results in the recruitment of the cytoplasmic phosphoprotein Dvl to the membrane (Tauriello et al., 2012). Dvl recruits Axin to the cell membrane, inhibiting the formation of the destruction complex (Bilić et al., 2007). As a result, β-catenin is no longer phosphorylated and escapes ubiquitin-mediated degradation. Stabilized β-catenin can translocate to the nucleus where-it displaces the transcriptional repressor Groucho and interacts with T cell factor/lymphoid enhancer factor (TCF/LEF) to activate gene transcription (Fig. 1.1) (Daniels & Weis, 2005). This transcriptional program controls cell fate, proliferation, and differentiation, and is therefore critical for proper development of tissues and maintenance of stem cells.

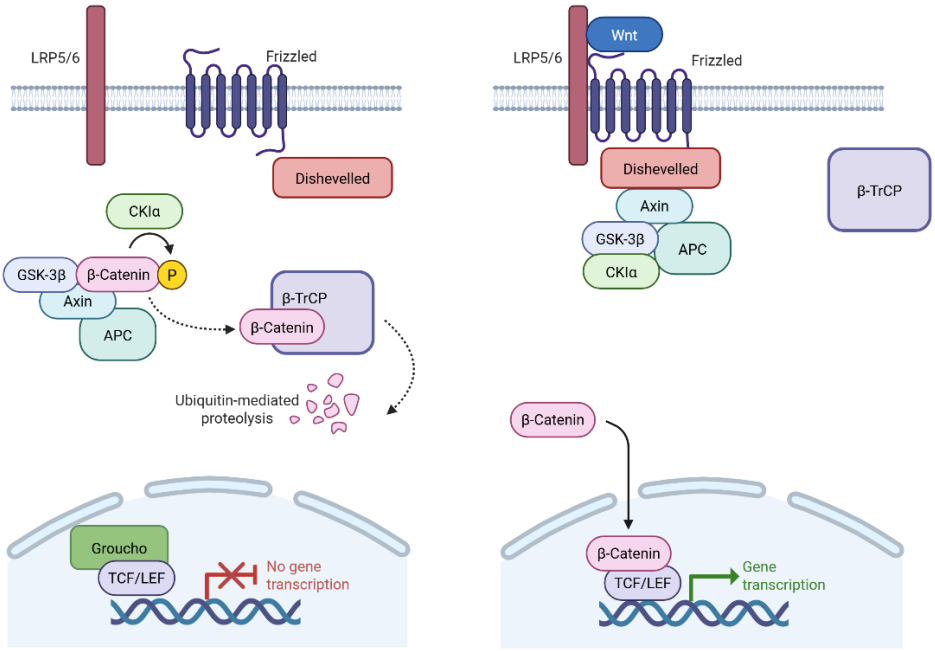

Figure 1.1: The Wnt/β-catenin signalling pathway. (Left) In the absence of a Wnt ligand, β-catenin is phosphorylated by CKI and GSK3β in the cytoplasm, binding it to the destruction complex made of scaffold proteins Axin and APC. It is then targeted by β-TrCP for ubiquitinylation and degradation. In the nucleus, Groucho represses transcription by binding to TCF/LEF. (Right) In the presence of Wnt, the dimerization of LRP5/6 and Frizzled is promoted, recruiting Dishevelled to promote the recruitment of Axin to the membrane and dissociation of the destruction complex. β-catenin is translocated to the nucleus, displacing Groucho to interact with TCF/LEF to activate gene transcription.

1.2: Biological Roles of the Wnt/β-Catenin Signaling Pathway

The Wnt signalling pathway can be characterized into three distinct pathways: the canonical Wnt pathway which is dependent on β-catenin, and the noncanonical β-catenin independent pathways consisting of the planar cell polarity and Wnt/calcium pathways (Komiya & Habas, 2008). This study focuses on the canonical Wnt/β-catenin signalling pathway. The canonical Wnt pathway is a key regulator in multiple systems in the human body. In the digestive system, the activation of the Wnt signalling pathway is crucial for maintaining homeostasis in the intestinal epithelium in adult organisms by perpetuating the stemness and undifferentiated state of intestinal stem cells, which allows for rapid regeneration of the epithelium (Fevr et al.,

2007). In brain morphogenesis, the Wnt pathway is responsible for brain formation and craniofacial development (Brault et al., 2001). In hair growth, Wnt signalling is required for the establishment of the hair follicle and hair formation, and loss of β-catenin results in the failure of stem cells to differentiate into follicular keratinocytes (Huelsken et al., 2001; Zhou et al., 1995). Importantly, Wnt signalling is essential for female sex determination in embryos and supports ovarian follicle maturation and ovulation in adult females (Hernandez Gifford, 2015).

1.3: β-Catenin as a Therapeutic Cancer Target

While Wnt/β-catenin signaling is essential for normal development and tissue homeostasis, dysregulation of this pathway shows pathological consequences. In humans, the β-catenin protein is encoded by the *CTNNB1* gene which is reported to have high frequency of mutations across endometrial (16%), hepatobiliary (12%), melanoma (7%), and colorectal (6%) cancers (National Academies of Sciences, 2016). Within the *CTNNB1* gene, exon 3 is reported hot-spot mutation site, which affects phosphorylation of β-catenin, thereby preventing proteasomal degradation (S. Kim & Jeong, 2019). Missense mutations in this exon are associated with an aggressive phenotype of low-grade endometrial, liver, and colorectal cancers (Y. Liu et al., 2014). Mutations in this exon also influence the inflammation signature of lesions in desmoid-type fibromatosis, which are rare, locally aggressive soft-tissue tumours that do not metastasize. Indeed, mutations in β-catenin, especially in exon 3, often lead to aberrant overexpression across multiple cancer types as the disruption of phosphorylation-dependant ubiquitination allows β-catenin to escape destruction and translocate to the nucleus, where it constitutively activates oncogenic transcriptional programs (G. Kim et al., 2018). Consistent with this mechanism, gain-of-function β-catenin studies have revealed that hyperactive β-catenin signalling often results in carcinoma or polyp formation. This is seen in transgenic mice models

where overexpressed β-catenin induced cancerous growths in mouse mammary tissue (Miyoshi & Hennighausen, 2003). Conversely, loss-of-function β-catenin studies were shown to inhibit cancer cell proliferation. For example, the knockdown of endogenous β-catenin in human U251 glioma cancer cells using small interfering RNA (siRNA) demonstrated that the silencing of β-catenin inhibited proliferation and increased apoptosis of U251 cells (Z. Wang & Chen, 2016). Knockout of *CTNNB1* in a mice model of the $BRAF^{V600E}$ mutation driven-papillary thyroid cancer showed reduction in thyroid tumour growth and increased survival compared with mice retaining wild-type *CTNNB1* (Zou et al., 2021). Together, these studies strongly support that β-catenin is a central driver of oncogenic progression.

1.4: Overview of β-Catenin in Ovarian Cancer

While aberrant β-catenin activation is implicated in numerous cancers, this thesis focuses on β-catenin in ovarian cancer (OC), particularly the effects of aberrant β-catenin in OC and therapeutic development targeting β-catenin. Ovarian cancer is the deadliest gynecologic malignancy and the 8th most common cancer in women (Webb & Jordan, 2024), with epithelial ovarian cancer (EOC) accounting for 90-95% of OC cases. EOC consists of five major histological subtypes: high-grade serous carcinoma (HGSC), accounting for 70-75% of cases, endometrioid carcinoma (EC) (7-24% of cases), clear cell carcinoma (10-26% of cases), low-grade serous carcinoma (3-5% of cases), and mucinous carcinoma (2-6% of cases) (National Academies of Sciences, 2016).

The standard chemotherapy treatment for EOC consists of a combination of a platinum product such as cisplatin or carboplatin with a taxane, such as paclitaxel or docetaxel (Jelovac & Armstrong, 2011). However, many patients develop resistance to these treatments and relapse after this first line treatment (Ledermann et al., 2013). The molecular heterogeneity of EOC

contributes in part to poor patient outcomes, and targeted therapies have been developed as third cytotoxic agents alongside platinum-taxane products. Anti-angiogenic agents such as bevacizumab, a monoclonal antibody targeting vascular endothelial growth factor (VEGF)-A, has been approved by the FDA to be used in combination with carboplatin and paclitaxel (Cortez et al., 2018). Additionally, several Poly (ADP-Ribose) Polymerase (PARP) inhibitors, which target the defective DNA repair pathway in HGSC, have been approved for treatment of BRCA-associated EOC (Parkes & Kennedy, 2016).

The role of the Wnt/β-catenin signalling pathway in cancer development has been reported in all subtypes of EOC, contributing to cancer stem cell (CSC) maintenance, chemoresistance, and metastasis (Arend et al., 2013; Nagaraj et al., 2015). Mutations of the β-catenin gene, *CTNNB1*, are most commonly observed in EC cases compared to other EOC subtypes. Studies suggest that up to 54% of EC cases contain mutated *CTNNB1*, leading to increased nuclear localization of β-catenin and a subsequent increase in transcription of its target genes (Gamallo et al., 1999). As a result, overactive β-catenin in EC regulates key aspects in cancer development, which collectively contributes to tumorigenesis and disease progression (Nguyen et al., 2019).

β-Catenin plays a critical role in modulating CSC properties in OC cells (Condello et al., 2015). CSCs are a small subset of cancer cells possess self-renewal and differentiation capabilities which contribute to heterogeneity within the tumour microenvironment. CSC cells are known to possess tumorigenic potential, driving metastasis and cancer recurrence (Tysnes, 2010; Ahmed et al., 2014). Ovarian CSCs (OCSCs) are characterized by the high expression of surface markers including CD133 and aldehyde dehydrogenase (ALDH). The combination of these two markers has been observed to increase angiogenic capacity of OCSCs and form

spheroids *in vitro* and tumours *in vivo*, contributing to the progression of OC (Kryczek et al., 2012). Additionally, β-catenin directly activates the transcription of aldehyde dehydrogenase 1 family member A1 (ALDH1A1), a specific member of the ALDH family. Knockdown of β-catenin decreased ALDH1A1 levels and disrupted ovarian cancer spheroid formation, cell viability, and chemoresistance, supporting the role of β-catenin in promoting OC cell tumorigenesis through modulating its CSC-like properties (Condello et al., 2015).

Chemoresistance is defined as a cancer cell's ability to evade the cytotoxic effects of chemotherapy (Zhao, 2016). The standard chemotherapy for EOC patients is a combination of a platinum product, such as cisplatin to block DNA replication and induce apoptosis, combined with a taxane such as paclitaxel to inhibit mitosis (Abal et al., 2003; Chandra et al., 2019; Florea & Büsselberg, 2011). However, many patients develop chemoresistance to these drugs and relapse (Zhao, 2016). Additionally, as mentioned earlier, the presence of OCSCs is implicated in chemoresistance, with $ALDH^+$ and $CD44^+$ OCSCs exhibiting resistances to cisplatin and paclitaxel (Wang et al., 2012). The β-catenin/TCF complex is also known to transcribe drug resistance genes such as multi drug resistance (MDR1) which upregulates P-glycoprotein (P-gp), an ATP-binding cassette (ABC) membrane transporter that pumps chemotherapeutic agents out of cells to attenuate drug-induced cytotoxicity (Shang et al., 2017). A study conducted by Zhang *et al.* (2015) showed that inhibition of Fz to suppress Wnt/β-catenin signalling downregulated MDR1 and P-gp expression, as well as significantly decreasing nuclear β-catenin levels and transcriptional activity in OC cells (Zhang et al., 2015).

Metastasis, the migration of cancer cells from the original tumour to other organs and tissues, is driven by epithelial-to-mesenchymal transition (EMT). EMT is a process by which epithelial cells lose their adhesion and transform into mobile mesenchymal cells, gaining migratory and

invasive capabilities. This invasive ability allows cells to break through the basement membrane to spread throughout the body through the blood or lymph system (Kalluri & Weinberg, 2009). Studies have observed the loss of E-cadherin, a transmembrane protein crucial for cell-cell adhesion, in OC cell types expressing EMT (Sawada et al., 2008). E-cadherin forms a complex with β-catenin to maintain low cytosolic β-catenin levels when the Wnt pathway is inactivated; therefore, the loss of E-cadherin would result in an increase in β-catenin signalling (Tian et al., 2011). This interaction will be elaborated on in the next section.

Within multiple human cancers including OC, aberrant β-catenin signalling drives tumorigenesis and disease progression. Inhibition of β-catenin activity has been shown to slow cancer progression and inhibit cancer cell proliferation (Arend et al., 2013). As such, β-catenin is a validated, bona fide therapeutic drug target to treat cancer. However, directly targeting β-catenin has proven challenging as it functions primarily through protein-protein interaction where it has multiple interaction partners with overlapping binding sites (Cui et al., 2018). Additionally, the protein structure itself is difficult to target as it has a flat surface that lacks the deep binding pockets found on most enzymes or receptors for small molecules to interact with (Lazo & Sharlow, 2016). To better understand the complexities surrounding β-catenin as a drug target, its protein structure, and the molecular basis for several important interactions with its binding partners are reviewed next.

2. Structural Overview of β-Catenin

2.1: Structure of β-Catenin

β-Catenin is a 781-amino acid protein which in humans is encoded by the *CTNNB1* gene located on the short arm of chromosome 3 with the locus 3p22.1 (Kraus et al., 1994). The structure of β-catenin is composed of three distinct regions: a disordered N-terminus, a central domain composed of 12 armadillo repeats (residues 141-664), and a C-terminus (Figure 1.2) (Xing et al., 2008). An armadillo repeat is characterized by a triangular arrangement of three alpha-helices containing a repetitive amino acid sequence of about 42 residues in length (Huber et al., 1997). β-Catenin is an evolutionary conserved protein, with mammalian β-catenin sharing >60% amino acid identity with cnidarian β-catenin with 80% similarity in the armadillo repeat region (Valenta et al., 2012). A specific α-helix at the N-terminal region of the C-terminal region of β-catenin, referred to as helix C, is highly conserved across species and is critical for the binding of transcriptional co-activators. The N-terminus and armadillo repeat regions contain binding surfaces for interaction partners that function in cell adhesion, Wnt signalling, and gene transcription (Xing et al., 2008).

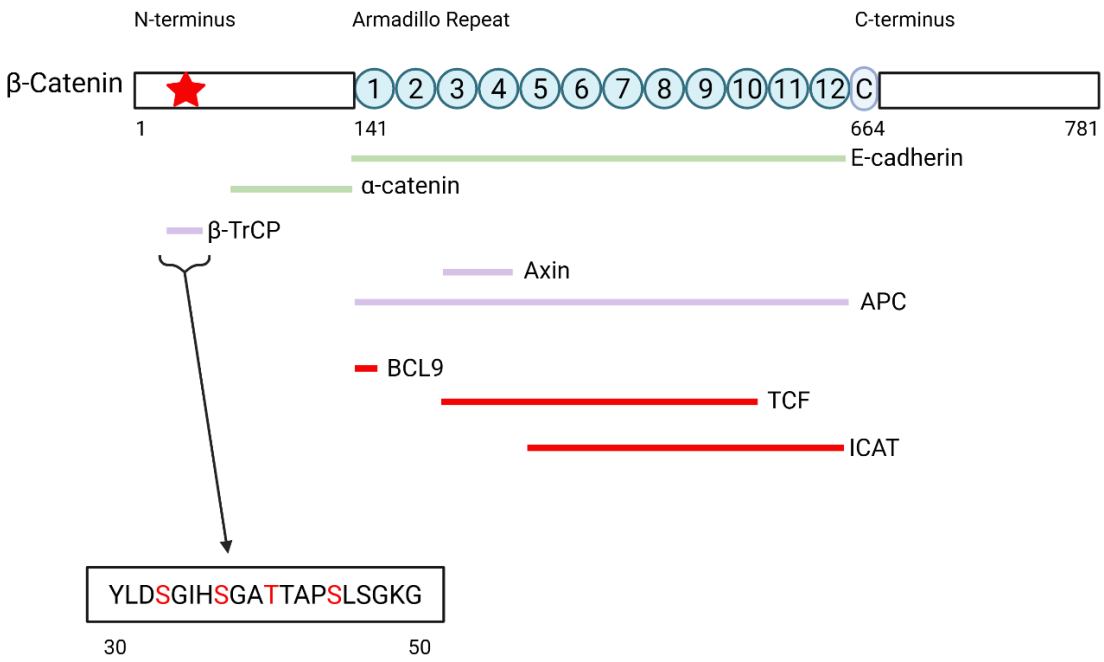

Figure 1.2: A summary of the β-catenin domains and its interaction partners. The circles represent the armadillo repeats, and the oval 'C' represents the conserved α-helix, known as helix C. The β-catenin binding partners are depicted below the domain structure, with the regions involved in each interaction highlighted. The green bars indicate binding partners that participate in structural regulation. Purple bars indicate binding partners of β-catenin in Wnt signalling in the cytoplasm. The red bars indicate the binding partners of β-catenin in the nucleus. The red star indicates the exon 3 residues that are phosphorylated to create the binding site for β-TrCP, namely Ser 33, Ser 37, Ser 45, and Thr 41.

2.2: β-Catenin Interactions in Structural Regulation

β-Catenin plays a critical role in maintaining structural integrity in cells outside of its role in gene transcription (Valenta et al., 2012). When the Wnt signalling pathway is inactivated, the transmembrane adhesion protein E-cadherin forms an adhesion complex with β-catenin, interacting along the armadillo repeat domain to maintain low cytosolic levels of β-catenin in the cell. This interaction is a key component of adherens junctions between cells and is crucial for maintaining tissue architecture and structural integrity. The association between E-cadherin and β-catenin is modulated by serine/threonine kinases casein kinase 2 (CKII) and GSK3β, which phosphorylate E-cadherin and increase its affinity with β-catenin. This interaction additionally

recruits α-catenin to the N-terminal domain of β-catenin, which links the adhesion complex to actin filaments to stabilize adherens junctions (Huber & Weis, 2001). When the Wnt signalling pathway is activated, β-catenin is dissociated from the adhesion complex through phosphorylation of tyrosine residues, namely Tyr 142 and Tyr 654. These residues are phosphorylated by a number of tyrosine kinases, notably the Fyn and Src tyrosine kinases which are part of the Src family kinases. The dissociation of the adhesion complex allows for the translocation of β-catenin to the nucleus to activate gene transcription (Shah & Kazi, 2022).

In the context of EOC, studies indicate that the dissociation of the adhesion complex induces the accumulation of free cytosolic β-catenin which can translocate to the nucleus to increase oncogene transcription. This dissociation has been shown to be regulated by tissue transglutaminase 2 (TG2), a cross-linking protein overexpressed in various cancers including OC and is known to enhance β-catenin transcriptional activity (Satpathy et al., 2007). TG2 normally binds to β-integrin, a transmembrane receptor subunit that acts as a crucial link between the cell cytoskeleton and the extracellular matrix, and this interaction facilitates the binding of fibronectin, a glycoprotein that bridges cells and their surrounding environment. The overexpression of TG2 and the β-integrin-fibronectin complex activates c-Src, another tyrosine protein kinase in the Src family that phosphorylates β-catenin at Tyr 654. As previously mentioned, this event dissociates the adhesion complex between E-cadherin and β-catenin, resulting in augmented accumulation of free cytosolic β-catenin which subsequently upregulates oncogene transcription upon translocation to the nucleus. TG2 overexpression also regulates EMT in cancer cells, which is associated with the loss of E-cadherin where it has been previously mentioned to be observed in ovarian cancer cell types expressing EMT (Condello et al., 2013).

2.3: β-Catenin Interactions in Wnt Signalling

In the absence of Wnt signalling, cytosolic β-catenin is targeted by the destruction complex, composed of a number of proteins that interact with β-catenin at its N-terminal domain and armadillo repeat domain. This interaction ultimately results in the degradation of β-catenin to inhibit translocation to the nucleus and subsequent gene transcription (Logan & Nusse, 2004).

2.3.1: N-terminus Region

The N-terminus includes exon 3 of *CTNNB1*, which has been previously mentioned to be a reported hot-spot mutation site which affects phosphorylation of β-catenin. Known missense mutations in exon 3 include S45, which is phosphorylated by CKI, and S33, S37, and T41, which are phosphorylated by GSK3β to create the binding site for βTrCP to ubiquitinate β-catenin, targeting it for degradation. Mutations in this phosphorylation site would render β-catenin resistant to degradation, increasing nuclear localization of β-catenin and transcription of β-catenin/TCF target genes (S. Kim & Jeong, 2019)

2.3.2: Armadillo Repeat Region

β-Catenin interacts with Axin at armadillo repeats 3-4, with Axin acting as a scaffold for the destruction complex. Axin contains a binding site for GSK3β to promote phosphorylation of β-catenin. Additionally, casein kinase 1 alpha 1 (CSNK1A1) phosphorylates Axin at its N-terminus to stabilize it and counteract its degradation by the tankyrase enzymes of the PARP family (S.-M. A. Huang et al., 2009a; Klement et al., 2023). The interaction between β-catenin and APC occurs at armadillo repeats 1-5 and 6-12. The APC protein contains 20-amino acid repeats which interact with β-catenin at armadillo repeats 3-4, which bind β-catenin with high affinity when phosphorylated by CKI and GSK3β (Ha et al., 2004; Xing et al., 2004). APC also contains 15-amino acid repeats which interact with β-catenin at armadillo repeats 5-8, which

have been suggested to aid in positioning the 20-amino acid repeats closer to the Axin-GSK3β site to promote phosphorylation of the former to enhance binding to β-catenin (Rubinfeld et al., 2001). Mutation of these components would render the destruction complex less effective or nonfunctional, which would drive β-catenin hyperactivation and subsequent oncogenesis. Although mutations of the destruction complex are less prevalent in OC compared to other types of cancer such as Axin mutations in liver cancer and APC mutations in colon cancer (Gryfe et al., 1997; Satoh et al., 2000), there are cases where such mutations have been reported for OC. In individual cases of EC, a nonsense Axin1 isoform mutation was observed in one case and a truncating frameshift mutation in Axin2 in another case (R. Wu et al., 2001).

2.4: β-Catenin Interactions in Gene Transcription

Upon translocation to the nucleus, β-catenin acts as a transcriptional coactivator to activate gene transcription through its interaction with TCF/LEF, inhibitor of β-catenin and TCF (ICAT), B cell CLL/lymphoma 9 (BCL9), and CREB-binding protein (CBP)/p300 (Valenta et al., 2012).

2.4.1: TCF/LEF/ICAT

β-Catenin activates gene transcription by directly binding members of the TCF/LEF family. TCF normally binds to Groucho, which prevents gene transcription when the Wnt pathway is inactivated. The interaction of β-catenin with TCF4 activates gene transcription of target genes that are crucial for cell proliferation and division, including known proto-oncogenes c-Myc and cyclin D1 (Clevers, 2006).

ICAT is a negative regulator that binds to β-catenin, preventing it from interacting with TCF/LEF(Tago et al., 2000). In cancer, the overexpression of ICAT plays conflicting roles

depending on the cancer type. In colorectal cancer, ICAT acts as a tumour suppressor by binding β-catenin and preventing cancer cell proliferation (Hu et al., 2021). Conversely, in cervical cancer, ICAT augments the migration and invasion capabilities of cervical cancer cells (Liao et al., 2024). The role of ICAT in ovarian cancer is currently unknown.

Studies suggest that ICAT is not likely to be a transcriptional target of the Wnt pathway, with cells normally possessing a free pool of ICAT in the cytoplasm to buffer cytosolic β-catenin when Wnt signalling is activated (Gottardi & Gumbiner, 2004). Within the nucleus, ICAT interacts with the armadillo repeats of β-catenin in a way that blocks TCF from binding to β-catenin, inhibiting gene transcription (Graham et al., 2002). This structural interaction will be addressed in the next section.

2.4.2: BCL9/Pygopus and CBP/p300

In addition to binding with TCF/LEF for gene transcription, BCL9 and the co-activator Pygopus function as co-activators of β-catenin to enhance gene transcription. BCL9 acts as an adaptor that interacts to bridge β-catenin and Pygopus. Pygopus recruits a complex known as the Wnt enhanceosome to further amplify transcription activation via modulating the chromatin state. The histone acetyltransferase CBP is part of the enhanceosome, binding to the helix C region of β-catenin and acting as another transcriptional coactivator. The helix C region is also the binding site for another histone acetyltransferase, p300, which is closely related to CBP and is another coactivator for gene transcription (Lévy et al., 2004; Wang et al., 2023)

2.5: Targeting β-Catenin/TCF4 for Cancer Treatment

Given the vital role of β-catenin in mediating Wnt-driven tumorigenesis, the development of small molecule inhibitors targeting the β-catenin/TCF4 complex is particularly attractive and

highly desired. Importantly, the interaction of β-catenin and TCF4 represents the terminal step in the Wnt signalling pathway, functioning as the final convergence point for pathway activation. As a result, inhibiting this interaction may block all aberrant activations regardless of alterations earlier in the signalling pathway, such as mutations in other components of the destruction complex such as Axin or APC. Additionally, cancers harboring activating mutations in the *CTNNB1* gene are often resistant to therapeutic strategies that target upstream proteins. In this context, directly targeting the β-catenin/TCF4 complex provides a rational approach to block Wnt-driven transcription (Yan et al., 2017).

2.6: β-Catenin/TCF4 Interaction for Drug Targeting

As the β-catenin/TCF4 interaction forms the core transcriptional complex of the canonical Wnt signaling pathway and represents a key therapeutic targeted in β-catenin driven cancer, multiple structural studies have attempted to reveal the mechanistic insights into how β-catenin engages TCF4, and how ICAT disrupts this interaction.

2.6.1: TCF/LEF Structure

The TCF/LEF family of transcription factors function as main downstream effectors of the Wnt signalling pathway, interacting with β-catenin to activate gene transcription. TCF4 is the most commonly expressed factor in the family across adult human tissue as well as the most intensely studied. TCF4 interacts with β-catenin through the first 53 amino acids in its N-terminal domain, which bind to β-catenin with high affinity (Omer et al., 1999). This region is termed as the catenin-binding domain (CBD).

The crystal structure mapping the interaction between β-catenin and the TCF CBD was first elucidated using *Xenopus* TCF3 (xTCF3, PDB: 1G3J) as it is sequentially very similar to

human TCF4 (hTCF4); the latter was found to also possess a similar binding mode (PDB: 1JPW) (Fig. 1.3A) (Graham et al., 2000; Poy et al., 2001). TCF overall interacts with β-catenin along armadillo repeats 5-9, running antiparallel to β-catenin. Residues 12-21 of both CBDs are structurally identical, forming a β-strand conformation, with residues 41-49 forming a conserved α-helix. There are two structural differences between xTCF3 and hTCF4: while residues 1-11 of the xTCF3 CBD form a β-hairpin that interact with armadillo repeats 9-11 in β-catenin, this region is disordered in the hTCF4 CBD and is not crucial for binding to β-catenin. Second, residues 22-29 in xTCF3 form a β-strand extending along the groove of β-catenin; this region forms a kinked α-helix in hTCF4. Consequently, residues 31-37 in hTCF4 form an extended strand to connect this kinked α-helix to the structurally conserved α-helix; this set of residues is not well ordered in xTCF3 and is unresolved (Graham et al., 2001).

Sequential alignment of xTCF3 and hTCF4 reveal conserved residues that are critical for the binding of the CBD to β-catenin. These residues form salt bridges with Lys 312 and Lys 435, known as the 'charged buttons' of β-catenin that are essential to the β-catenin/TCF interaction. The first conserved residue in xTCF3 and hTCF4 is Asp 16 which forms a salt bridge with Lys 435. The section of residues 23-29 are also identical in xTCF3 and hTCF4, containing glutamic acid residues that form a second salt bridge with Lys 312 of β-catenin (Graham et al., 2000). In xTCF3, Glu 24 forms a salt bridge with Lys 312, while this interaction can happen at either Glu 24 or Glu 29 in hTCF4 depending on its conformation. Mutation of either lysine residue abolishes binding of both xTCF3 and hTCF4 (Graham et al., 2001). Asp 16 and Glu 24 are also conserved across the rest of the members of the TCF/LEF family in humans, namely TCF1 and LEF (Fig. 1.3B) (Graham et al., 2000).

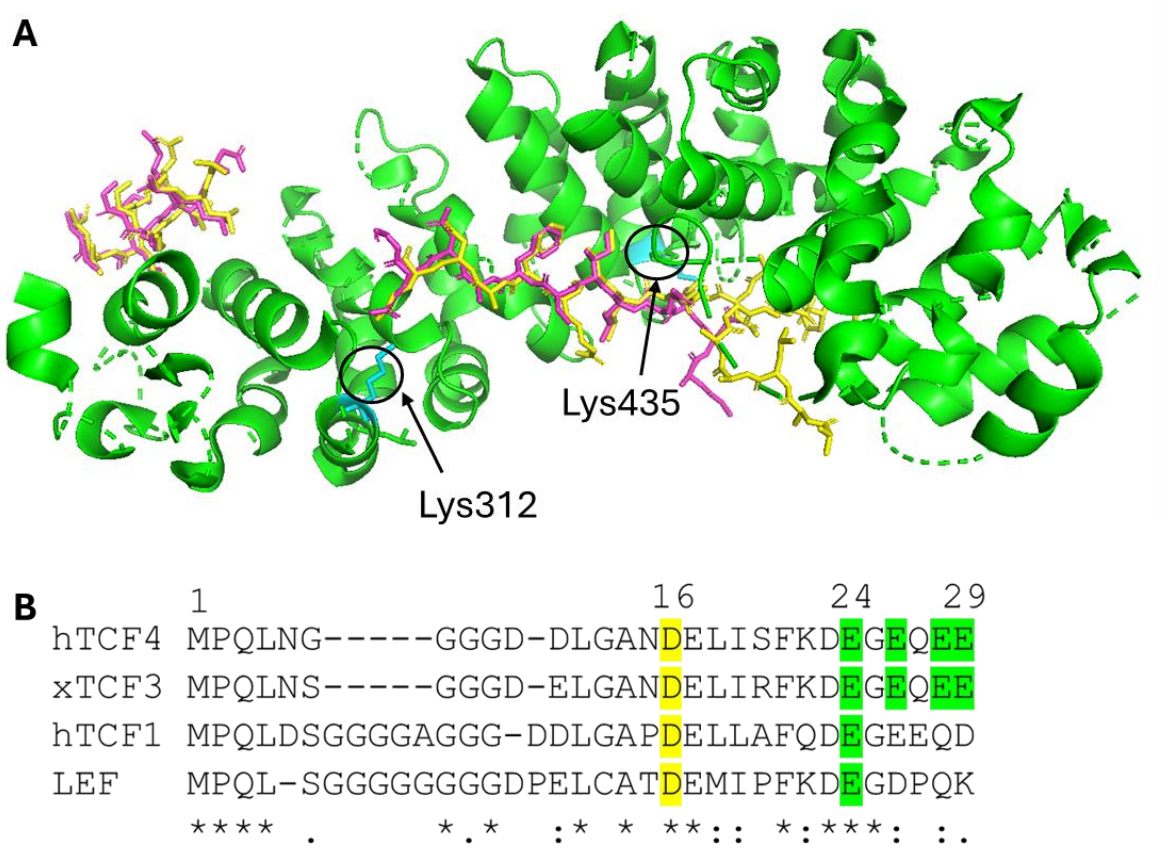

Figure 1.3: Crystal structure of β-catenin in complex with xTCF3 and hTCF4 and their sequence alignments. A: The two TCFs are sequentially and structurally similar, with the exception of the β-hairpin that is formed from residues 1-11 in xTCF3 (yellow) which is disordered in hTCF4 (pink). The lysine residues Lys 312 and Lys 435 which interact with Glu 24 (xTCF3)/Glu 29 (hTCF4) and Asp 16 respectively are coloured cyan. For the PDB files used, residues 26-39 are unresolved for xTCF3, while residues 25-39 are unresolved for hTCF4. Image generated with PyMOL. **B: Alignment of *Xenopus* TCF3 and members of the human TCF/LEF family.** The conserved aspartate residue that forms a salt bridge with Lys 435 of β-catenin is highlighted in yellow, and the conserved glutamate residue that forms a salt bridge with Lys 312 of β-catenin is highlighted in green. In the case of xTCF3 and hTCF4, residues 23-29 are identical, and hTCF4 can additionally form a salt bridge with Lys 312 at Glu 29.

Interestingly, the importance of Lys 312 and Lys 435 extends to ICAT, which is unrelated to the TCF/LEF family, but is a protein that naturally inhibits binding of TCF to β-catenin. ICAT binds to β-catenin at armadillo repeats 10-12, with its tail region extending to interact with armadillo repeats 5-9 (Fig. 1.4A) (Graham et al., 2002). Similar to TCF, ICAT contains an aspartate residue (Asp 66) and glutamate residue (Glu 75) that form salt bridges with Lys 435

and Lys 312 respectively (Fig. 1.4B), and this interaction is able to displace TCF to block gene transcription.

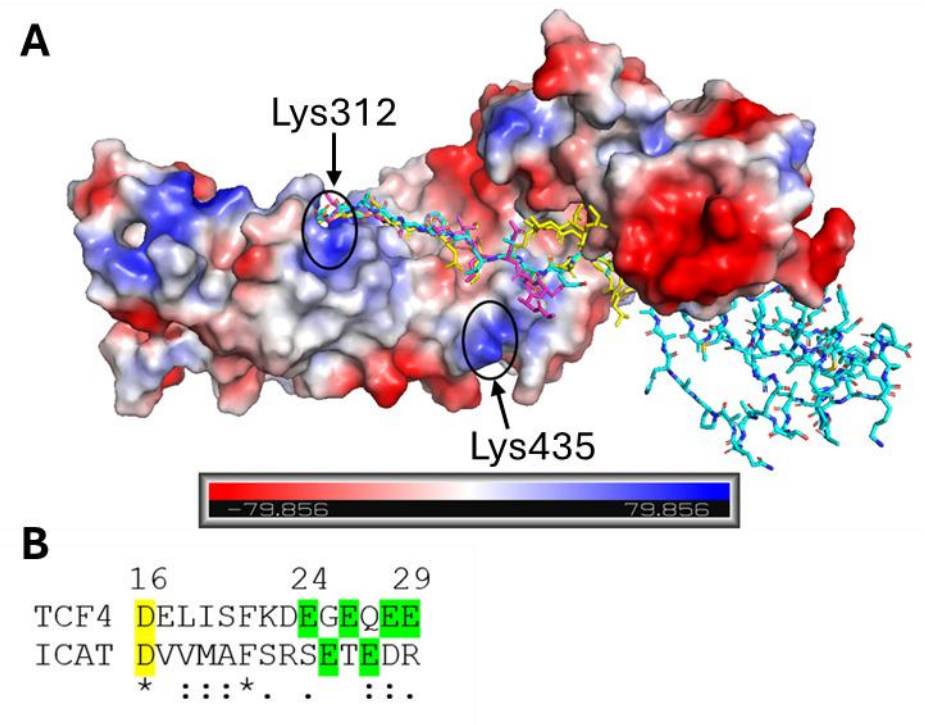

Figure 1.4: Crystal structure of β-catenin in complex with ICAT, xTCF3 and hTCF4 with sequence alignments. A: The electrostatic surface of β-catenin shows positively charged areas in red and negatively charged areas in blue. ICAT is in cyan, xTCF3 is in yellow, and hTCF4 is in pink. The circled areas in the blue surfaces are the locations of the charged buttons Lys-312 and Lys-435. Within the armadillo repeat section between the positively charged lysine residues, ICAT shares some structural similarity with xTCF3 and hTCF4. Image generated with PyMOL. **B:** The sequence for ICAT starts at Asp 66. The aspartate residues highlighted in yellow form salt bridges with Lys 435 of β-catenin, and the glutamate residues highlighted in green form salt bridges with Lys 312 of β-catenin.

2.6.2: Hot-Spot Region of β-Catenin for Drug Targeting

As β-catenin interacts with numerous partners across the armadillo repeat region, research has focused on the specific region of armadillo repeats 8-9 to abolish only β-catenin and TCF4 binding without disrupting interactions with other proteins. Lys 435, previously mentioned to be a highly critical residue that forms a salt bridge with the CBDs of xTCF3 and hTCF4, falls

within this region. Additional amino acids of note include His-470 and Asn-426 which align TCF with the groove, Arg-469 which stabilizes the TCF side chain, and Lys-508, which interacts with the extended region of TCF (Graham et al., 2000). Mutational analysis of the mentioned amino acids to alanine specifically abolished TCF4 binding but did not affect binding with Axin or APC. As such, this region has been identified as a 'hot spot' for TCF/LEF binding (Birchmeier et al., 2000). Targeting this region for drug design is therefore a viable approach in targeting cancers with aberrant Wnt signalling.

2.7: Small Molecule Inhibitors and Treatments Targeting the Wnt/β-Catenin Pathway

Over the past decade, several small molecules and peptides targeting the Wnt signalling pathway have been discovered through the use of high-throughput screening (HTS) and virtual screening (VS), where libraries containing chemical compounds are assessed for interaction with a protein target (McCoy et al., 2022).

Early preclinical molecules targeted along the Wnt pathway upstream of β-catenin/TCF4 interaction, such as the development of PORCN inhibitors to inhibit Wnt ligand lipidation and secretion to the cell membrane. A notable PORCN inhibitor is LGK974 (WNT974), which has entered early clinical trials (J. Liu et al., 2013; Rodon et al., 2021). Another small molecule, XAV939, stabilizes Axin through tankyrase inhibition to enhance the destruction complex (S.-M. A. Huang et al., 2009b). Other small molecule inhibitors have been found to target β-catenin interactions with CBP/p300 in the nucleus, such as PRI724 and ICG001 to inhibit formation of the β-catenin dependant transcriptional enhanceosome (Emami et al., 2004). Notably, PRI724 has progressed to phase 2 clinical trials (Kimura et al., 2022). In addition to small molecule inhibitors, monoclonal antibodies have also been developed to the Wnt ligand and its receptors. Vantictumab, an IgG2 monoclonal antibody, targets the Fzd receptor to block Wnt ligand binding

and made it to phase 1 clinical trials, although the trials were discontinued due to reports of bone related toxicity (Diamond et al., 2020).

The development of a small molecule inhibitor targeting β-catenin/TCF4 interaction has long been an area of interest in drug discovery, although few have proceeded past the preclinical phase. Within the ChEMBL database (https://www.ebi.ac.uk/chembl/), a database of bioactive drug-like small molecules curated from primary scientific literature, there are 283 reported β-catenin/TCF4 small molecule inhibitors. All compounds are reported to inhibit β-catenin/TCF activity based on their IC_{50} values from luciferase-based transcriptional reporter assays, although there are no published functional studies to validate their mechanisms of action. The exception is the set of 2,4-diaminoquinazoline derivatives, which have been studied *in vitro*, although their mechanism of action also remains to be elucidated. Aside from the reported β-catenin/TCF4 inhibitors in the ChEMBL database, several separate documentations of β-catenin/TCF4 inhibitors are addressed further.

In 2004, the first small molecules of β-catenin/TCF4 interaction were discovered through HTS of natural compounds. Six molecules were found to be positive hits, exhibiting IC_{50} values lower than 10 μM, indicating a measure of affinity with β-catenin. These compounds disrupted β-catenin/TCF4 interaction and complex formation, and showed selectivity by also inhibiting β-catenin/APC interaction without disrupting β-catenin/E-cadherin interaction. PKF115-584 and its related analogue PKF222-815 also disrupted the binding of TCF4 to DNA, suggesting that they interact with TCF4 instead of β-catenin (Lepourcelet et al., 2004).

In 2006, the small molecule PNU-74654 was the first reported β-catenin/TCF4 inhibitor discovered through VS, which was used in combination with *in silico* docking targeting the pocket around the residues Lys-435 and Arg-469. A binding affinity of 450 nM against the β-

catenin armadillo repeat region was reported from isothermal titration calorimetry experiments, indicating strong binding, and *in vitro* studies on pancreatic and hepatocellular carcinoma suggest that PNU-74654 interferes with the NF-κB pathway (Chien et al., 2023; M.-Y. Wu et al., 2022).

As of 2023, the first cocrystal structure of β-catenin with the small molecule inhibitor RS6452, discovered through VS, was reported (PDB: 7ZRB). The study conducted by Nalli et al. observed that RS6452 binds to the hotspot of β-catenin/TCF4 interaction, and exhibits inhibitory activity in both *in vitro* and *in vivo* studies; however, it has low potency in the *in vitro* assays (Nalli et al., 2023).

As of 2024, a peptidomimetic known as FOG-001 has progressed to phase 2 trials. Early clinical trials indicate that FOG-001 leads to notable tumour shrinkage, with no notable side effects. The structure of FOG-001 appears to mimic the structure of ICAT to outcompete TCF4 binding to β-catenin in the armadillo repeat region (Papadopoulos et al., 2024).

Although many β-catenin/TCF4 small molecule inhibitors have been discovered, little is known about their binding mechanisms or their modes of action. A biophysical survey conducted in 2022 by McCoy et al investigated existing small molecules that claimed to bind to β-catenin including β-catenin/TCF4 inhibitors, including the aforementioned PKF115-584, PKF222-815 and PNU-74654. Their findings showed that none of the small molecules examined were found to exhibit actual *in vitro* binding to the armadillo repeat domain of β-catenin. Moreover, several reported molecules were found chemically labile due to pan assay interference (PAINS) structures (McCoy et al., 2022). PAINS structures are promiscuous chemical substructures that react non-specifically with numerous biological targets, resulting in false positives in screening campaigns (Baell & Holloway, 2010). Their results shed doubts on the mechanism of action

behind existing molecules, which suggests that additional approaches to ligand screening and optimization will be useful to validate future small molecule inhibitors.

Table 1.1: Existing small molecule inhibitors of the β-catenin/TCF4 and Wnt signalling pathway.

Compound Name	Proposed Mechanism of Action/Target	Developmental Stage in Clinical Trials	Current State in Research	References
PKF115-584 and related compounds	Disrupt formation of β-catenin/TCF4 complex, suggested to inhibit TCF binding to DNA	Preclinical	High *in vivo* toxicity in mice over long term, binding site unknown	(Lepourcelet et al., 2004; Wei et al., 2010; McCoy et al., 2022)
PNU-74654	Bind to β-catenin and partially competes with TCF4	Preclinical	Contrasting binding results in isothermal titration calorimetry (ITC) assays	(Chien et al., 2023; McCoy et al., 2022; M.-Y. Wu et al., 2022)
***R*-etodolac and analogues**	Inhibit β-catenin/TCF signaling and decrease nuclear β-catenin levels	Phase 1/2 (trials terminated)	Linked to rare cases of drug induced liver disease with fatal cases described, no binding observed to β-catenin in ITC	(Mabee et al., 1995; Reuben et al., 2010; Schmeltzer et al., 2016; McCoy et al., 2022)
2,4-diaminoquinazoline derivatives	Inhibit β-catenin/TCF4 protein-protein interaction	Preclinical	No binding observed to β-catenin in ITC, low bioavailability and solubility observed	(Chang et al., 2020; Chen et al., 2009; Dehnhardt et al., 2010; Mao et al., 2012; McCoy et al., 2022)
2,3,6-trisubstituted quinoxaline derivates	Decrease nuclear β-catenin levels, suppressed β-	Preclinical	No binding observed to β-catenin in ITC	(S. B. Lee et al., 2013; S.-B. Lee et al.,

	catenin/TCF4 transcriptional activity			2010; McCoy et al., 2022)
CCT031374	Block TCF-dependent transcription	Preclinical	No binding observed to β-catenin in ITC	(Ewan et al., 2010; McCoy et al., 2022)
iCRT3	Inhibit β-catenin/TCF4 complex formation without noticeable effects with E-cadherin and α-catenin	Preclinical	No binding observed to β-catenin in ITC	(Gonsalves et al., 2011; McCoy et al., 2022)
BC21	Decrease β-catenin dependent TCF reporter activity and downregulated Wnt target genes	Preclinical	Also inhibits protein phosphatase 2C, low solubility	(Daniel et al., 2004; McCoy et al., 2022; Rogers et al., 2006; W. Tian et al., 2012)
Carboxylic acid-containing derivatives	Selective inhibition of β-catenin/TCF4 interaction without disrupting APC and E-cadherin interaction, proposed to interact at Lys 435	Preclinical	PAINS alerts for reactive and promiscuous, indiscriminate reactions with different biological targets	(Henen et al., 2012; McCoy et al., 2022)
UU-T01 and derivatives	Inhibit β-catenin/TCF4 protein-protein interaction and confirmed to bind directly to β-catenin	Preclinical	Poor cell permeability observed in derivative UU-T02, biological activity of UU-T01 unknown	(Z. Huang et al., 2014; B. Yu et al., 2013)
LF3	Inhibit β-catenin/TCF4 protein-protein interaction	Preclinical	No binding observed to β-catenin in ITC	(Fang et al., 2016; McCoy et al., 2022)

HI-B1	Inhibit β-catenin/TCF4 transcriptional activity	Preclinical	No binding observed to β-catenin in ITC	(McCoy et al., 2022; Shin et al., 2017)
RS6452	Abolished association between β-catenin/TCF4, binds to β-catenin/TCF4 hotspot region	Preclinical	Crystal structure of RS6452 and β-catenin reported	(Nalli et al., 2023)
Peptidomimetics and other small molecule inhibitors of the Wnt/β-catenin Signalling Pathway				
FOG-001	Outcompete TCF4 binding with β-catenin to inhibit interaction	Phase 1/2	Clinical trials in progress, no side effects reported in treatment	(Papadopoulos et al., 2024)
LGK794	Inhibits PORCN activity	Phase 1	Bone toxicity observed in murine models	(J. Liu et al., 2013; Lung et al., 2024; Rodon et al., 2021)
PRI724	Inhibits CBP/ β-catenin interaction	Phase 1/2A	Clinically applicable equivalent of ICG001	(Kimura et al., 2022)
ICG-001	Inhibits CBP/ β-catenin interaction	Preclinical	Precursor of PRI724	(Emami et al., 2004)
XAV939	Axin stabilizer through tankyrase inhibition	Preclinical	Effective lethal dose of drug in free form is high, around 178 μM	(Afifi et al., 2014; S.-M. A. Huang et al., 2009a)

The development of a potent β-catenin/TCF4 inhibitor with the potential to become a clinical drug has remained elusive. HTS and VS of multiple chemical libraries have resulted in the discovery of promising compounds that have the potential to inhibit β-catenin/TCF4 activity, but it is nearly impossible for a perfect drug to be discovered immediately from existing libraries. As such, these initial structures, or positive ‘hits’ are chosen as ‘lead’, or candidate molecules,

which need to undergo cycles of optimization to improve selectivity, potency, and pharmacokinetic properties such as solubility to increase their druglikeness, or drug potential (Hughes et al., 2011). Previous studies of β-catenin/TCF4 inhibitors mostly lacked pharmacokinetics data and did not take medicinal chemistry into account (McCoy et al., 2022). This highlights the urgent need for a medicinal chemistry driven approach to develop and optimize β-catenin inhibitors with potency, specificity, and drug-like properties necessary to advance into clinical trials. Improving drug potency can be conducted virtually using structure-activity relationship (SAR) analysis.

3. SAR Analysis and Molecular Similarity

3.1: Structure-Activity Relationship Analysis

Structure-activity relationship (SAR) analysis refers to the analysis of the relationship of a molecule's biological activity with its structure, with the concept dating back to the 19th century with the investigation of ammonium bases derived from medicinal plants and their common physiological effects on humans. Analysis of SAR allows for the determination of the chemical group or scaffold responsible for exerting a biological effect on the target, from which further improvement to the rest of the structure can be made (Brown & Fraser, 1868). SARs are key along the drug discovery process, ranging from primary screening to lead optimization.

Lead optimization is a cyclic, iterative process, where new analogues of the lead compound are designed, synthesized, tested, analyzed, and redesigned to improve potency, selectivity, metabolic stability and bioavailability while reducing toxicity (Raymond et al., 2009). Strategies for lead optimization often rely on the availability of the three-dimensional structure of the ligand-receptor complex; however, there are cases where the structure cannot be obtained

through methods such as X-ray crystallography or nuclear magnetic resonance (NMR). As such, SAR analysis can be used to fill the knowledge gaps to optimize and improve the lead compound as it is strictly ligand-based (Shim & MacKerell, 2011). Ideally, early in the optimization process, the drug-like characteristics of an active compound needs to be considered, which include ADME/Tox (Absorption, Distribution, Metabolism, Excretion, and Toxicology) (Andricopulo & Montanari, 2005). These properties describe how a body processes a drug to determine its concentration, duration, and intensity of effect, and improvement of these properties via SAR analysis is critical in decreasing the late-stage failure rate traditionally associated with the discovery process (Nelson, 1961).

3.2: Molecular Similarity in SAR

SAR technology is based conceptually on the principle of molecular similarity, one of the most heavily exploited concepts in drug discovery, which operates under the principle that structurally similar molecules have similar properties (Johnson & Maggiora, 1990). Under this principle, virtual screening can be conducted on known active compounds to discover structurally similar compounds that are likely to share the same activity to find new leads for drug discovery. Upon discovery of a scaffold, molecular similarity analyses can be conducted to investigate structurally similar compounds, which further enhances understanding of SARs.

A prominent case for molecular similarity analyses is the development of the synthetic HMG-CoA reductase atorvastatin calcium. Initial studies of this structure came from the discovery of fungal metabolite-derived inhibitors mevastatin and lovastatin. SAR analysis of these molecules and their synthetic derivatives revealed a common scaffold, or pharmacophore, from which structurally similar compounds, or analogues, were derived, namely, a double-ringed system with a hydrophobic group. However, with the advent of safety concerns from toxicology

reports, the double-ringed portion of the scaffold was replaced with a similar system that had similar inhibitory activity. Following optimization through the replacement or substitution of the R-groups where potency and toxicity were prioritized, atorvastatin was eventually developed and is now marketed today as Lipitor (Roth, 2002).

One of the common tools for structural similarity analysis is DataWarrior, an open-source software for chemical data visualization and analysis. Structural similarity analysis was conducted using fragFP, a built-in descriptor containing a predefined library of 512 predefined substructure fragments. This library contains common fragment types such as functional groups or ring systems that occur frequently within typical organic molecule structures with little overlap. Inputted chemical structures are encoded into a binary bit string, or a sequence of 0s and 1s based on the fragFP library. If a structure contains a feature in the library, the bit position in the string is set to 1 (ON); otherwise, it is set to 0 (OFF) (Fig. 1.5). Each chemical structure analyzed using fragFP would have its own unique binary string, or fingerprint, which can be used to calculate molecular similarity between two molecules (Sander et al., 2015).

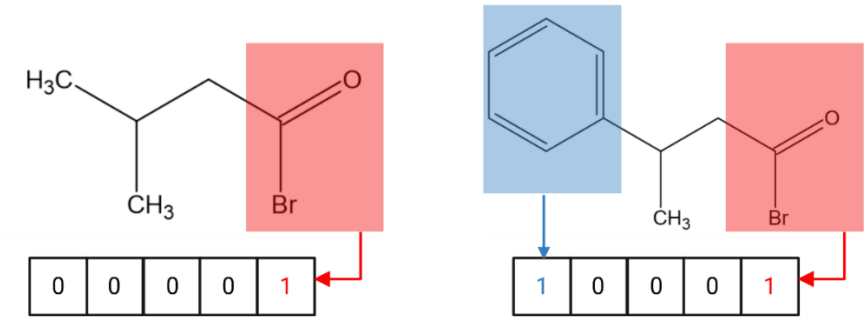

Figure 1.5: Example of a binary bit string between two example structures. Both structures share a carbonyl bromide group indicated in red, setting the bit position to 1. The structure on the right has an additional phenyl group indicated in blue, setting the bit position to 1. As the structure on the left lacks the phenyl group, the bit position is set to 0.

Molecular similarity in DataWarrior is calculated using the Tanimoto coefficient, which is a standard in similarity calculations. It is calculated by the quantification of the fraction of features common between two chemical structures to the total number of features across both structures, illustrated as "c/[(a+b)-c]", where a and b are the number of features present in structures A and B, and c is the number of features shared by A and B. The values of a, b and c are based on the molecular fingerprints of A and B. The Tanimoto coefficient results in a value between 0 and 1, where a Tanimoto coefficient closer to 1 indicates that the structures are very similar (Bajusz et al., 2015). Upon generation of a structural similarity plot on DataWarrior, structures that have a high Tanimoto coefficient are connected and clustered together, while dissimilar structures with lower coefficients are randomly scattered throughout the plot. As molecular fingerprints are based off the predefined fragments in the fragFP library, differences in the presence or absence of fragment types may greatly alter the Tanimoto coefficient.

Rationale

Aberrant Wnt/β-catenin signalling is associated with a number of diseases and cancer types. Dysregulation of Wnt signalling has been shown to initiate cancer progression, especially in EOC. A particular mechanism in the dysregulation of Wnt signalling is the hyperactivation of β-catenin, where mutations of the *CTNNB1* gene encoding for β-catenin has been found in many ovarian cancer cases, specifically in the EC subtype of EOC. Hyperactive β-catenin has also been implicated in angiogenesis, metastasis, and the maintenance of CSCs, which increase chemoresistance to current cancer treatments through the upregulation of oncogenes. The interaction between β-catenin and its coactivator TCF4 is critical in the transcription of oncogenes; therefore, targeting this interaction would eradicate Wnt signalling without off-target toxicities. Although current β-catenin/TCF4 inhibitors exist, many fail at the preclinical trials as

they lack pharmacological data and do not possess a druglike nature, reducing their likelihood of proceeding to clinical trials.

Preliminary research conducted in our lab used *in silico* screening to identify promising inhibitors from a virtual library containing 200,000 compounds. The target was the hotspot in armadillo repeats 8-9 of the β-catenin structure described earlier as it abolishes binding between β-catenin and TCF4 but avoids the disruption of β-catenin with Axin and APC. Eleven top hits, termed C1 to C11, were commercially available and purchased to test their ability to inhibit β-catenin/TCF4 signalling. Two of the compounds, C2 to C10, were further tested, with C10 performing better than C2. Analogues of C10 were then synthesized, termed C12 to C44, and characterized by previous members of the lab. One of the compounds, C21, exhibited inhibitory activity on par with C10.

However, the druglike nature of C10 has been impeded by mediocre solubility and binding affinity, as it is only able to inhibit β-catenin at micromolar concentrations; ideally, a β-catenin/TCF4 inhibitor would be able to exert anti-tumour effects at nanomolar concentrations which correlate with high binding affinity and potency. Additionally, the low solubility of C10 has prevented the generation of a cocrystal structure of the molecule in complex with a β-catenin. As previously mentioned, SAR analysis can fill the knowledge gap in the case where the three-dimensional structure is not available. As C1-C44 have been previously characterized in functional assays, SAR analysis can be conducted on the structures to confirm bioactive substructures and determine areas of optimization to improve solubility and potency.

Further analogues of C10 have also been synthesized in-house, termed C45-C62. They will be characterized similarly through biochemical and cell-based assays as the previous compounds

to determine their SARs, and a compound that surpasses C10 in potency and solubility is anticipated to further optimize the β-catenin/TCF4 inhibitor.

Objectives

The goal of my project is to analyze and compare C10 with its newly synthesized analogues C45-C62 using structure-activity relationship (SAR) analysis and correlate the findings with *in vitro* assays. SAR has been shown to be critical in drug discovery to investigate the pharmacophore, or critical structure which can then be optimized to increase the druglike nature of new analogues

Objective 1: Structural similarity analysis of existing β-catenin/TCF4 inhibitors with in-house compounds to investigate SAR and druglike nature

As C10 and its analogues are unreported in public domain, verification of their structural uniqueness compared to existing β-catenin/TCF4 inhibitor is crucial to prove their worth for future investigation. Additionally, as bioactivities of C1-C44 exist from previous data, the SARs for these compounds can be determined to identify bioactive substructures. As C45-C62 do not have any previously existing bioactivity data, *in silico* analyses will be carried out to determine their predicted binding affinity to β-catenin through molecular docking; in addition, their ADME profile will be characterized to assess their druglikeness.

Objective 2: Determine if C45-C62 bind directly to β-catenin

As C45-C62 are designed to directly bind to β-catenin to inhibit activity, biolayer interferometry (BLI) assays will be conducted to determine their *in vitro* binding affinity compared to the virtually predicted affinities. This measure of bioactivity will be used to determine their SARs to identify areas for optimization.

Objective 3: Determine inhibitory effects of C45-C62 on cancer cells

It is expected that inhibition of β-catenin activity disrupts cancer cell growth and proliferation. As such, proliferation and clonogenic assays will be conducted using TOV112D cells, an ovarian cancer cell line that expresses hyperactive β-catenin, as a model for EC. A comparison between C10, the candidate molecule, will be made with C45-C62.

Chapter 2: Materials and Methods

Purification of Recombinant β-Catenin Protein

E. coli strain BL21+ (DE3) with the M57 pPET28a-TEV-full-length human β-catenin plasmid was inoculated in 50 mL of lysogeny broth (LB) medium containing 50 µg/mL of kanamycin at 37°C overnight before culture in 1 L LB broth containing 50 µg/mL at 21°C. When the OD_{600} reached 0.6-0.8, the bacterial cells were induced with 0.5mM of isopropyl-beta-D-thiogalactopyranoside (IPTG) for recombinant protein expression at 16°C for approximately 18-20 hours. The plasmid was purchased from Addgene (plasmid #17198; originally deposited by Randall Moon).

After the bacterial pellet was harvested, it was suspended in lysis buffer (20 mM Tris, pH 8.0, 500 mM NaCl, 10% glycerol, 0.1% Triton X-100, 1 mM β-mercaptoethanol (BME), 10 mM imidazole, 0.5 mM PMSF, 1 mM benzamidine) at 4°C and sonicated at 25% amplitude, 10 seconds off, 2 seconds on for 2 minutes to lyse the cells. After sonication, the soluble protein was harvested and incubated with 2 mL of nickel-nitrilotriacetic (Ni-NTA) beads for an hour. The beads were transferred to an affinity chromatography column pre-equilibrated with lysis buffer and washed with a wash buffer (20 mM Tris, pH 8.0, 500 mM NaCl, 10% glycerol, 1 mM BME, 10 mM imidazole, 0.5 mM PMSF, 1 mM benzamidine) and eluted in 1 mL fractions with elution buffer (20 mM Tris, pH 8.0, 500 mM NaCl, 10% glycerol, 1 mM BME, 300 mM imidazole, 0.5 mM PMSF, 1 mM benzamidine).

Protein fractions were then dialyzed into BLI buffer (20 mM Tris, pH 8.0, 150 mM NaCl, 10% glycerol). Elutions collected from the affinity column were visualized using SDS-PAGE.

Compound Preparation

C1 to C11, and commercially available C10 analogues C12 to C28 were purchased from Molport. In-house synthesized C10 analogues C29 to C62 were provided by Dr. Arturo Orellana's lab. All compounds were dissolved in DMSO at the concentration of 100 mM and diluted with DMSO to required concentrations.

Confidentiality and Disclosure Statement

Due to potential IP applications, the structural details of the compounds investigated in this thesis have been withheld from the publicly available version of this document out of considerations for confidentiality. The omission of these details does not affect the scientific interpretation of the results presented herein.

Biolayer Interferometry with Octet R4

The binding kinetics of C45-C62 with β-catenin was detected and quantified using the Sartorius Octet R4 system. Protein-compound interaction was conducted at 25°C in BLI buffer supplemented with 0.001 g/mL BSA as blocking buffer. Ni-NTA probes were activated in PBS prior to use. Samples were added to black 96-well plates with a volume of 200 µL per well. Sensor tips were initially wet in BLI buffer for baseline establishment, before being moved to wells containing 1 mg/mL of purified full-length His_6-tagged β-catenin protein to load the protein onto sensor tips. A washing step was then conducted to remove excess protein before a new baseline was established. C45-C62 and C10 were prepared as a serial dilution of 2.5, 5, 10, 20, 40 and 60 µM. Sensor tips were then dipped into wells containing a single concentration of compound before being washed to dissociate binding before proceeding to the next

concentration. A negative control of 0.1% DMSO was included in each run. Data was processed using Octet Analysis software using reference subtraction. Experiments were conducted twice.

Cell line and Culturing

TOV112D cells were purchased from the American Type Culture Collection (Manassas, VA, USA). TOV112D cells were maintained in a 1:1 ratio of MCDB105/M199 media supplemented with 15% fetal bovine serum (FBS). The cells were subcultured every 2-3 days upon reaching confluency in 10 cm plates.

Proliferation Assay

TOV112D cells were seeded onto 96-well plates with 2500 cells per well and treated with 10 μM of C45-C62, C10, or 0.1% DMSO. Plates were placed in the IncuCyte for imaging every 4 hours. Plates were removed after 72 hours in the IncuCyte and confluency was graphed using GraphPad. Experiments were conducted three times.

Clonogenic Assay

TOV112D cells were seeded into 12-well plates with 500 cells/well and allowed to adhere to the wells for 24 hours. Media was discarded and media containing 10 μM of C45-C62, C10, or 0.1% DMSO was added, and refreshed every 3 days. After 3 treatments, cells were fixed and stained with crystal violet (0.2% w/v, 20% ethanol, 10% formaldehyde) and counted manually. Experiments were conducted three times.

Statistical Analysis

For *in vitro* analyses, results were expressed as mean ± SEM. Statistical analysis and graph generation were conducted using GraphPad Prism 11.0 with significance determined at

$p<0.05$. Each experiment was independently repeated two or more times to ensure consistency in the results. IC_{50} values were determined using nonlinear regression analysis with a dose-response inhibition model. Additionally, one-way ANOVA and Tukey's tests were used for comparisons among C45-C62 and comparison with C10.

Determination of Survival Fraction and Relative Inhibition for Data Representation

To represent clonogenic assay data in numerical form, the survival fraction formula [colonies counted/(cells plated*plating efficiency of control)] was used, where DMSO, with a survival fraction of 1, was used as the control for the determination of plating efficiency (colonies observed/cells seeded) (Franken et al., 2006; Rafehi et al., 2011).

To represent proliferation assay data in numerical form, the relative inhibition was calculated using DMSO, with a relative inhibition of 0%, as the scale. Relative inhibition was calculated as the relative cell inhibition derived from net confluency over 72 hours (Ahmad et al., 2025).

Chapter 3: Results

3.1: Structural Analysis of β-catenin/TCF4 Small Molecule Inhibitors in ChEMBL Database

As our study focuses on the inhibition of the interaction between β-catenin and TCF4, we first analyzed existing β-catenin/TCF4 inhibitors in the ChEMBL database (https://www.ebi.ac.uk/chembl/). The analysis served as a reference landscape (Fig. 3.1) for comparison with the candidate compounds developed in the Peng lab.

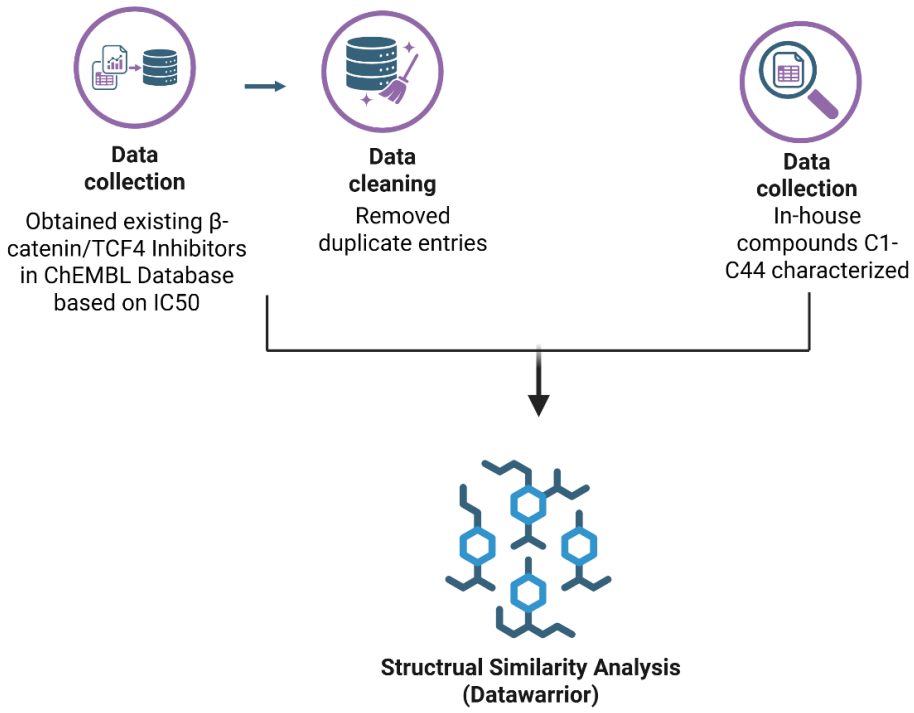

Figure 3.1: Workflow outline for structural similarity analysis of existing β-catenin/TCF4 inhibitors and in-house synthesized inhibitors. The existing inhibitors were obtained from the ChEMBL database and cleaned to remove duplicates before they were combined with data from the candidate compounds C1 to C44 to undergo structural similarity analysis using DataWarrior software.

Among the β-catenin/TCF4 inhibitors in ChEMBL (ChEMBL target ID: 3038511), 549 compounds have reported IC_{50} values derived from various luciferase-based reporter assays. After removing duplicate entries, the dataset of ChEMBL compounds was reduced to 283

compounds. Because the reported bioactivity values spanned several orders of magnitude (8.5×10^{-9} M to 2.5×10^{-5} M), the values were normalized by converting the IC_{50} values to the negative logarithmic scale (pIC_{50}) also referred to as pChEMBL value for subsequent analysis.

To explore the relationship between structural similarity in the ChEMBL compounds and the differences in their bioactivities, the data analysis software DataWarrior was used. The activities of the compounds are represented by their pIC_{50} values, while their structural similarity was calculated by the default FragFP similarity descriptor in DataWarrior and illustrated as a cluster diagram (Fig. 3.2). This descriptor identifies common substructure fragments shared in typical organic molecule structures to assess similarity between two compounds. In the cluster diagram, each marker represents an individual compound from the dataset. The colour represents the pIC_{50} (pChEMBL) values, ranging from a log scale of 4 to 7, where a smaller value corresponds to a lower bioactivity and larger vales indicates stronger inhibitory activity. Compounds with identical chemical scaffolds are connected by lines and clustered together, whereas dissimilar structures are scattered throughout the visualized chemical space.

The ChEMBL compounds cluster diagram reveals a diverse range of structures. Three large clusters are observed, each containing around 30 compounds (labeled 1-3). There are additional smaller clusters scattered throughout the landscape, each containing less than 10 structurally similar compounds. The remaining compounds appear as isolated markers, representing structures that are unique within the dataset.

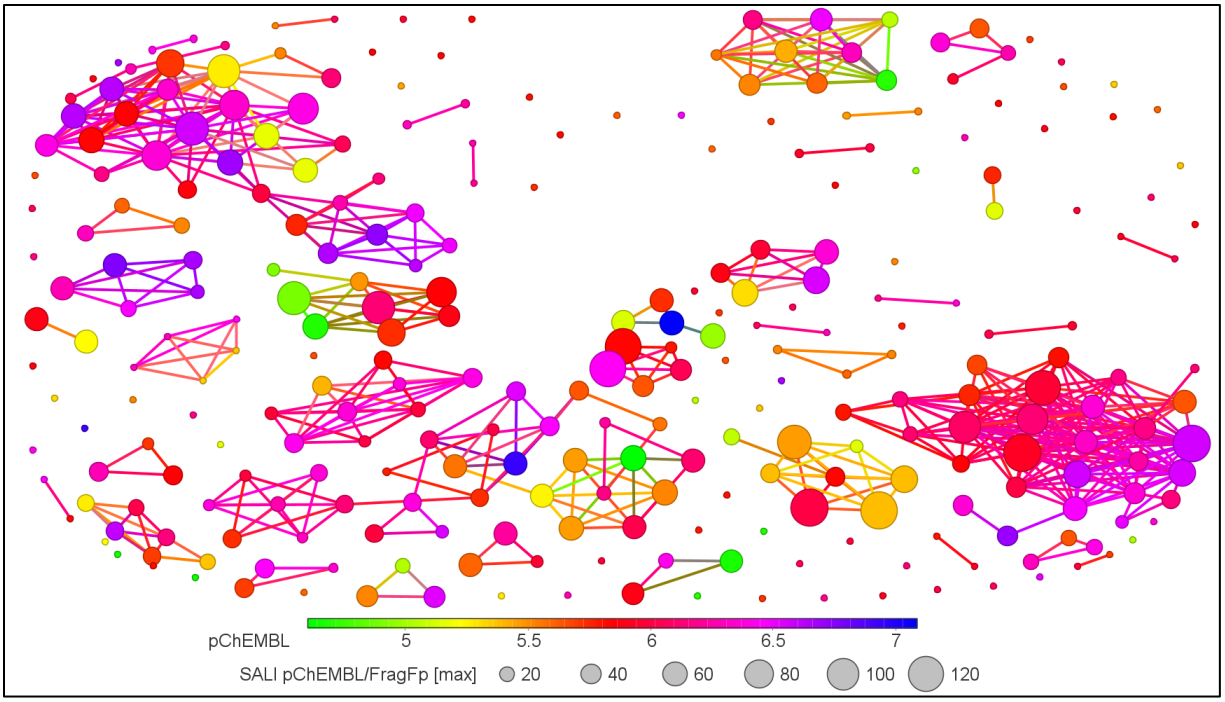

Figure 3.2: The structural similarity analysis for 283 existing β-catenin/TCF4 inhibitors in the ChEMBL database. Compounds with identical structural skeletons are connected by lines and clustered together, and dissimilar structures are scattered throughout the visualized chemical space. The colour of the circles represents the pIC_{50} (negative log of IC_{50}) values of each compound. The sizes of the circles reflect the SALI value for each compound. The SALI value is defined by the measure of the difference in structure and the difference in bioactivity. This analysis was done by DataWarrior software.

To further identify structural features that strongly influence β-catenin/TCF4 inhibitory activity, a structure-activity landscape index (SALI) was calculated to characterize activity cliffs. Activity cliffs are pairs of chemically similar molecules that exhibit a large, unexpected difference in biological activity, and this metric is quantified through the calculation of the SALI value and visualized as the circular markers as seen in Figure 3.2. A larger marker, i.e. a higher SALI value, represents a large difference in activity but a small difference in structural similarity. These markers provide insights into substructures and functional groups that strongly affect bioactivity of these β-catenin/TCF4 inhibitors.

3.2: Structural Analysis of Candidate Compounds C1-C44

SAR analysis was then performed on a group of 44 compounds previously identified through *in silico* screening targeting β-catenin in the Peng lab. Ranked by the calculated potential free energy of the compounds binding to β-catenin, the 11 top-scoring compounds in the screening were named C1 to C11 and tested in the Peng lab for their ability to inhibit β-catenin/TCF4 activity *in vitro*. Functional assays found C10 to exhibit the strongest inhibitory activity on β-catenin. Additional analogues of C10, termed C12-C44, were further purchased or synthesized and characterized by previous lab members.

A structural comparison of C1 to C44 with the ChEMBL compounds was performed using DataWarrior and illustrated in Fig. 3.3. The ChEMBL compounds are shown in yellow, and C1 to C44 are shown in cyan. C1 to C44 occupy a unique region in the landscape without overlapping with any of the existing compounds. These candidate compounds are therefore structurally distinct and are potentially worth investigating as a potential new family of β-catenin/TCF4 inhibitors.

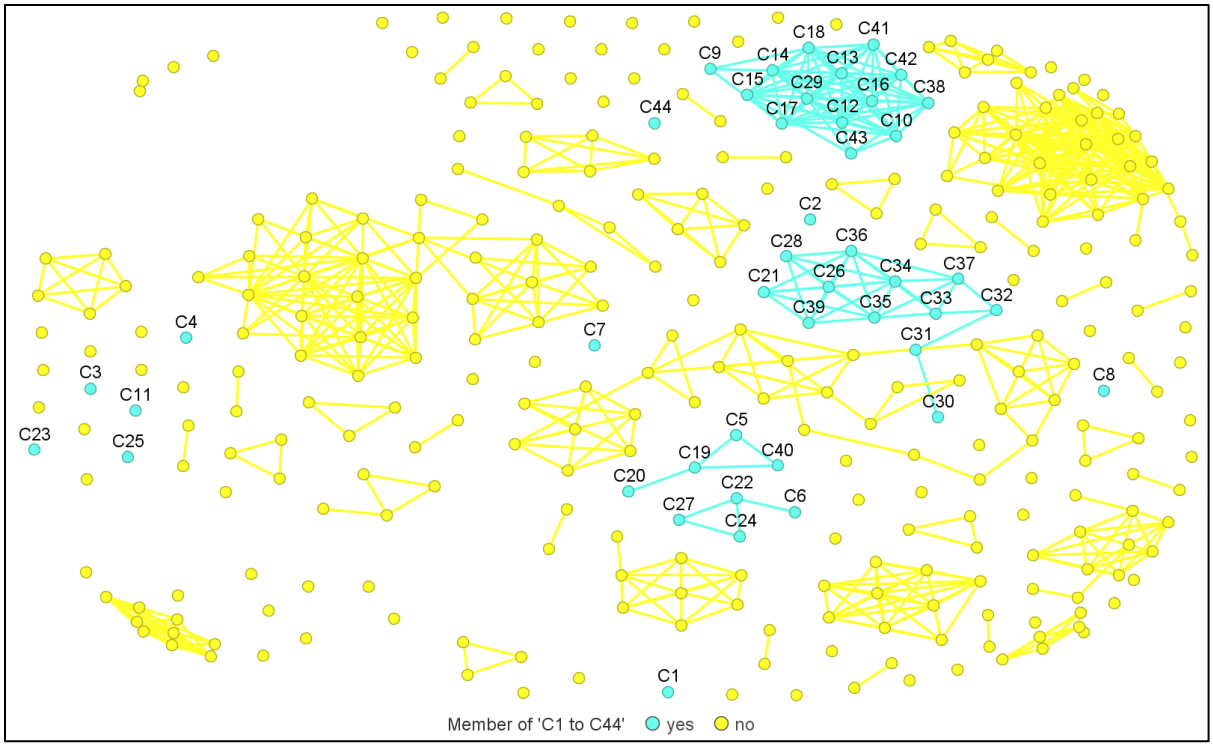

Figure 3.3: The structural similarity analysis for all reported β-catenin/TCF4 inhibitors in the ChEMBL database in comparison with the structures of C1 to C44. The ChEMBL compounds are shown in yellow, and C1 to C44 are shown in cyan. C1 to C44 do not overlap with any of the existing compounds and are therefore structurally distinct and worth investigation.

To explore the relationship between structural difference and changes in bioactivity within C1 to C44, DataWarrior was used to perform a similar SAR analysis as was conducted on the ChEMBL compounds. Structural similarity is represented by the FragFP similarity descriptor. The activities of these compounds are represented by their inhibitory effect (potency) ranked relative to C10 on a scale of 0 (no inhibition) to 1 (total inhibition) based on the dataset provided by a previous lab member. This dataset was generated using clonogenic assays on TOV112D cells with C10 as a reference of 1 as it exhibited total inhibition at 10 µM (Table S1). This relationship was visualized as a cluster diagram (Fig. 3.4).

In Figure 3.4, structural comparison of C1 to C44 reveals two major clusters of compounds denoted as the C10 and C21 clusters respectively. C10 and C21 are the representative compounds as they were previously tested to have the highest inhibitory activity. Each cluster contains compounds that share an identical structural scaffold. The C10 cluster is composed of 12 compounds including itself. The C21 cluster is composed of 12 compounds including itself. Within the C21 cluster of compounds, major structural changes are observed in C30 to C32 as they diverge from the main cluster but remain connected to the main scaffold. In addition, there are individual compounds represented by dots that possess scaffolds distinct from other compounds. The size of the compound markers represents the SALI score between two compounds. The C10 and C21 clusters were further compared based on the differences at specific substructure sites derived from DataWarrior analysis.

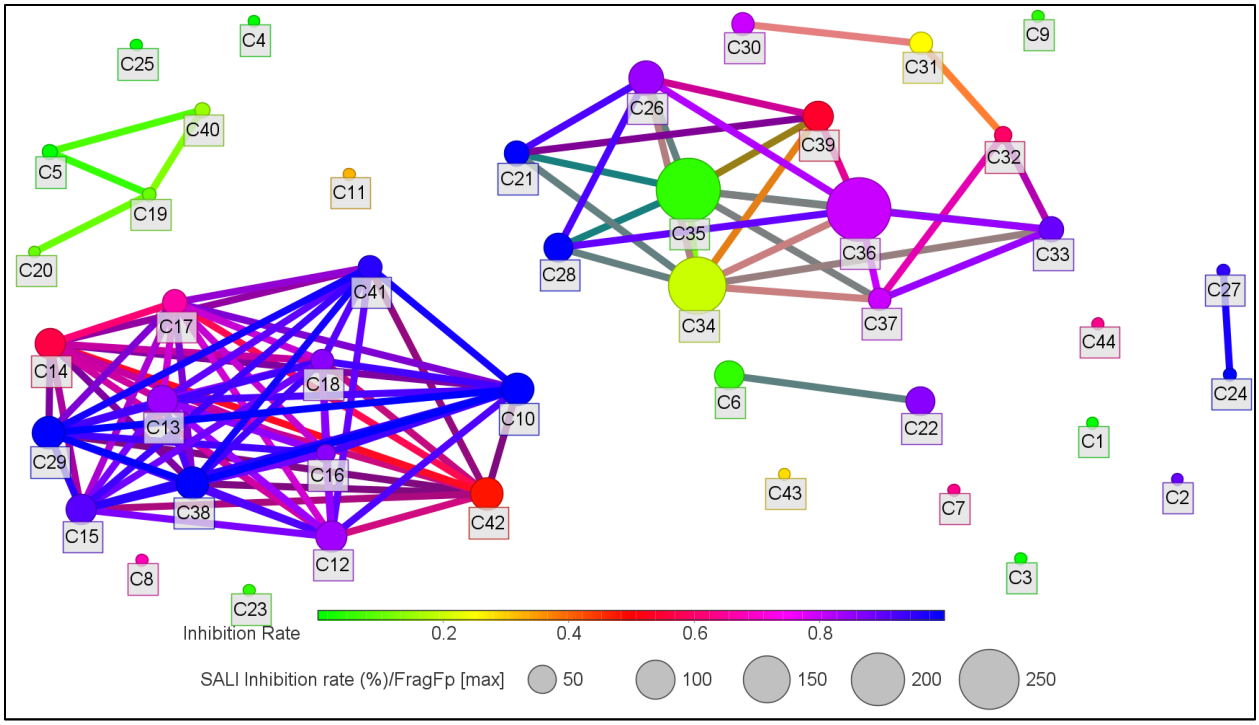

Figure 3.4: The structural similarity analysis for C1 to C44. The colour of the markers represents the inhibitory rate of each compound, and the sizes reflect the SALI value for each pair of compounds. Compounds with identical structural skeletons are connected by lines and clustered together, and dissimilar structures are scattered throughout the visualized chemical space.

Based on the SALI clusters, Table 3.1 summarizes the structural changes are found at specific substructure sites indicated as R1 to R5 within the C10 cluster of compounds. Notably, compounds C15, C29 and C38 have the same chemical structure as C10 but differ in stereochemistry. All three have similar inhibitory activity ranging from 0.9 to 1, and the slight activity differences are likely due to changes in stereochemistry.

Table 3.1: Chemical structure differences and bioactivity of C10 and its structurally similar analogues.

Compound	R1	R2	R3	R4	R5	% Inhibition
10	H	H	methyl	H	Cl	1
12	H	H	H	H	Cl	0.84
13	H	H	methyl	H	methyl	0.85
14	H	H	methyl	H	H	0.57
15[1]	H	H	methyl	H	Cl	0.91
16	H	H	methyl	methyl	H	0.87
17	H	H	H	H	F	0.66
18	H	H	ethyl	H	H	0.87
29[1]	H	H	methyl	H	Cl	1
38[1]	H	H	methyl	H	Cl	1
41	methyl	H	methyl	H	Cl	0.96
42	H	methyl	methyl	H	Cl	0.48

Comparing the impact of each R group on activity, substitutions at R2, R3 and R5 appear to have greater influence on the compound's activity, where R1 and R4 tolerate small substitutions and are therefore less critical for activity. First, compounds C41 and C42 are structurally similar to C10, each containing a single methyl substitution at R1 and R2 respectively. The addition of a methyl group at R1 has a mild impact on activity as C41 retains an inhibitory activity of 0.96. In contrast, the addition of a methyl group at R2 greatly impacts activity as C42 has an inhibitory activity of only 0.48. Moreover, R3 prefers a methyl as in C10, and the loss of it results in decreased activity as seen in C12 and C17. Additionally, R5 favours a chlorine substituent as seen in C10. The loss of this halogen reduces activity as seen in C13 and C14. Overall, based on the SALI scores, the substitutions and R2 and R5 lead to the biggest changes in inhibitory activity.

[1] C15, C29 and C38 are stereoisomers of C10.

Based on the SALI clusters, Table 3.2 summarizes the structural changes within the C21 cluster of compounds focusing on substitutions at positions R1 to R3. Out of the three R-groups, changes in R1 appear to have the greatest impact on activity. First, replacing aromatic group at R1 in C21 with an aliphatic substitution greatly reduced activity. For example, C34 and C35 with aliphatic substitutions in R1 exhibit reduced inhibitory activity (less than 0.25) compared to C21 (inhibitory rate of 1), suggesting R1 prefers an aromatic substructure. In addition, the polarity of R1 also seems to affect activity. Examples include C36 and C39, which possess a benzyl and pyridine group at R1 respectively. These structures are more polar than the aryl halide that C21 has at R1, and both C36 and C39 have decreased inhibitory activity compared to C21. Altogether, this corroborates the importance of the R1 site for inhibitory activity and its preference for a nonpolar aromatic group.

Table 3.2: Chemical structure differences and bioactivity of C21 and its structurally similar neighbours.

Compound	R1	R2	R3	% Inhibition
21	3-chloro-4-fluorophenyl	methyl	Cl	1
26	phenyl	methyl	Cl	0.85
28	cyclohexyl	ethyl	Cl	1
30	2,3-dihydro-1H-indene	ethyl	H	0.8
31	n-propylacetamide	ethyl	H	0.25
32	1-methoxy-4-methylphenyl	ethyl	H	0.6
33	1-methoxy-4-methylphenyl	ethyl	Cl	0.9
34	n-propylacetamide	ethyl	Cl	0.2
35	n-butylacetamide	ethyl	Cl	0.05
36	benzyl	methyl	Cl	0.8
37	1-methoxy-4-methylphenyl	methyl	Cl	0.8
39	pyridine	methyl	Cl	0.54

3.3: Predicted Druglikeness of Initial Candidate Compounds

'Druglikeness' is a qualitative concept applied to compounds to compare their properties with existing drugs. The druglikeness of small molecules are often evaluated using Lipinski's Rule of 5, a set of guidelines in drug discovery based on existing drugs that assesses the chance for a molecule to become an oral drug with respect to bioavailability. Properties calculated include solubility, lipophilicity, and molecular mass (Lipinski et al., 2001). Violation of the guidelines decreases the druglikeness of a small molecule, although a singular violation does not greatly impact druglikeness. The druglike properties of C1 to C44 were predicted using SwissADME, a drug discovery software that computes predicted physicochemical descriptors including parameters for Lipinski's Rule of 5 (Table 3.3) (Daina et al., 2017). Solubility and lipophilicity are critical in drug discovery as drugs need to be soluble enough for absorption and lipophilic enough to pass through cellular membranes. Solubility is assessed as a log score, or log S, calculated with three different models and a scoring range between -10 to -6 (insoluble), -6 to -4 (moderately soluble), -4 to -2 (soluble), and $-2 < 0$ (highly soluble) (Sorkun et al., 2019). Lipophilicity is measured as the octanol-water partition coefficient, measuring the relationship between lipophilicity and hydrophilicity of a substance, known as the Log Po/w value. This value typically ranges between -3 (very hydrophilic) and 10 (extremely lipophilic) (Cumming & Rücker, 2017). Further parameters were also calculated by SwissADME but will not be included for clarity.

Based on earlier structural analysis, C1 to C44 tend to be nonpolar and are therefore less hydrophilic. Consistent with this observation, further analysis SwissADME indicated that C10 and its analogues were poorly to moderately soluble. In addition, many of these compounds had molecular weights over 500 kDa, thereby violating the Lipinski's rule of five guidelines. Taken

together, the SAR and SwissADME analysis described above have identified the critical and bioactive substructures and provide proof- of principle for future structure guided optimization to increase the druglikeness of future analogues.

Table 3.3: Physicochemical properties of C1 to C44.

Compound	Solubility (Log S)	Lipophilicity (Log P o/w)	Druglikeness (Lipinski Violations)
C1	-6.04	3.71	0
C2	-4.35	2.56	0
C3	-7.38	5.4	1
C4	-3.53	2.9	0
C5	-5.18	2.51	1
C6	-5.35	3.11	1
C7	-4.85	2.17	2
C8	-5.27	3.03	2
C9	-4.6	2.6	1
C10	-5.52	3.4	1
C11	-6.86	4.12	2
C12	-5.15	3.09	1
C13	-5.25	3.22	1
C14	-4.88	2.91	1
C15	-5.52	3.41	1
C16	-5.25	3.22	1
C17	-4.6	2.87	1
C18	-5.32	3.2	1
C19	-3.84	2.48	0
C20	-3.74	2.29	0
C21	-6.19	4.41	2
C22	-5.73	3.42	1

Compound	Solubility (Log S)	Lipophilicity (Log P o/w)	Druglikeness (Lipinski violations)
C23	-4.32	1.75	0
C24	-6.21	3.76	1
C25	-1.62	1.81	0
C26	-5.43	3.56	1
C27	-5.83	3.42	1
C28	-6.14	4.01	1
C29	-5.52	3.41	1
C30	-5.61	3.71	1
C31	-3.89	2.19	1
C32	-5.33	3.41	1
C33	-5.98	3.94	1
C34	-4.53	2.68	1
C35	-4.9	3.04	1
C36	-5.36	3.61	1
C37	-5.53	3.57	1
C38	-5.52	3.43	1
C39	-4.59	2.81	1
C40	-2.97	1.83	0
C41	-5.82	3.66	1
C42	-5.53	3.61	1
C43	-3.77	1.89	1
C44	-6.03	3.83	1

3.4: Structural Analysis of New Analogues of C10

Analysis of C1 to C44 revealed areas of improvement that were carried forward into further analogue synthesis and design. These new compounds, developed in-house, are aimed to improve solubility and potency and designated as C45 to C62. To determine whether these new compounds are more potent than C10, they will be compared against C10 in terms of structural similarity, biochemical and biological properties.

Similar to previous chemometric analyses performed on C1 to C44, a structural similarity analysis was applied on these new analogues (C45 to C62). As demonstrated in Figure 3.5, C45 to C62 are structurally unique from the ChEMBL compounds. Interestingly, these new compounds form two distinct clusters. C45 to C49 are connected to C10, indicating a similar structural backbone, and C50 to C62 form a cluster unique from C10 or C21, suggesting another unique structural backbone in this group of analogues.

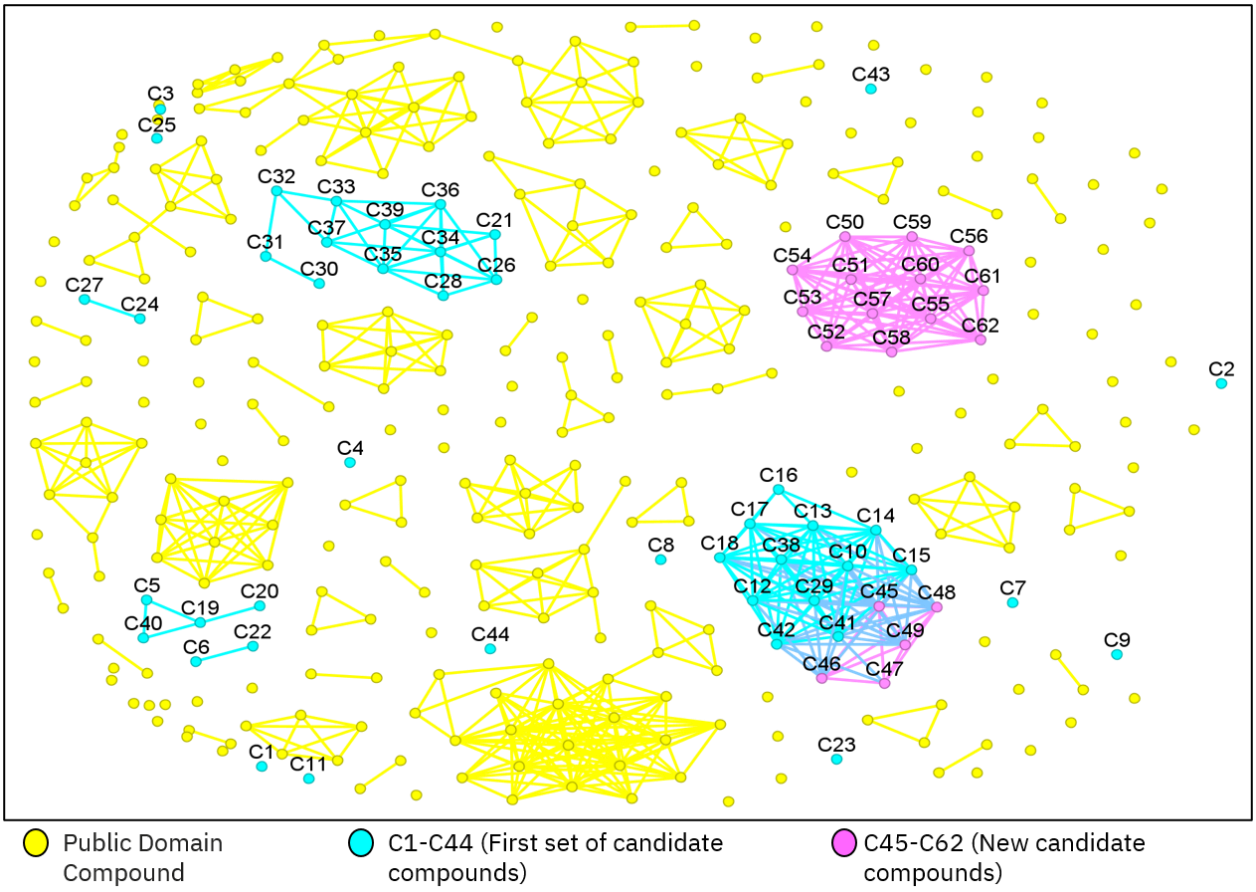

Figure 3.5: The structural similarity analysis for C1 to C62 compared to the ChEMBL compounds. The ChEMBL compounds are indicated in yellow, initial candidate compounds C1 to C44 are indicated in cyan, and new candidate compounds C45-C62 are indicated in magenta. C1 to C44 do not overlap with any of the existing compounds and are therefore structurally distinct and worth investigation. C45 to C62, the new compounds, are circled. C45-C49 share the same scaffold as C10 and are added into the original cluster, while C50-C62 form a new cluster within the space.

To characterize the new compounds, a predicted measure of binding affinity with β-catenin was generated, represented as docking scores. The new compounds were docked within the crystal structure of β-catenin (PDB: 2Z6H) using the molecular docking software AutoDock Vina following established protocols for C1 to C44 (Eberhardt et al., 2021). Given these values are derived from virtual prediction, direct comparisons with activity measured in cell-based assays cannot be made. However, it is possible to identify substructural changes that impact

potential binding within this group of new C10 analogs. To achieve a comparison of predicted binding affinity, the docking scores (kcal/mol) were converted to approximate K_d values using the Gibbs free energy equation ($\Delta G° = -RT\ln(K_d)$) and converted to pK_d values (i.e. $-\log K_d$) to maintain consistency in scaling (Table 3.4) (Du et al., 2016). A higher pK_d value indicates stronger predicted binding affinity, potentially identifying compounds with a higher actual bioactivity.

Table 3.4. Docking scores and K_d values of C45-C62 in comparison with C10

Compound	Docking Score (kcal/mol)	Computed K_d (μM)	pK_d
C10	-9.5	0.109	6.96
C45	-8.8	0.354	6.45
C46	-8.9	0.299	6.52
C47	-8.7	0.42	6.38
C48	-8.9	0.299	6.52
C49	-9.6	0.092	7.04
C50	-7.8	1.917	5.72
C51	-8.2	0.976	6.01
C52	-8	1.368	5.86
C53	-8.5	0.588	6.23
C54	-8.7	0.42	6.38
C55	-8.5	0.588	6.23
C67	-8.2	0.976	6.01
C57	-8.4	0.696	6.16
C58	-8.6	0.497	6.30
C59	-8.2	0.976	6.01
C60	-8.4	0.696	6.16
C61	-8.7	0.42	6.38
C62	-8.9	0.299	6.52

Next, similar to the SAR analysis on C1 to C44, a structural similarity plot was generated in DataWarrior for C45 to C62 using their pK_d values (Fig. 3.6). Similar to Figure 3.5 and as shown in Figure 3.6, three distinct clusters were observed: two clusters represented by compound C10 and C21 respectively, and a third new cluster consisting of compounds C50-C62 with a

unique structural backbone. C45-C49, being structurally similar to C10, also have relatively similar theoretical binding affinities with C10, suggesting potentially similar bioactivity. Within the new cluster consisting of C50-C62, the predicted binding affinities trend lower, suggesting potentially lower bioactivity than C10.

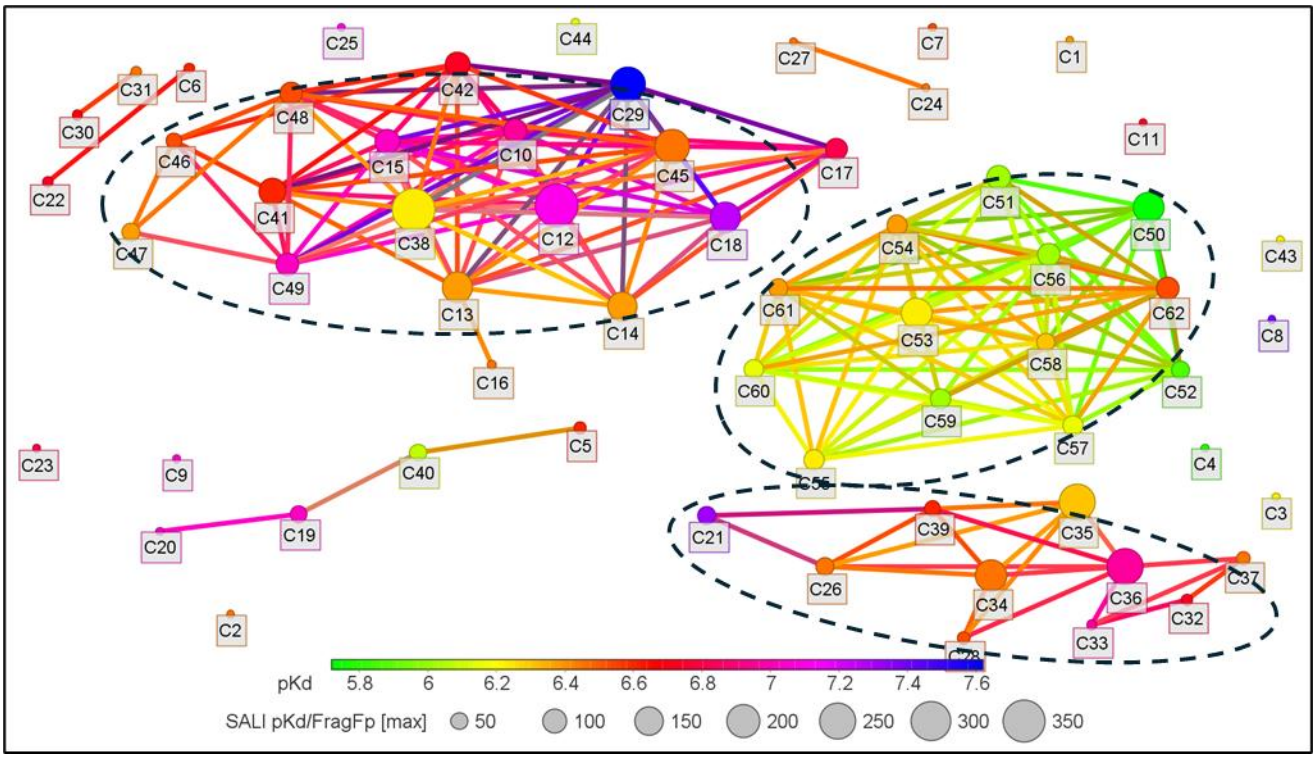

Figure 3.6: The structural similarity analysis for C1 to C62. A predicted measure of bioactivity to compare the SARs of C1 to C44 in comparison to C45 to C62 was generated using the conversion between docking scores and K_d using the Gibbs free energy equation and subsequent conversion to pK_d values, where a lower score indicates a lower predicted affinity. The colour of the markers represents the pK_d of each compound, and the sizes reflect the SALI value for each pair of compounds. Compounds with identical structural skeletons are connected by lines and clustered together, and dissimilar structures are scattered throughout the visualized chemical space.

Following the structural analysis of this group of compounds, the physicochemical properties of C45-C62 including solubility, lipophilicity, and druglikeness was analyzed using SwissADME (Table 3.5). There are no major improvements in solubility; rather, for C54-C62,

they are less soluble and more lipophilic than C10. In terms of druglikeness, all new compounds break one or two Lipinski rules, namely with sizes over 500 kDa; the exceptions are C50-C53, which do not break any rules. Presently, further optimization of the structure is needed to increase the solubility for this family of compounds.

Table 3.5. Physicochemical properties of C10 in comparison with C45 to C62

Compound	Solubility (Log S)	Lipophilicity (Log P o/w)	Druglikeness (Lipinski) Violations
C10	-5.52	3.40	1
C45	-5.25	3.44	1
C46	-5.83	3.82	1
C47	-5.56	3.81	1
C48	-5.25	3.63	1
C49	-5.54	3.68	1
C50	-5.44	3.37	0
C51	-5.09	3.24	0
C52	-5.85	3.70	0
C53	-5.82	3.72	0
C54	-7.23	4.85	1
C55	-7.24	4.97	2
C56	-6.14	4.55	1
C57	-7.24	5.03	2
C58	-6.65	4.61	1
C59	-6.25	4.89	2
C60	-6.69	4.67	1
C61	-6.04	4.34	1
C62	-6.85	5.03	1

3.5: Preparation of Protein for BLI

To examine how the new analogs C45-C62 of C10 interact with the β-catenin protein, the binding affinities were measured using biolayer interferometry (BLI). This method analyzes biomolecular interactions using the difference in optical interference in reflected white light when sensor-bound protein binds a ligand in solution (N. B. Shah & Duncan, 2014). These changes can be quantified to determine kinetic rates of binding and dissociation, providing *in vitro* binding affinity values of C45-C62 with β-catenin (Fig. 3.7).

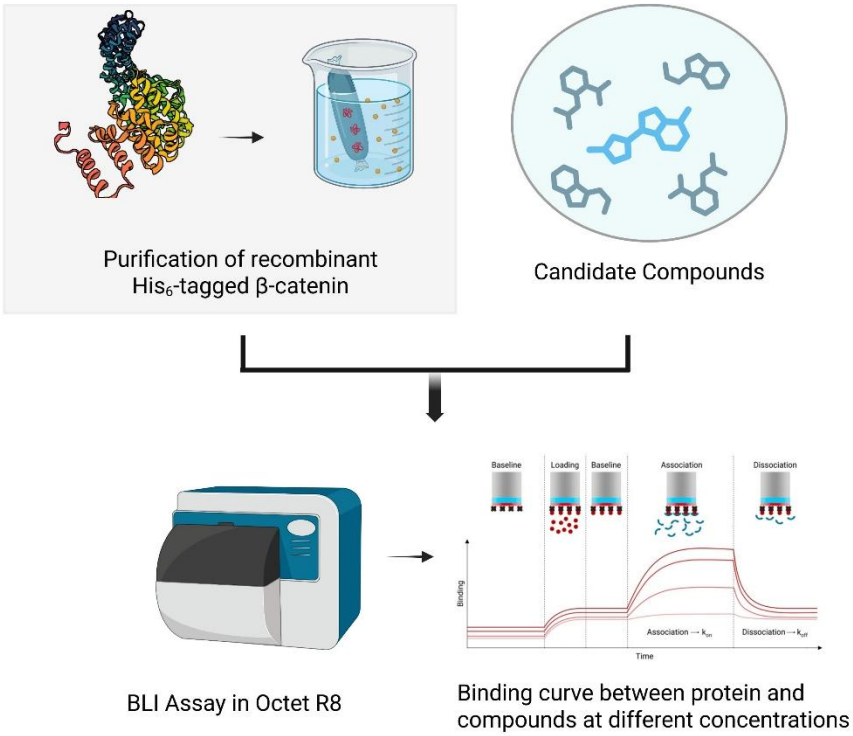

Figure 3.7: Graphical abstract of BLI workflow. Recombinant full-length His_6-tagged β-catenin was purified and candidate compound diluted to appropriate concentrations before preparation of the BLI assay on the Octet R4 system.

The interaction between C45 to C62 and β-catenin was first examined with full-length β-catenin protein, which was prepared in two steps. First, the protein was expressed from BL21+

E. coli transformed with the pET28a M57 plasmid encoding for full-length β-catenin. As the candidate binding site is closer to the C-terminus of β-catenin, an N-terminus His_6-tag was used to allow for nickel affinity purification. A representative β-catenin purification is shown in Figure 8A. The full-length β-catenin, with a predicted molecular weight of 92 kDa, was purified with a general purity of about 80% with a size close to 100 kDa (Figure 3.8A).

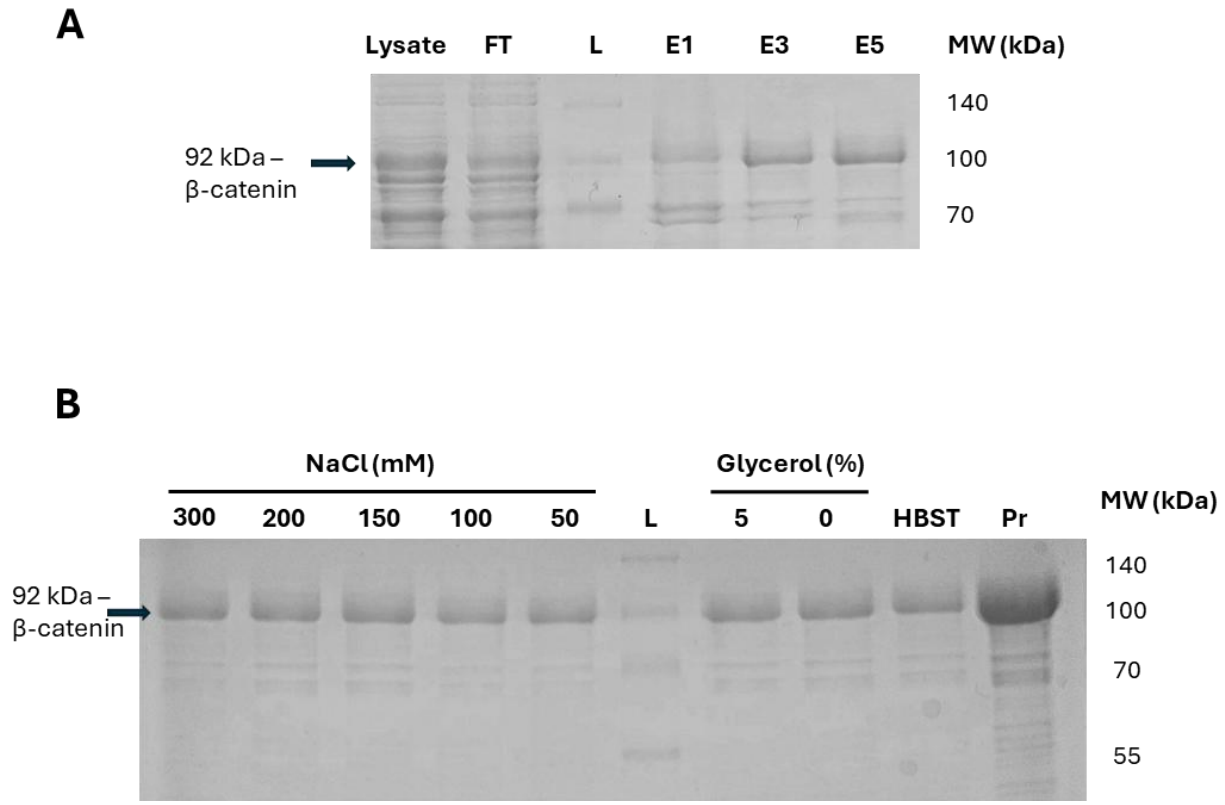

Figure 3.8: Purification and optimization of protein purification for BLI. A. Representative SDS-PAGE gel of protein purification. His-tagged β-catenin was purified from BL21+ E. coli transformed with the pET28a vector containing the full-length β-catenin insert. FT: flowthrough, L: ladder, E = elution. **B.** Due to high protein loss in original HBST buffer, the buffer was changed to a Tris-based buffer to retain the original elution buffer characteristics and optimized by testing various sodium chloride and glycerol concentrations and visualized on an SDS-PAGE gel. L: ladder, HBST: original buffer, Pr = original eluted protein.

The purified protein was next subject to a buffer exchange before BLI analysis. Initially, the purified protein was dialyzed against a HEPES-based buffer, HBST, based on the

manufacturer's guidelines. However, it was found that the protein precipitated heavily in HBST. Therefore, buffer optimization was conducted on the conditions of buffer base, salt and glycerol concentrations to enhance protein stability and compatibility with BLI use. Out of the conditions tested, it was found that the most stable buffer consisted of a Tris-based buffer of 150 mM NaCl and 10% glycerol (Fig. 3.8B). This condition was then used to test all new compounds as it was compatible with BLI, and produced the most robust and reproducible binding results.

3.6: Assessment of Protein-Compound Interactions using BLI

To access β-catenin-compound interactions using BLI, generally two main steps are involved: immobilization of β-catenin on a probe, and the protein-compound binding measurement.

Initial BLI immobilization involved the usage of His_6-tag binding antibody-coated probes (Anti-Penta-HIS) to capture the His_6-tag of the purified β-catenin protein. However, due to the hydrophobicity of the compounds, non-specific binding was observed in the background where they directly bound the antibody-coated probes instead of the protein. To avoid this issue, His_6-tagged β-catenin was immobilized on nickel-coated probes. Figure 3.9 shows a direct comparison between the Anti-Penta-HIS probe and the Ni-NTA probe for C10. With the Anti-Penta-HIS probes, a K_d value of 3.2 μM was observed; with the Ni-NTA probes, a K_d value of 9.8 μM was observed.

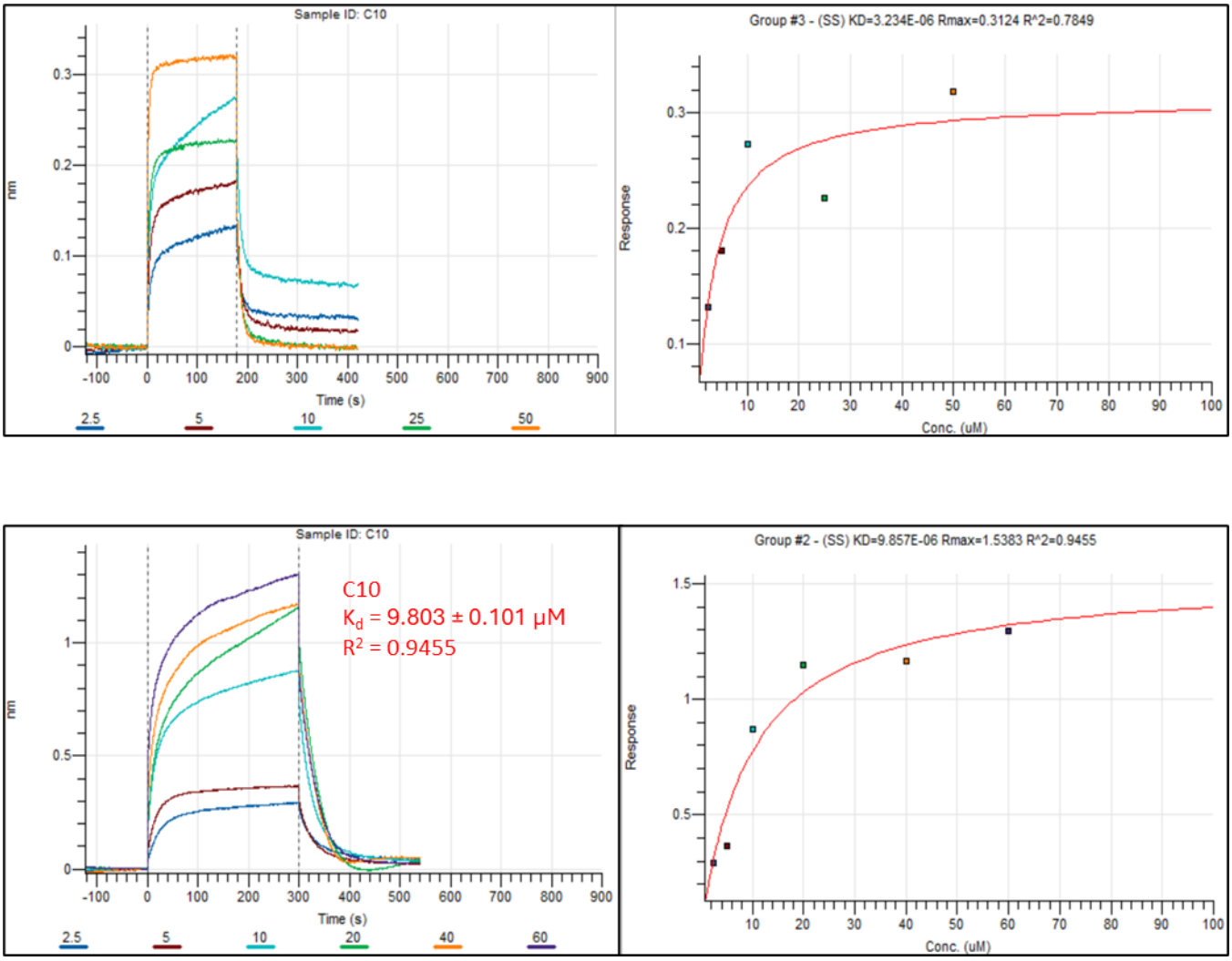

Figure 3.9: Comparison between Anti-Penta-HIS and Ni-NTA probes for BLI assays assessing binding interaction between β-catenin and C10. Nonspecific binding is observed for the Anti-Penta-HIS probes (top) compared to the Ni-NTA probes (bottom) as binding does not reach saturation.

Analysis of binding affinity between β-catenin and C45-C62 was conducted using Ni-NTA probes. The probes are dipped into solutions containing increasing concentrations of compound, ranging from 2.5 µM to 60 µM. The association and dissociation of ligand is measured at each concentration, and binding affinity is calculated as the equilibrium dissociation constant K_d, where a smaller K_d value correlates with a greater binding affinity of the ligand to

its target. C10 was used as a comparison reference against C45 to C62, and DMSO (vehicle control) was used as a normalized baseline.

The binding curves of C45 to C62 to the full-length β-catenin are shown in Supplementary Figure 1. The K_d values for C45 to C62 are summarized in Table 6 with a graphical visualization in Figure 3.10A. A new structural similarity plot was generated using the pK_d values to compare with Figure 2.6 to assess predicted and actual binding affinities (Fig. 3.10B).

Table 3.6. BLI values of C45-C62 in comparison with C10.

Compound	K_d (μM)
C10	9.8 ± 0.1
C45	6.8 ± 0.1
C46	4.9 ± 0.1
C47	14.4 ± 0.9
C48	9.4 ± 2.8
C49	4.9 ± 0.1
C50	44.0 ± 0.8
C51	21.1 ± 0.3
C52	22.3 ± 0.3
C53	23.7 ± 0.4
C54	51.7 ± 0.6
C55	7.8 ± 0.1
C56	58.6 ± 0.7
C57	6.1 ± 0.1
C58	11.0 ± 0.2
C59	5.5 ± 0.1
C60	53.5 ± 0.8
C61	52.2 ± 1.0
C62	49.6 ± 0.9

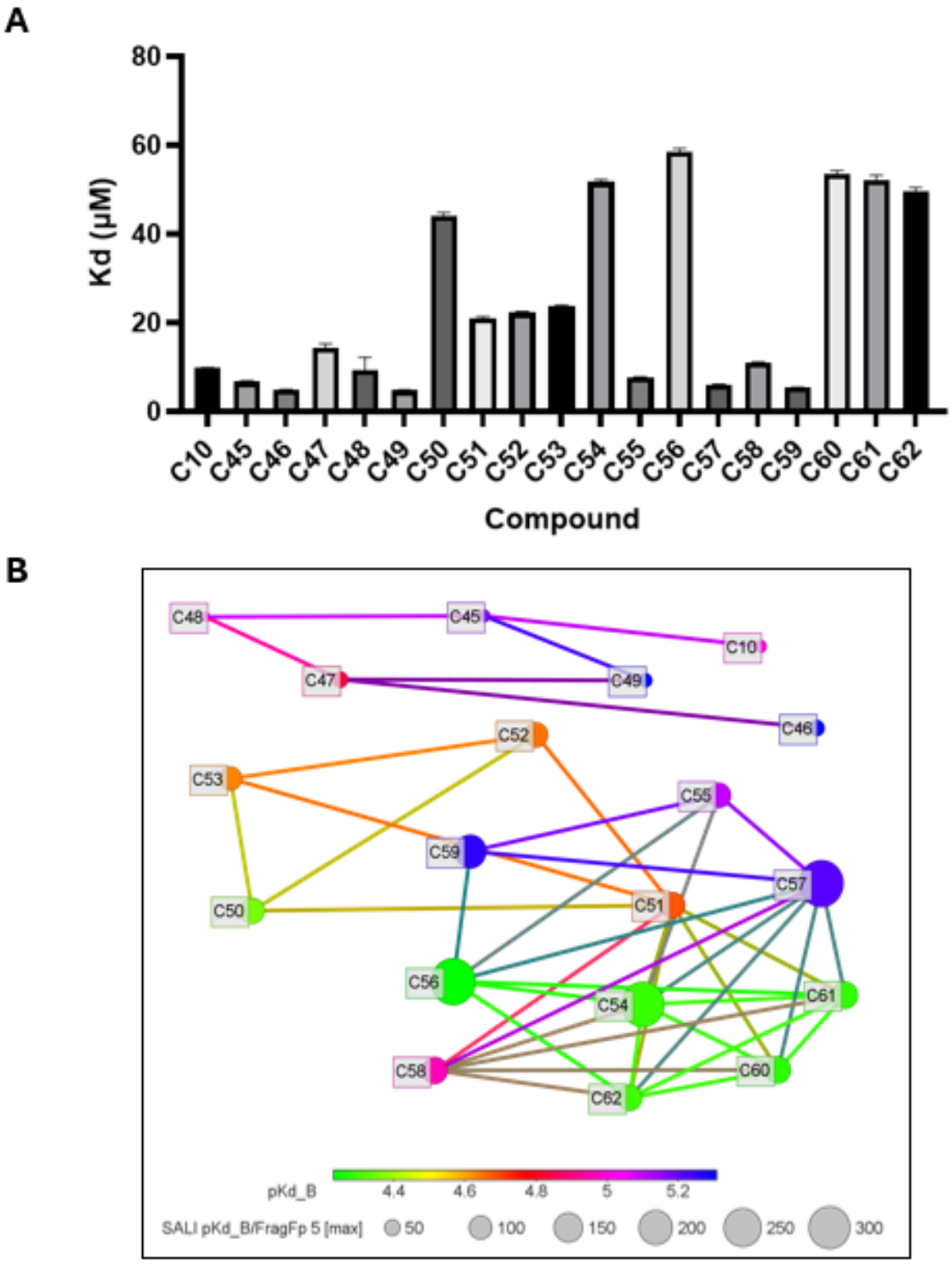

Figure 3.10: Representations of K_d values from BLI assays. A: Graphical representation of K_d values. B: Structural similarity plot for C10, C45-C62 with pK_d as activity. The colours represent the pK_d where the lower the pK_d, the stronger the binding affinity to β-catenin. Marker sizes represent the SALI score between two compounds.

From the BLI analysis, the K_d values for C45-C49 range from 4.9 μM to 14 μM, which are relatively similar to C10, which has a K_d of 9.8 μM. Interestingly, the earlier structural similarity analysis plot showed that C45-C49 are in the same cluster as C10 with similar predicted binding affinities. With the exception of C47, the rest of the compounds exhibit a slightly higher affinity for β-catenin than C10. The cluster of C10 and C45-C49 in Figure 3.10B also show low SALI scores as seen by the small markers, indicating that the structural differences in this set of compounds are minor and have little difference in binding activity. This observation is reflected in the earlier predicted binding affinity for this subset of compounds, as well as the structural analysis of C10 in comparison to C45-C49 (Table 3.7).

Table 3.7: Structural analysis and K_d comparisons for C45-C49 in comparison with C10

Compound	R1	R2	R3	K_d (μM)
10	H	H	H	9.8
45	methyl	H	H	6.8
46	H	methyl	methyl	4.9
47	methyl	methyl	methyl	14.4
48	methyl	H	methyl	9.4
49	methyl	methyl	H	4.9

A greater variance in K_d values is observed in C50-C62 which form a separate cluster in Figure 2.6 and Figure 2.10B, with K_d values ranging from 5.5 μM to 58 μM. With the exception of C55, C57, and C59, all compounds in this group exhibit lower affinity for β-catenin than C10 with high K_d values. Analysis of the new cluster of C50-C62 reveal a variety of SALI scores, indicating that the structural differences in this set of compounds greatly impact binding affinity. In addition, the predicted K_d values are lower than the actual values on the plots, indicating stronger affinities for β-catenin than was calculated (Table 3.8). This cluster of compounds vary only by the singular variable R1 group which corresponds to the same R1 group previously

mentioned in the C21 cluster, which was noted to prefer a nonpolar aromatic group. This preference is noted with C50-C53, which exhibit low binding affinity with polar pyridine-based groups at R1. C55, C57 and C59 exhibit a slightly stronger affinity for β-catenin than C10 with K_d values lower than 9.8 μM. The reason for notable differences between binding affinities in the rest of the compounds is currently unknown, although the specific placements of the halogens may have an effect. The *in vitro* results will be noted later in this thesis.

Table 3.8: Structural analysis and K_d comparisons for C50-C62

Compound	R1	Actual K_d (μM)
50	2-pyridinyl	44.0
51	3-pyridinyl	21.1
52	6-methylpyridin-2-yl	22.3
53	4-methylpyridin-2-yl	23.7
54	naphthalenyl	51.7
55	3, 4-dichlorophenyl	7.8
56	3, 5-difluorophenyl	58.6
57	3, 5-dichlorophenyl	6.1
58	2-bromophenyl	11.1
59	3, 4, 5-trifluorophenyl	5.5
60	2, 4-dimethylphenyl	53.5
61	2-fluorophenyl	52.2
62	2-(trifluoromethyl)phenyl	49.6

3.7: Assessment of Truncated Protein Interactions with Select Compounds

As a lower K_d value corresponds with higher affinity for a target protein, i.e. β-catenin, the compounds that had lower K_d values than C10 were selected for further BLI analysis. This was conducted using a truncated form of β-catenin consisting of only the armadillo repeat domain (aa 141-664) (Fig. 3.11A) to validate the binding of the small compounds to the target site on the protein. This recombinant His_6-tagged truncated β-catenin was purified similarly to

the full-length protein and visualized (Fig. 3.11B) before being dialyzed for use in BLI analysis. The K_d values are shown in Table 3.9.

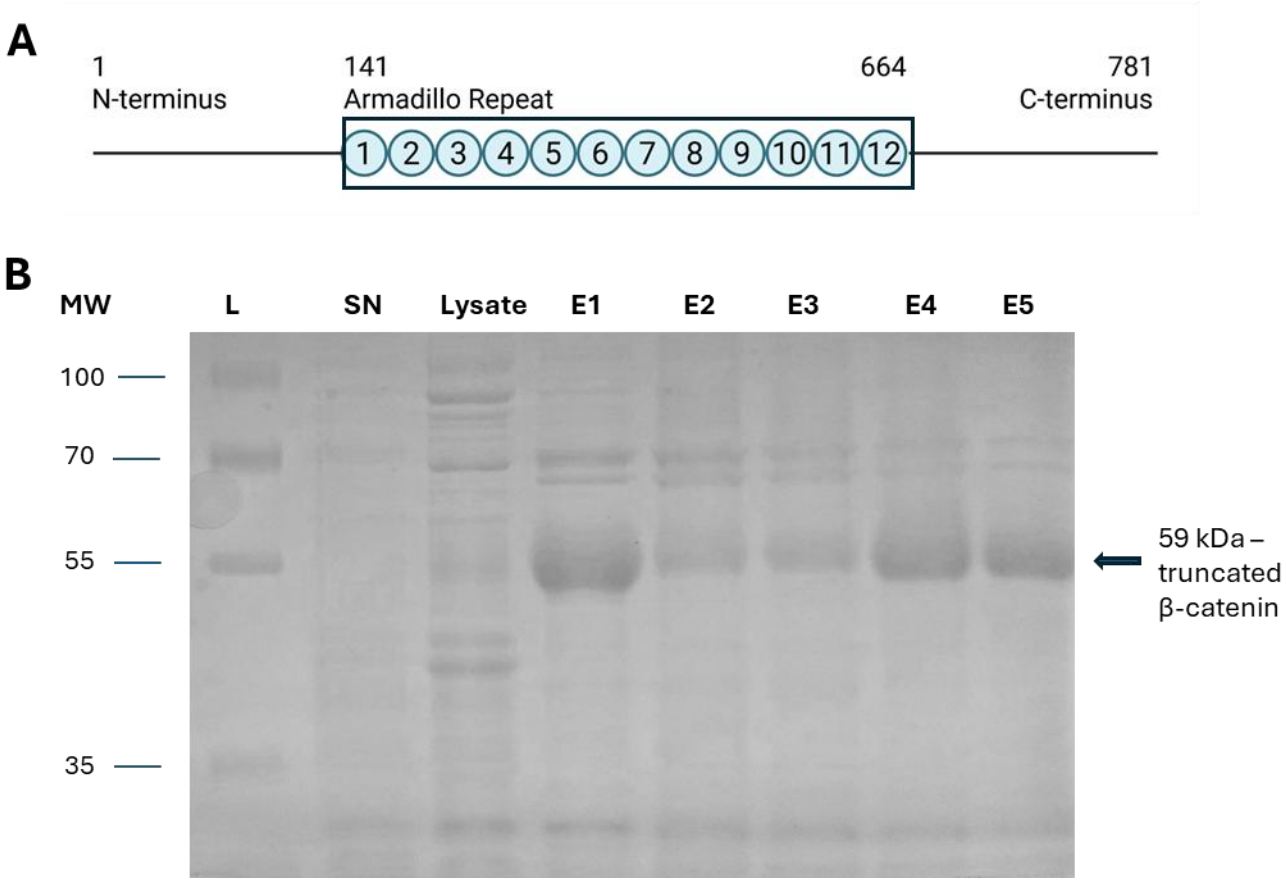

Figure 3.11: Structure of β-catenin structure and truncated protein purification. A: Summary of β-catenin structure. The purified truncated protein contains only the armadillo repeat domain. **B: SDS-PAGE gel of truncated protein purification.** L= ladder, SN = supernatant, E = Elution.

Table 3.9. Comparison between full length and truncated protein K_d for select compounds.

Compound	Full-Length Protein K_d (μM)	Truncated Protein K_d (μM)
C10	9.8 ± 0.1	7.4 ± 0.1
C45	6.8 ± 0.1	11.2 ± 0.1
C46	4.9 ± 0.1	5.1 ± 0.1
C48	9.4 ± 2.8	8.0 ± 0.2
C49	4.9 ± 0.1	3.9 ± 0.1
C55	7.8 ± 0.1	11.2 ± 0.1
C57	6.1 ± 0.1	29.7 ± 0.3
C59	5.5 ± 0.1	10.0 ± 0.1

As the differences between the K_d values of full length and truncated β-catenin are relatively small, a notable increase or decrease in affinity to the armadillo repeat domain cannot be determined. A notable difference in affinity is seen in C57, with a decrease in affinity with the truncated protein to 29 μM as opposed to its affinity of 6 μM with the full-length protein. These results confirm that the above compounds bind to the armadillo repeat domain of β-catenin; however, the exact binding location remains to be determined.

3.8: Determining Efficacy in Inhibiting Cancer Cell Growth

Following biochemical characterization of the new compounds C45-C62, the cytotoxic effects of these compounds were examined on cancer cells (Fig. 3.12). The TOV112D ovarian cancer cell line was used for the cell-based assays as it expresses hyperactive β-catenin due to harbouring a mutation in *CTNNB1* at the GSK3β phosphorylation site.

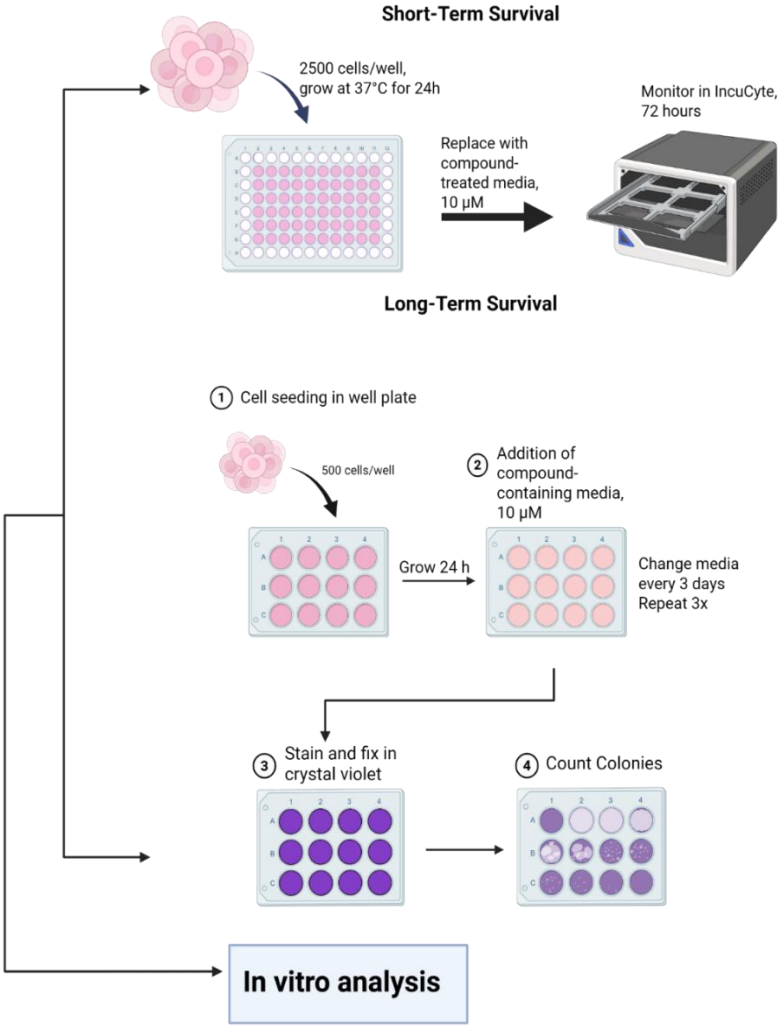

Figure 3.12: Graphical abstract for cell-based assays. Proliferation and clonogenic assays were carried out using TOV112D cells as they express hyperactive β-catenin. Cells were treated with 10 µM of C45-C62 with C10 as a positive control and DMSO as a vehicle.

3.9: Effect of New Compounds on Cancer Cell Proliferation

Uncontrolled proliferation is a hallmark of cancer cells, as they lack the signals to terminate cell division (Hanahan & Weinberg, 2011). To assess the effects of C45 to C62 on short-term cancer cell proliferation, a previously established protocol was followed where cells were treated with 10 μM of compound, and cell confluency was monitored in the IncuCyte for 3 days. As C10 was previously established as the top-performing compound, it was used as the positive control. DMSO was used as the vehicle as all compounds are dissolved in DMSO. Among the compounds tested, C46, C48, C54 and C59 exhibited a greater inhibitory effect on cell proliferation, with lower cell confluency after 3 days compared to C10. C47, C53 and C55 exhibited similar growth inhibition to C10 (Fig. 3.13).

A

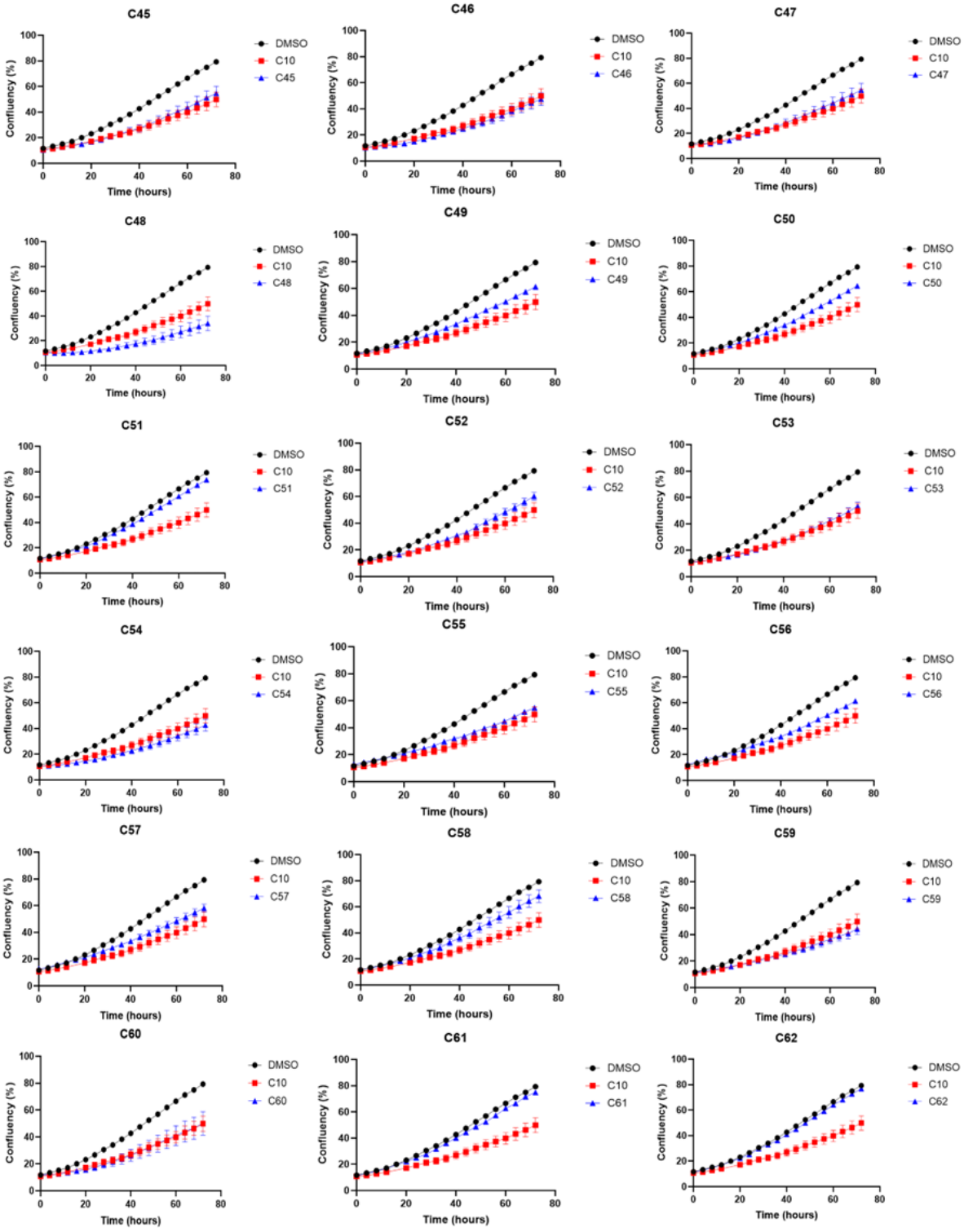
C45
C46
C47
C48
C49
C50
C51
C52
C53
C54
C55
C56
C57
C58
C59
C60
C61
C62
DMSO
C10
Confluency (%)
Time (hours)

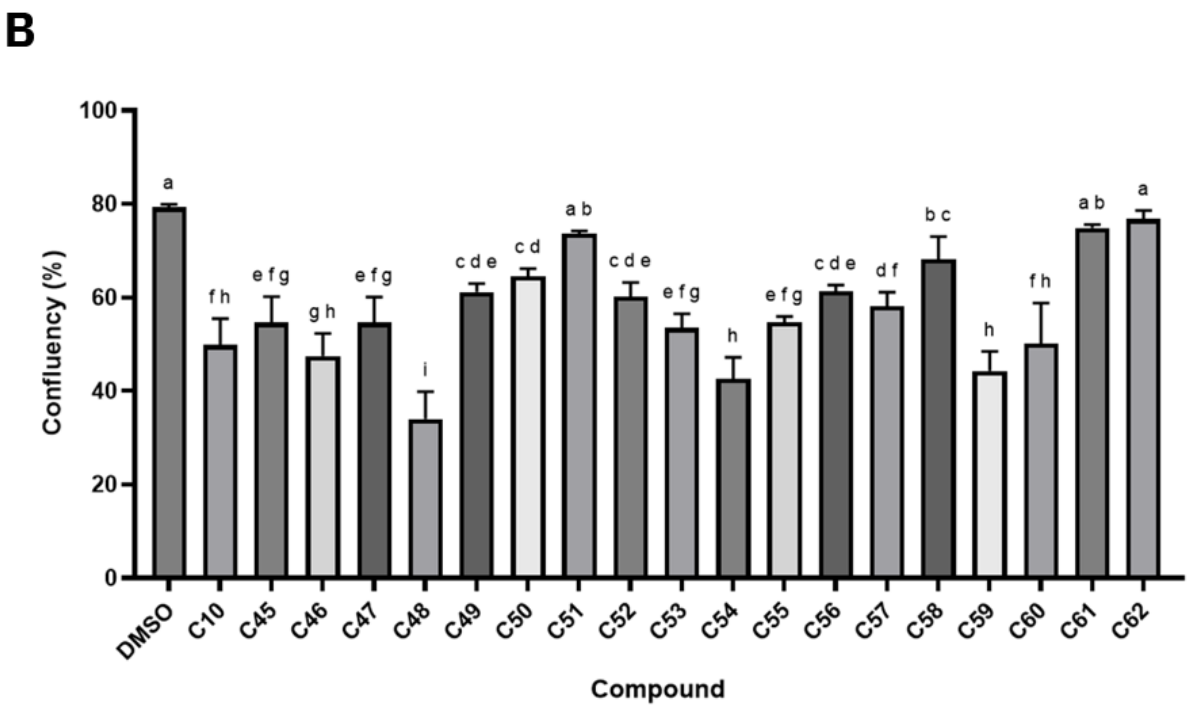

Figure 3.13: Effects of C45-C62 in comparison with C10 at 10 µM on TOV112D cells. A: Individual graphs for C45-C62 in comparison with C10. DMSO was used as the negative control. Data represents Mean ± SEM (n=10). **B: Summary of cell confluency for proliferation assays after 72 hours of treatment.** Data represents Mean ± SEM (n=10, $p<0.05$). Statistical analyses were performed using one-way ANOVA and Tukey's multiple comparison test. Different letters above bars denote statistical significance against every other compound. This experiment was conducted three times.

Part 3.10: Effect of New Compounds on Colony Growth

Another feature of cancer cells is their clonogenic ability, or their capacity to proliferate and form a colony. Clonogenic assays were carried out on C45-C62 to assess cell growth inhibition over time (1-2 weeks). C10 was used as a positive control at 10 µM, as it has been previously documented in the lab that 100% of TOV112D growth is inhibited at this concentration. Similar to the proliferation assay, DMSO was used as the vehicle as all compounds are dissolved in DMSO. Following previously established protocols for the clonogenic assay, cells were seeded at a density of 500 cells/well and refreshed with media

containing 10 μM of compound three times before undergoing staining on the 8th day. The summary of the manual count of the stained colonies is presented in Figure 3.14A. Compared to C10, C55, C56 and C59 exhibited similar inhibition of colony growth of TOV112D cells, with very few colonies counted on the final day. The rest of the compounds do not possess strong inhibitory activity, instead exhibiting increased colony growth (Fig. 3.14B).

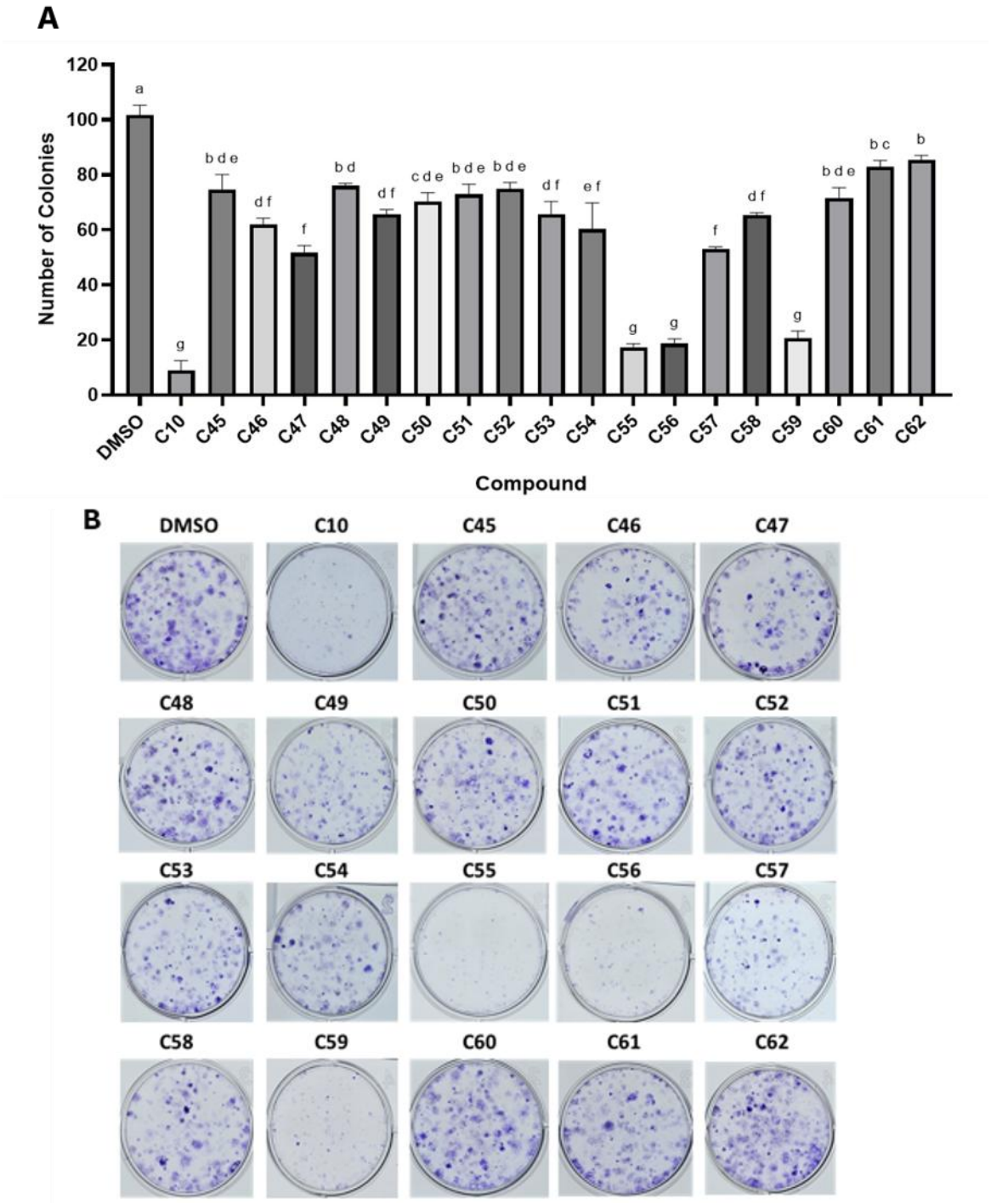

Figure 3.14: Summary of clonogenic assays. A: Summary of colony count after staining with crystal violet. Colonies were manually counted. Data represents Mean ± SEM (n=3, $p<0.05$) Statistical analyses were performed using one-way ANOVA and Tukey's multiple comparison test. Different letters above bars denote statistical significance against every other compound. **14B: Representative images of colony formation of TOV112D cells after being treated for 8 days.** This experiment was conducted three times.

Although C54 exhibited inhibition of TOV112D proliferation short-term, its effects long-term are less effective. The opposite is observed with C48 and C56, which exhibited lower inhibitory activity short-term in the proliferation assay but exhibited higher activity long-term. Altogether, across both biochemical and cell-based assays, C55 and C59 are consistently exhibiting high bioactivity. In the BLI assays, they were seen to exhibit a slightly stronger affinity for β-catenin than C10. In addition, in the proliferation and clonogenic assays, C55 and C59 both performed on par with C10. C54 also performs similarly to C10 in the cell-based assays, although it exhibits a weaker binding affinity with β-catenin. Titration assays using varying concentration of the compounds were carried out using C54, C55 and C59 to determine their IC_{50} values. It was found that C54 had the lowest IC_{50} value of 4.9 μM, C55 and C59 have IC_{50} values of 8.2 and 6.1 μM respectively, indicating high bioactivity (Fig. 3.15).

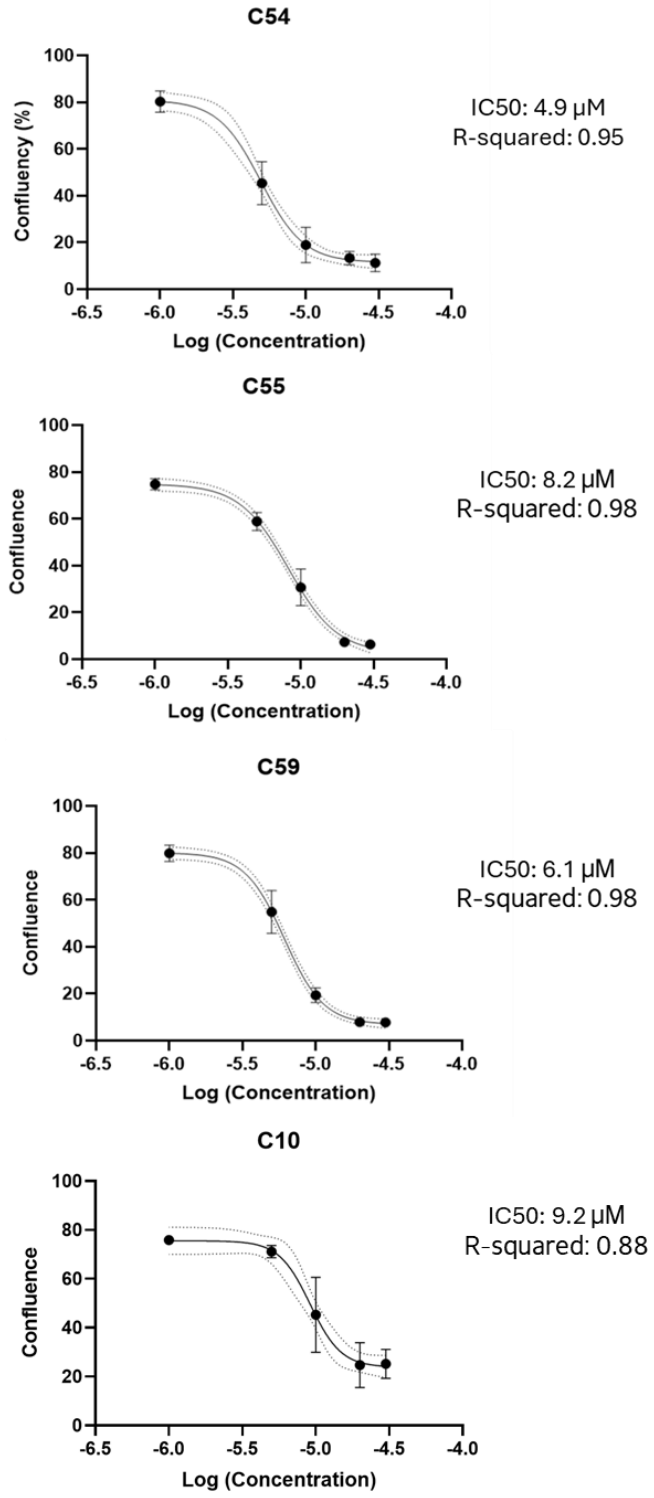

Figure 3.15: Sigmoidal interpretation of IC50 calculations for C10, C54, C55 and C59.
Image generated using GraphPad Prism. Data represents Mean ± SEM (n=10, $p<0.05$)

Chapter 4: Discussion

4.1: General Summary

The aberrant activation of the Wnt signalling pathway plays a critical role in carcinogenesis, especially in ovarian cancer. Mutations along this pathway lead to the hyperactivation of β-catenin and its interaction with TCF4, resulting in overexpression of oncogenes that result in cancer development and progression. Although a number of small molecules have been developed to inhibit the interaction between β-catenin and TCF4, many of them fail at preclinical stages, and none have been approved as targeted therapies for EOC or any other cancer type. Previous studies in this lab resulted in the characterization of C10, a novel small molecule found to inhibit β-catenin activity. Further studies of C10 resulted in the analysis and characterization of its analogues C12-C44, leading to the further development of novel analogues C45-C62. The goals for my study were to characterize the structure-activity relationships of C45-C62 in comparison to C10, determine the interaction between C45-C62 to β-catenin, and determine the tumorigenic effects of C45-C62 *in vitro* on cancer cells.

4.2: Substructure Differences in C10 and its Analogues Identify Areas for Optimization

For the purposes of this study, DataWarrior was used to interpret structural similarity analyses between C1-C62 in comparison with public domain β-catenin/TCF4 inhibitors on the ChEMBL database. Similarity was calculated using the Tanimoto index, with the default coefficient cutoff of 0.96 was used for similarity analysis. Compounds with Tanimoto coefficients greater than the cutoff would be clustered together. Although C1-C62 were found to be structurally distinct from the ChEMBL compounds, an interesting observation was observed in how C21 was classified as structurally distinct from C10, forming its own structurally distinct cluster along with compounds C50-C62. This is likely due to the internal fragFP library in DataWarrior marking the different substructures between C10 and C21 in a way that the

Tanimoto coefficient was lower than 0.97. As such, the same principle would apply for the cluster of C50-C62.

Pharmacokinetic analysis of these compounds also indicates their low solubility, identifying future paths for potential optimization. The new analogues remain poorly soluble and are too large, decreasing their druggability as per the Lipinski Rule of 5. However, as SAR analysis focuses only on the ligand itself, there are still many limitations to this study. The method was mainly utilized to analyze the differences in substructures of C10 and its already-studied analogues and the effects on cell-based and biochemical activity to create a relationship between structure and activity. Although the findings on the new analogues corroborated the data of previous saturation-transfer difference NMR experiments and provided possible points for future optimization, the actual mechanism of action between the protein and ligand remains to be elucidated.

4.3: C45-C62 Bind Directly to β-Catenin

Although β-catenin has long been a target protein of interest, the development of small-molecule inhibitors targeting this protein has been hindered by the structure and nature of β-catenin. β-Catenin acts as a transcription factor, interacting and binding with multiple protein partners. Its surface is shallow and flat, lacking clear druggable pockets for small molecules to directly bind to. Indeed, many reported β-catenin inhibitors discovered through HTS did not actually bind directly to the armadillo repeat domain of β-catenin. Through the use of BLI, the direct interaction of C45-C62 to β-catenin has been confirmed at micromolar concentrations. Additionally, BLI analysis using the truncated version of β-catenin confirmed that select compounds interact directly with the armadillo repeat domain of β-catenin. However, as BLI only confirms the direct binding or absence of it, it is unknown where specifically on the protein

that the compounds bind to. Additionally, the mechanism of actions of C45-C62 remain to be elucidated, as it is currently unknown whether they specifically inhibit β-catenin/TCF4 activity.

4.4: C45-C62 Inhibit Cancer Cell Growth and Proliferation

Finally, the cytotoxic effects of C45 to C62 were determined through cell-based growth assays on TOV112D cells, an ovarian cancer cell line with hyperactive β-catenin. Across both proliferation and clonogenic assays to determine the effects of C45-C62 on cancer cell proliferation and colony-forming ability, C55 and C59 overall seem to perform nearly on par with C10, but do not notably outperform C10 by a noticeable magnitude. C54 also performs relatively on par with C10, but exhibits low binding affinity with β-catenin.

4.5: Summary of Key Findings

Across the biochemical and cell-based assays, several compounds performed on par with C10 in one or more assay, but performed poorly in other assays. Although C45 had a strong affinity for the β-catenin protein and performed on par with C10 in the proliferation assay, it failed to inhibit colony growth in the clonogenic assay. C46 to C49 perform similarly, although C48 had a stronger inhibitory activity than C10 in the proliferation assay. In the cases of C53, C54, and C56, which exhibited a weaker affinity for β-catenin compared to C10, C53 and C54 exhibited inhibitory activity on par with C10 in the proliferation assay but not in the clonogenic assay, and the reverse is true for C56. This suggests that these compounds may not bind directly to β-catenin, but may exert inhibitory effects elsewhere. C55 and C59 overall perform on par with C10 throughout all three assays. C57 has a strong affinity for β-catenin but performed poorly in the cell-based assays, suggesting that it may not possess *in vitro* inhibitory activity. The IC_{50}s were calculated for C54, C55, and C59 based on their overall performance, and the values suggest that they have overall similar bioactivity with C10.

Table 4.1: Collective summary of top-performing compounds across assays[2]

Compound	K_d (μM) (From BLI)	K_d (μM) (Truncated Protein)	Survival Fraction (from Clonogenic Assay at 10 μM	% Relative Inhibition (from Proliferation Assay) at 10 μM	IC50 (μM)
DMSO	N/A	N/A	1.00	0	N/A
C10	9.8	7.4	0.09	43	9.2
C45	6.8	11.2	0.73	34	N/A
C46	4.9	5.1	0.61	45	N/A
C48	9.4	8.0	0.75	64	N/A
C49	4.9	3.9	0.65	25	N/A
C54	51.7	N/A	0.59	52	4.9
C55	7.8	11.2	0.17	37	8.2
C56	58.6	N/A	0.18	27	N/A
C57	6.1	29.7	0.52	33	N/A
C59	5.4	10.0	0.20	52	6.1

4.6: Limitations and Future Directions

One major challenge of developing successful and specific inhibitors for β-catenin/TCF4 interaction is the absence of co-crystal structures of β-catenin bound to these small molecules, which hampers our understanding of their binding mechanisms. Previous research conducted in the lab has attempted to generate a cocrystal structure of β-catenin and C10, but the low solubility of C10 impeded the experiment. C10 and its analogues continue to remain poorly soluble, and their structures need to be further optimized to improve their pharmacokinetics. It is also unknown whether C45-C62 actually inhibit β-catenin/TCF4 activity *in vitro*. Preliminary TOPflash luciferase assays and co-immunoprecipitation assays conducted previously have confirmed that C10 suppresses transcriptional activity of β-catenin/TCF4 and their target genes,

[2] Survival fraction and % relative inhibition values are calculated according to the equations listed in Materials and Methods. DMSO is listed as a reference value.

but it is unknown whether C45-C62 will perform similarly. Similar assays would need to be performed on C45-C62 to determine if these compounds also suppress β-catenin/TCF4 transcriptional activity. Additionally, Western blot analyses can be carried on cells treated with differing concentrations of ligand to determine protein levels of β-catenin/TCF4 target genes, as this has also been previously conducted with C10. Furthermore, luciferase reporter assays can be used to determine whether C45-C62 suppress β-catenin/TCF4 transcriptional activity, which would help confirm the mechanism of action of the compounds. Additionally, as the specificity of C45-C62 in targeting β-catenin/TCF4 interaction are unknown, similar cell-based assays can be carried out on β-catenin independent cell lines to confirm their effects.

Concerns regarding the limitation of the BLI techniques for this study should also be addressed. Following data analysis using the BLI software, the steady state K_d (measured in μM) and theoretical maximum binding signal R_{max} (measured in nm or shift in light wavelength) are calculated based on the plotted values of R_{eq}, or the equilibrium response (also measured in nm or shift in light wavelength) across the aforementioned six concentrations ranging from 2.5 to 60 μM. The equation for R_{max} is based on the ratio of the molecular weights of the analyte (C45-C62) and ligand (β-catenin), multiplied by the ligand response (as observed by the machine) and the binding stoichiometry as defined by the number of binding sites on the ligand (Yang et al., 2016). Given the significant difference in molecular weights between β-catenin (92 kDa) and C45-C62 (~500 Da), the observed response curves may not reflect a true interaction between the protein and analyte as a theoretical R_{max} would be much smaller than the R_{max} observed by the assay. This may be in part due to mass analyte aggregation at the surface of the probe independent of binding to β-catenin, resulting in a binding curve that has a far larger R_{max} than what is theoretically possible (Giannetti et al., 2008) and result in discrepancies between

measured K_d values compared to compound activity in the cell-based assays. To address this concern, confirmation of binding of the compounds to β-catenin can be determined through mutational analysis studies, where the critical amino acids that β-catenin hotspot for TCF4 binding are mutated to alanine to be tested with the compounds to observe changes in binding affinity. Additionally, a competitive BLI assay can be designed using both β-catenin and TCF4 to assess protein-protein binding and changes upon addition of the compounds.

In this study, the newly synthesized C10 analogues, C45-C62, have been analyzed at a preliminary level. They are novel inhibitors synthesized in-house, and are structurally unique from molecules existing in public domain. Although they do not outperform the lead molecule C10, we have found that our novel inhibitors retain their cytotoxic effects even with changes in their substructures when compared to the original template molecule, C10. Additionally, they also exhibit direct binding to the β-catenin protein, and are therefore a promising step in the development of a β-catenin/TCF4 inhibitor. Additionally, it has been found that C55 and C59, two of the new analogues, perform on par with C10, and should undergo further analysis to elucidate their mechanism of action. As they are C10 analogues, understanding the structure-activity relationship of these molecules will enhance understanding of the overall scaffold of C10, and aid in future optimization efforts to increase solubility and potency of the novel β-catenin/TCF4 inhibitor.

Supplementary Data

Table S1: Characterization of C1 to C44 as provided by Yumin Qiu.

Compound	Inhibition Rate at 10 μM in TOV112D Cells	Compound	Inhibition Rate at 10 μM in TOV112D Cells
C1	0%	C23	5%
C2	90%	C24	100%
C3	0%	C25	0%
C4	0%	C26	85%
C5	0%	C27	95%
C6	5%	C28	100%
C7	64%	C29	100%
C8	68%	C30	80%
C9	4%	C31	25%
C10	100%	C32	60%
C11	32%	C33	90%
C12	84%	C34	20%
C13	85%	C35	5%
C14	57%	C36	80%
C15	91%	C37	80%
C16	87%	C38	100%
C17	66%	C39	54%
C18	87%	C40	15%
C19	10%	C41	96%
C20	10%	C42	48%
C21	100%	C43	28%
C22	87%	C44	64%

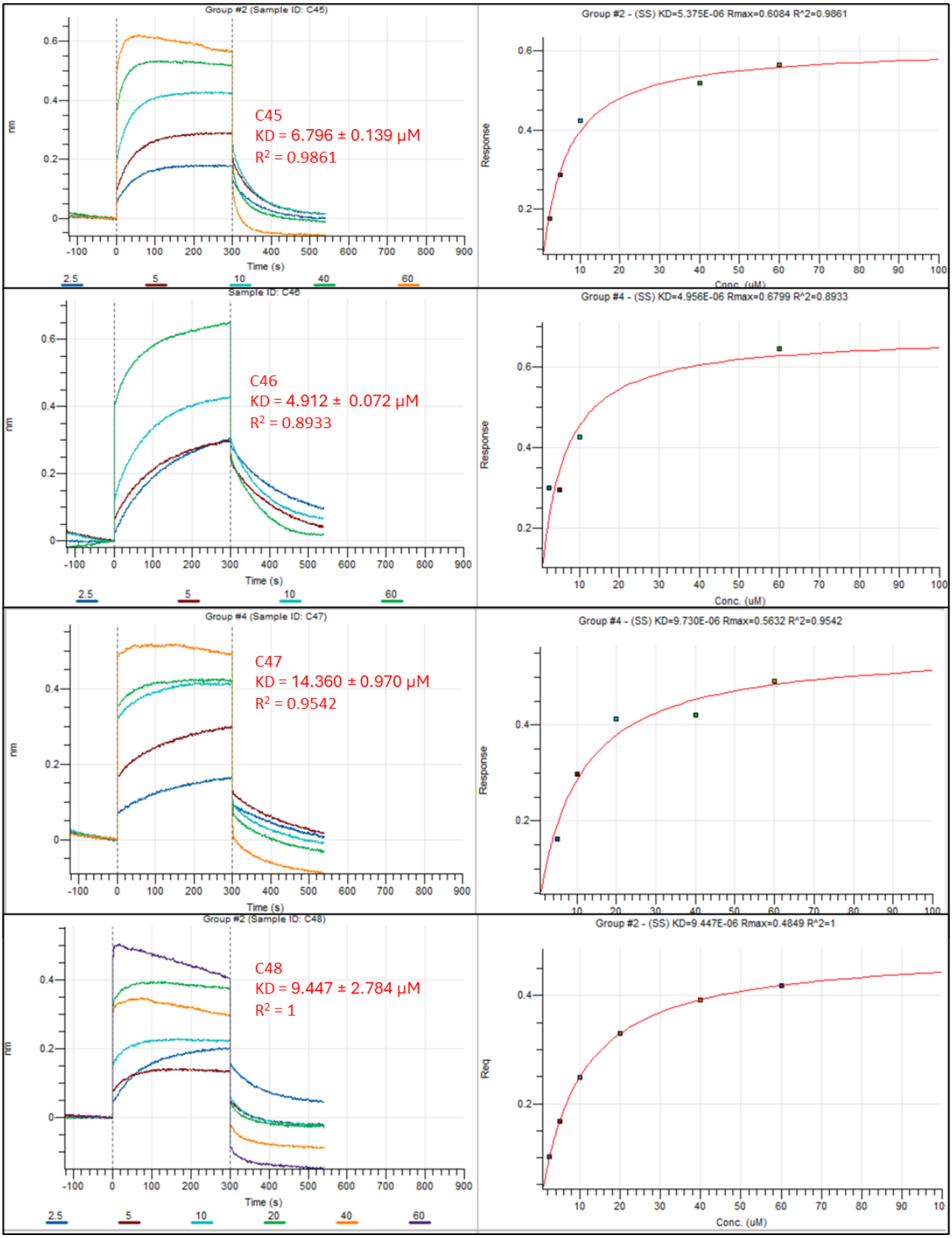
Group #2 (Sample ID: C45)
C45
KD = 6.796 ± 0.139 µM
R2 = 0.9861
Group #2 - (SS) KD=5.375E-06 Rmax=0.6084 R^2=0.9861
Response
Conc. (uM)
Sample ID: C46
C46
KD = 4.912 ± 0.072 µM
R2 = 0.8933
Group #4 - (SS) KD=4.956E-06 Rmax=0.6799 R^2=0.8933
Group #4 (Sample ID: C47)
C47
KD = 14.360 ± 0.970 µM
R2 = 0.9542
Group #4 - (SS) KD=9.730E-06 Rmax=0.5632 R^2=0.9542
Group #2 (Sample ID: C48)
C48
KD = 9.447 ± 2.784 µM
R2 = 1
Group #2 - (SS) KD=9.447E-06 Rmax=0.4849 R^2=1
nm
Time (s)
Req

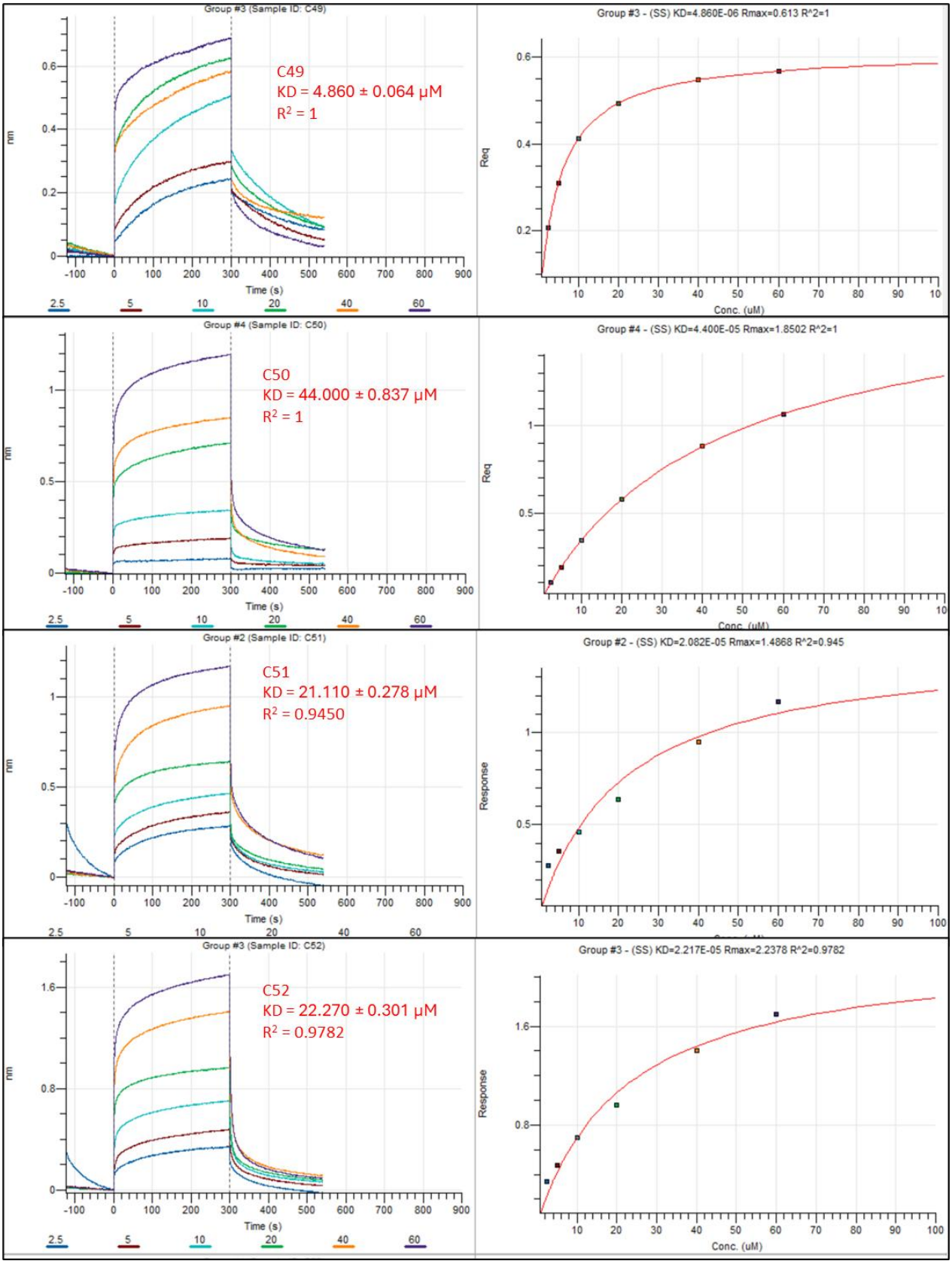
Group #3 (Sample ID: C49)
C49
KD = 4.860 ± 0.064 µM
R² = 1
Group #3 - (SS) KD=4.860E-06 Rmax=0.613 R^2=1
Group #4 (Sample ID: C50)
C50
KD = 44.000 ± 0.837 µM
R² = 1
Group #4 - (SS) KD=4.400E-05 Rmax=1.8502 R^2=1
Group #2 (Sample ID: C51)
C51
KD = 21.110 ± 0.278 µM
R² = 0.9450
Group #2 - (SS) KD=2.082E-05 Rmax=1.4868 R^2=0.945
Group #3 (Sample ID: C52)
C52
KD = 22.270 ± 0.301 µM
R² = 0.9782
Group #3 - (SS) KD=2.217E-05 Rmax=2.2378 R^2=0.9782
nm
Time (s)
Req
Response
Conc. (uM)
2.5
5
10
20
40
60

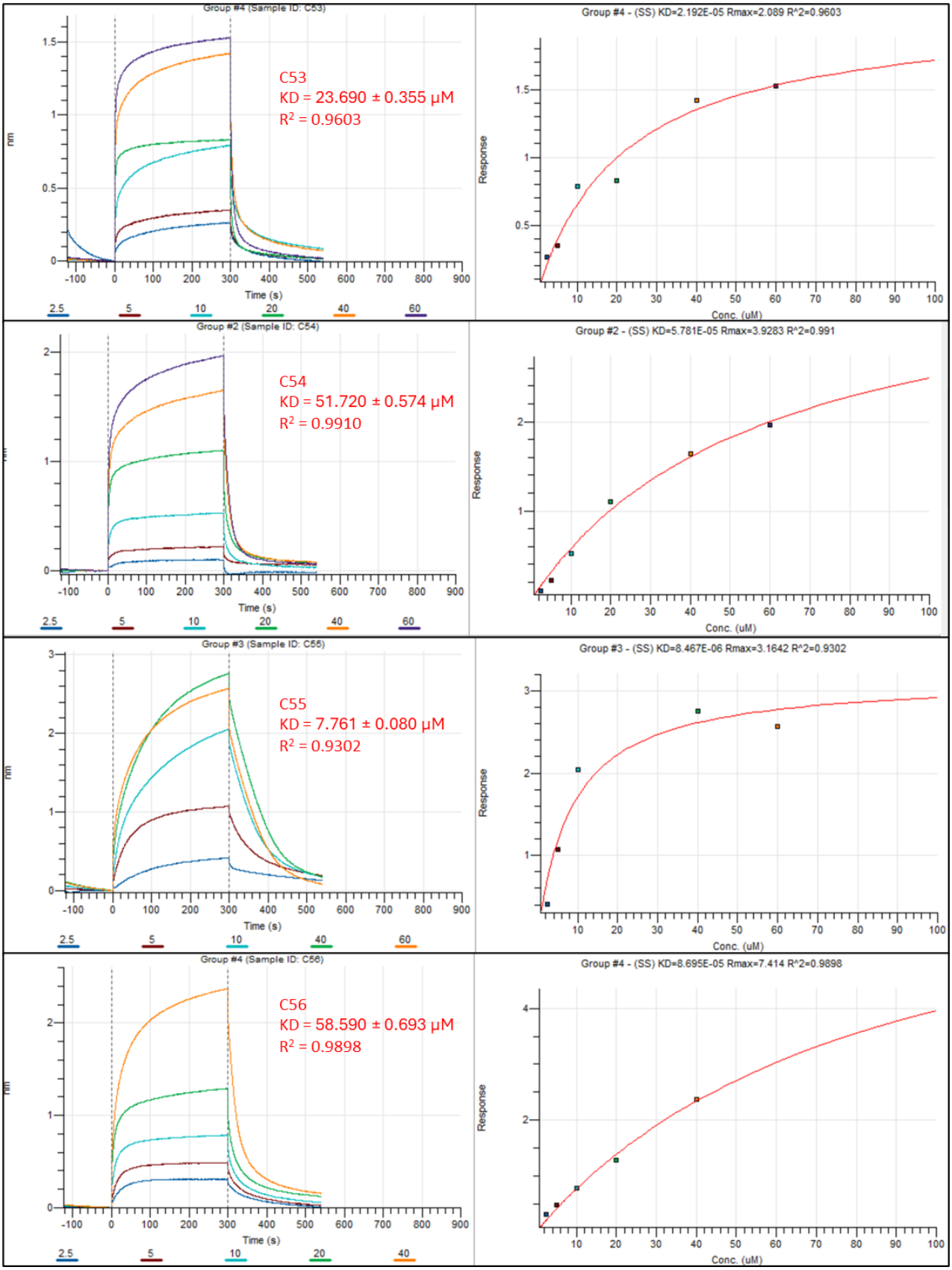
Group #4 (Sample ID: C53)
C53
KD = 23.690 ± 0.355 µM
R2 = 0.9603
Time (s)
Group #4 - (SS) KD=2.192E-05 Rmax=2.089 R^2=0.9603
Response
Conc. (uM)
Group #2 (Sample ID: C54)
C54
KD = 51.720 ± 0.574 µM
R2 = 0.9910
Time (s)
Group #2 - (SS) KD=5.781E-05 Rmax=3.9283 R^2=0.991
Response
Conc. (uM)
Group #3 (Sample ID: C55)
C55
KD = 7.761 ± 0.080 µM
R2 = 0.9302
Time (s)
Group #3 - (SS) KD=8.467E-06 Rmax=3.1642 R^2=0.9302
Response
Conc. (uM)
Group #4 (Sample ID: C56)
C56
KD = 58.590 ± 0.693 µM
R2 = 0.9898
Time (s)
Group #4 - (SS) KD=8.695E-05 Rmax=7.414 R^2=0.9898
Response
Conc. (uM)

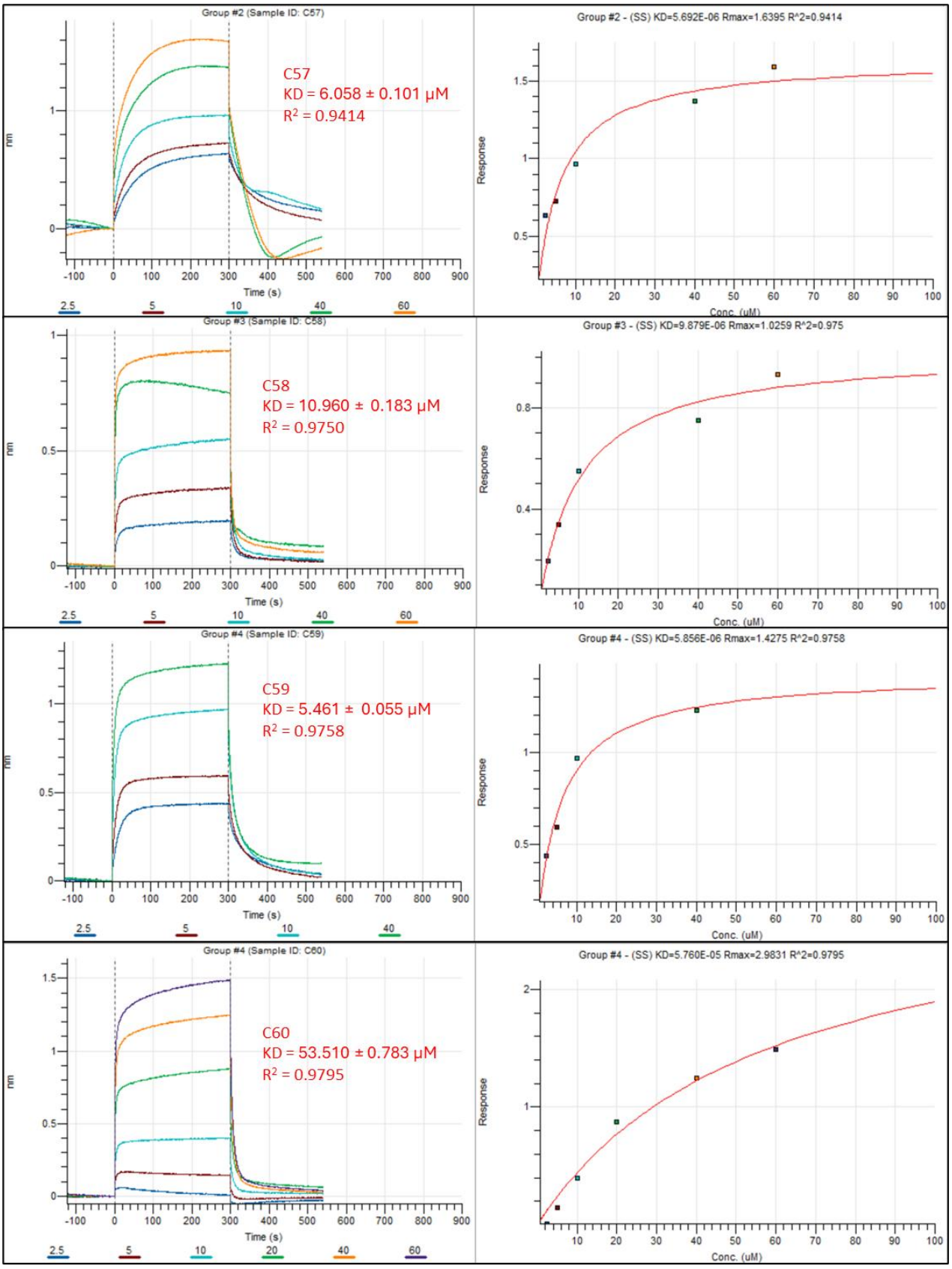
Group #2 (Sample ID: C57)
C57
KD = 6.058 ± 0.101 µM
R² = 0.9414
Group #2 - (SS) KD=5.692E-06 Rmax=1.6395 R^2=0.9414
Response
Conc. (uM)
Group #3 (Sample ID: C58)
C58
KD = 10.960 ± 0.183 µM
R² = 0.9750
Group #3 - (SS) KD=9.879E-06 Rmax=1.0259 R^2=0.975
Group #4 (Sample ID: C59)
C59
KD = 5.461 ± 0.055 µM
R² = 0.9758
Group #4 - (SS) KD=5.856E-06 Rmax=1.4275 R^2=0.9758
Group #4 (Sample ID: C60)
C60
KD = 53.510 ± 0.783 µM
R² = 0.9795
Group #4 - (SS) KD=5.760E-05 Rmax=2.9831 R^2=0.9795
nm
Time (s)

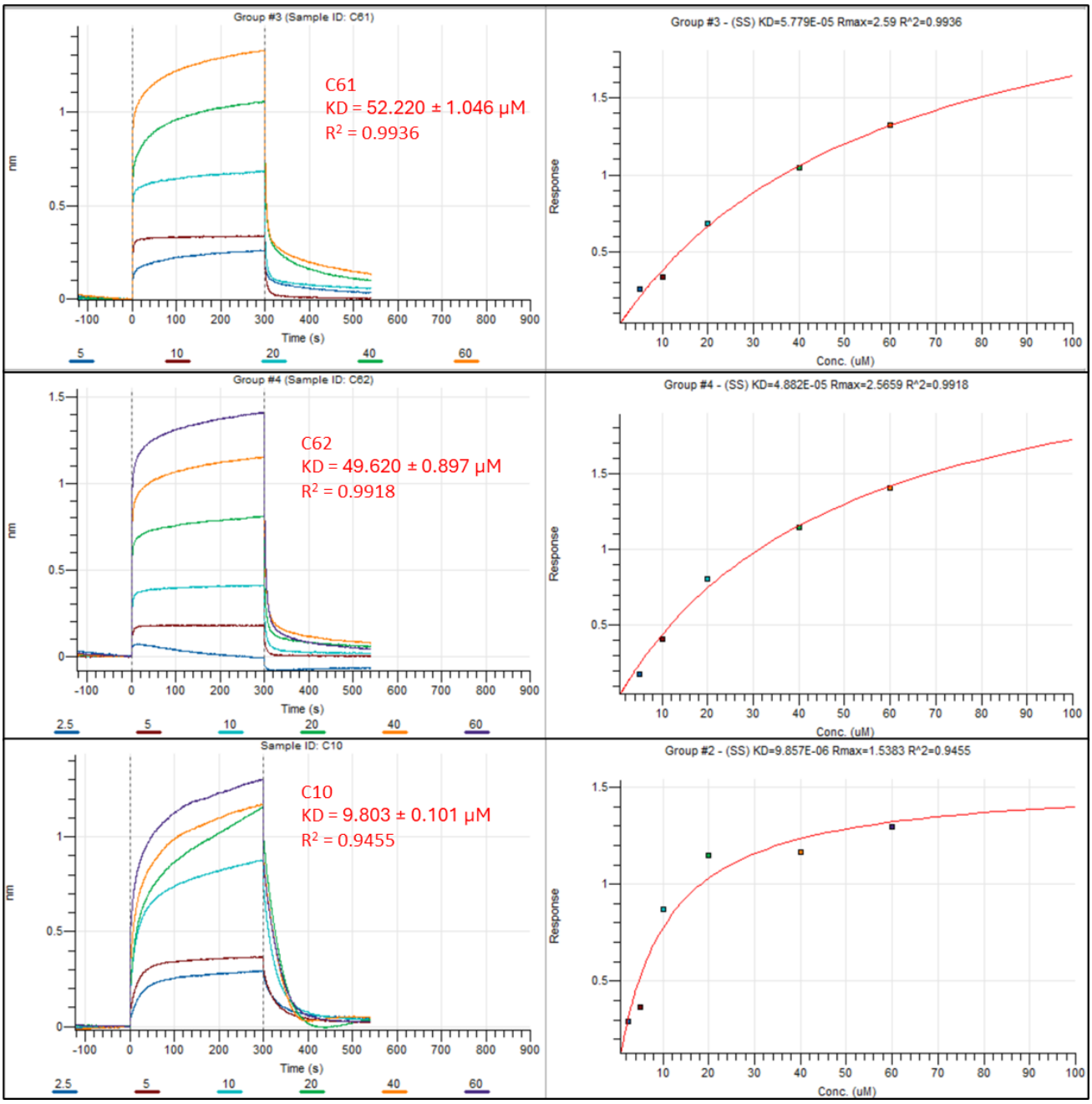

Figure S1: Binding and steady-state curves from BLI assays for C45-C62.

References

Abal, M., Andreu, J., & Barasoain, I. (2003). Taxanes: Microtubule and Centrosome Targets, and Cell Cycle Dependent Mechanisms of Action. *Current Cancer Drug Targets*, *3*(3), 193–203. https://doi.org/10.2174/1568009033481967

Afifi, M. M., Austin, L. A., Mackey, M. A., & El-Sayed, M. A. (2014). XAV939: From a Small Inhibitor to a Potent Drug Bioconjugate When Delivered by Gold Nanoparticles. *Bioconjugate Chemistry*, *25*(2), 207–215. https://doi.org/10.1021/bc400271x

Ahmad, S., Kandil, S., Williams, K., & Scott, J. (2025). Identification of non-oncology drugs with activity against inflammatory and triple-negative breast cancer cell lines. *Oncology Letters*, *31*(2), 1–18. https://doi.org/10.3892/ol.2025.15428

Ahmed, N., Abubaker, K., & Findlay, J. K. (2014). Ovarian cancer stem cells: Molecular concepts and relevance as therapeutic targets. *Molecular Aspects of Medicine*, *39*, 110–125. https://doi.org/10.1016/j.mam.2013.06.002

Andricopulo, A., & Montanari, C. (2005). Structure-Activity Relationships for the Design of Small-Molecule Inhibitors. *Mini-Reviews in Medicinal Chemistry*, *5*(6), 585–593. https://doi.org/10.2174/1389557054023224

Arend, R. C., Londoño-Joshi, A. I., Straughn, J. M., & Buchsbaum, D. J. (2013). The Wnt/β-catenin pathway in ovarian cancer: A review. *Gynecologic Oncology*, *131*(3), 772–779. https://doi.org/10.1016/j.ygyno.2013.09.034

Baell, J. B., & Holloway, G. A. (2010). New Substructure Filters for Removal of Pan Assay Interference Compounds (PAINS) from Screening Libraries and for Their Exclusion in Bioassays. *Journal of Medicinal Chemistry*, *53*(7), 2719–2740. https://doi.org/10.1021/jm901137j

Bajusz, D., Rácz, A., & Héberger, K. (2015). Why is Tanimoto index an appropriate choice for fingerprint-based similarity calculations? *Journal of Cheminformatics*, *7*(1), 20. https://doi.org/10.1186/s13321-015-0069-3

Bilić, J., Huang, Y.-L., Davidson, G., Zimmermann, T., Cruciat, C.-M., Bienz, M., & Niehrs, C. (2007). Wnt Induces LRP6 Signalosomes and Promotes Dishevelled-Dependent LRP6 Phosphorylation. *Science*, *316*(5831), 1619–1622. https://doi.org/10.1126/science.1137065

Birchmeier, W., von Kries, J. P., Winbeck, G., Asbrand, C., Schwarz-Romond, T., Sochnikova, N., Dell'Oro, A., & Behrens, J. (2000). Hot spots in beta-catenin for interactions with LEF-1, conductin and APC. *Nature Structural Biology*, *7*(9), 800–807. https://doi.org/10.1038/79039

Brault, V., Moore, R., Kutsch, S., Ishibashi, M., Rowitch, D. H., McMahon, A. P., Sommer, L., Boussadia, O., & Kemler, R. (2001). Inactivation of the β-catenin gene by Wnt1-Cre-mediated deletion results in dramatic brain malformation and failure of craniofacial development. *Development*, *128*(8), 1253–1264. https://doi.org/10.1242/dev.128.8.1253

Brown, A. C., & Fraser, T. R. (1868). On the Connection between Chemical Constitution and Physiological Action; with special reference to the Physiological Action of the Salts of the Ammonium Bases derived from Strychnia, Brucia, Thebaia, Codeia, Morphia, and Nicotia. *Journal of Anatomy and Physiology*, *2*(2), 224–242.

Chandra, A., Pius, C., Nabeel, M., Nair, M., Vishwanatha, J. K., Ahmad, S., & Basha, R. (2019). Ovarian cancer: Current status and strategies for improving therapeutic outcomes. *Cancer Medicine*, *8*(16), 7018–7031. https://doi.org/10.1002/cam4.2560

Chang, T.-S., Lu, C.-K., Hsieh, Y.-Y., Wei, K.-L., Chen, W.-M., Tung, S.-Y., Wu, C.-S., Chan, M. W. Y., & Chiang, M.-K. (2020). 2,4-Diamino-Quinazoline, a Wnt Signaling Inhibitor, Suppresses Gastric Cancer Progression and Metastasis. *International Journal of Molecular Sciences*, *21*(16), 5901. https://doi.org/10.3390/ijms21165901

Chen, Z., Venkatesan, A. M., Dehnhardt, C. M., Santos, O. Dos, Santos, E. D., Ayral-Kaloustian, S., Chen, L., Geng, Y., Arndt, K. T., Lucas, J., Chaudhary, I., & Mansour, T. S. (2009). 2,4-Diamino-quinazolines as inhibitors of β-catenin/Tcf-4 pathway: Potential treatment for colorectal cancer. *Bioorganic & Medicinal Chemistry Letters*, *19*(17), 4980–4983. https://doi.org/10.1016/j.bmcl.2009.07.070

Chien, T.-L., Wu, Y.-C., Lee, H.-L., Sung, W.-W., Yu, C.-Y., Chang, Y.-C., Lin, C.-C., Wang, C.-C., & Tsai, M.-C. (2023). PNU-74654 Induces Cell Cycle Arrest and Inhibits EMT Progression in Pancreatic Cancer. *Medicina*, *59*(9), 1531. https://doi.org/10.3390/medicina59091531

Clevers, H. (2006). Wnt/β-Catenin Signaling in Development and Disease. *Cell*, *127*(3), 469–480. https://doi.org/10.1016/j.cell.2006.10.018

Committee on the State of the Science in Ovarian Cancer Research; Board on Health Care Services; Institute of Medicine; National Academies of Sciences, E. and Medicine. (2016). *Ovarian Cancers: Evolving Paradigms in Research and Care*. National Academies Press. https://doi.org/10.17226/21841

Condello, S., Cao, L., & Matei, D. (2013). Tissue transglutaminase regulates β-catenin signaling through a c-Src-dependent mechanism. *The FASEB Journal*, *27*(8), 3100–3112. https://doi.org/10.1096/fj.12-222620

Condello, S., Morgan, C. A., Nagdas, S., Cao, L., Turek, J., Hurley, T. D., & Matei, D. (2015). β-Catenin-regulated ALDH1A1 is a target in ovarian cancer spheroids. *Oncogene*, *34*(18), 2297–2308. https://doi.org/10.1038/onc.2014.178

Cortez, A. J., Tudrej, P., Kujawa, K. A., & Lisowska, K. M. (2018). Advances in ovarian cancer therapy. *Cancer Chemotherapy and Pharmacology*, *81*(1), 17–38. https://doi.org/10.1007/s00280-017-3501-8

Cui, C., Zhou, X., Zhang, W., Qu, Y., & Ke, X. (2018). Is β-Catenin a Druggable Target for Cancer Therapy? *Trends in Biochemical Sciences*, *43*(8), 623–634. https://doi.org/10.1016/j.tibs.2018.06.003

Cumming, H., & Rücker, C. (2017). Octanol–Water Partition Coefficient Measurement by a Simple ^{1}H NMR Method. *ACS Omega*, *2*(9), 6244–6249. https://doi.org/10.1021/acsomega.7b01102

Daina, A., Michielin, O., & Zoete, V. (2017). SwissADME: a free web tool to evaluate pharmacokinetics, drug-likeness and medicinal chemistry friendliness of small molecules. *Scientific Reports*, *7*(1), 42717. https://doi.org/10.1038/srep42717

Daniel, K. G., Gupta, P., Harbach, R. H., Guida, W. C., & Dou, Q. P. (2004). Organic copper complexes as a new class of proteasome inhibitors and apoptosis inducers in human cancer cells. *Biochemical Pharmacology*, *67*(6), 1139–1151. https://doi.org/10.1016/j.bcp.2003.10.031

Daniels, D. L., & Weis, W. I. (2005). β-catenin directly displaces Groucho/TLE repressors from Tcf/Lef in Wnt-mediated transcription activation. *Nature Structural & Molecular Biology*, *12*(4), 364–371. https://doi.org/10.1038/nsmb912

Dann, C. E., Hsieh, J.-C., Rattner, A., Sharma, D., Nathans, J., & Leahy, D. J. (2001). Insights into Wnt binding and signalling from the structures of two Frizzled cysteine-rich domains. *Nature*, *412*(6842), 86–90. https://doi.org/10.1038/35083601

Dehnhardt, C. M., Venkatesan, A. M., Chen, Z., Ayral-Kaloustian, S., Dos Santos, O., Delos Santos, E., Curran, K., Follettie, M. T., Diesl, V., Lucas, J., Geng, Y., DeJoy, S. Q., Petersen, R., Chaudhary, I., Brooijmans, N., Mansour, T. S., Arndt, K., & Chen, L. (2010). Design and Synthesis of Novel Diaminoquinazolines with *in Vivo* Efficacy for β-Catenin/T-Cell Transcriptional Factor 4 Pathway Inhibition. *Journal of Medicinal Chemistry*, *53*(2), 897–910. https://doi.org/10.1021/jm901370m

Diamond, J. R., Becerra, C., Richards, D., Mita, A., Osborne, C., O'Shaughnessy, J., Zhang, C., Henner, R., Kapoun, A. M., Xu, L., Stagg, B., Uttamsingh, S., Brachmann, R. K., Farooki, A., & Mita, M. (2020). Phase Ib clinical trial of the anti-frizzled antibody vantictumab (OMP-18R5) plus paclitaxel in patients with locally advanced or metastatic HER2-negative breast cancer. *Breast Cancer Research and Treatment*, *184*(1), 53–62. https://doi.org/10.1007/s10549-020-05817-w

Du, X., Li, Y., Xia, Y.-L., Ai, S.-M., Liang, J., Sang, P., Ji, X.-L., & Liu, S.-Q. (2016). Insights into Protein–Ligand Interactions: Mechanisms, Models, and Methods. *International Journal of Molecular Sciences*, *17*(2), 144. https://doi.org/10.3390/ijms17020144

Eberhardt, J., Santos-Martins, D., Tillack, A. F., & Forli, S. (2021). AutoDock Vina 1.2.0: New Docking Methods, Expanded Force Field, and Python Bindings. *Journal of Chemical Information and Modeling*, *61*(8), 3891–3898. https://doi.org/10.1021/acs.jcim.1c00203

Emami, K. H., Nguyen, C., Ma, H., Kim, D. H., Jeong, K. W., Eguchi, M., Moon, R. T., Teo, J.-L., Oh, S. W., Kim, H. Y., Moon, S. H., Ha, J. R., & Kahn, M. (2004). A small molecule inhibitor of β-catenin/cyclic AMP response element-binding protein transcription. *Proceedings of the National Academy of Sciences*, *101*(34), 12682–12687. https://doi.org/10.1073/pnas.0404875101

Ewan, K., Pająk, B., Stubbs, M., Todd, H., Barbeau, O., Quevedo, C., Botfield, H., Young, R., Ruddle, R., Samuel, L., Battersby, A., Raynaud, F., Allen, N., Wilson, S., Latinkic, B., Workman, P., McDonald, E., Blagg, J., Aherne, W., & Dale, T. (2010). A Useful Approach to Identify Novel Small-Molecule Inhibitors of Wnt-Dependent Transcription. *Cancer Research*, *70*(14), 5963–5973. https://doi.org/10.1158/0008-5472.CAN-10-1028

Fang, L., Zhu, Q., Neuenschwander, M., Specker, E., Wulf-Goldenberg, A., Weis, W. I., von Kries, J. P., & Birchmeier, W. (2016). A Small-Molecule Antagonist of the β-Catenin/TCF4 Interaction Blocks the Self-Renewal of Cancer Stem Cells and Suppresses Tumorigenesis. *Cancer Research*, *76*(4), 891–901. https://doi.org/10.1158/0008-5472.CAN-15-1519

Fevr, T., Robine, S., Louvard, D., & Huelsken, J. (2007). Wnt/β-Catenin Is Essential for Intestinal Homeostasis and Maintenance of Intestinal Stem Cells. *Molecular and Cellular Biology*, *27*(21), 7551–7559. https://doi.org/10.1128/MCB.01034-07

Florea, A.-M., & Büsselberg, D. (2011). Cisplatin as an Anti-Tumor Drug: Cellular Mechanisms of Activity, Drug Resistance and Induced Side Effects. *Cancers*, *3*(1), 1351–1371. https://doi.org/10.3390/cancers3011351

Franken, N. A. P., Rodermond, H. M., Stap, J., Haveman, J., & van Bree, C. (2006). Clonogenic assay of cells in vitro. *Nature Protocols*, *1*(5), 2315–2319. https://doi.org/10.1038/nprot.2006.339

Gamallo, C., Palacios, J., Moreno, G., Calvo de Mora, J., Suárez, A., & Armas, A. (1999). β-Catenin Expression Pattern in Stage I and II Ovarian Carcinomas. *The American Journal of Pathology*, *155*(2), 527–536. https://doi.org/10.1016/S0002-9440(10)65148-6

Giannetti, A. M., Koch, B. D., & Browner, M. F. (2008). Surface Plasmon Resonance Based Assay for the Detection and Characterization of Promiscuous Inhibitors. *Journal of Medicinal Chemistry*, *51*(3), 574–580. https://doi.org/10.1021/jm700952v

Gonsalves, F. C., Klein, K., Carson, B. B., Katz, S., Ekas, L. A., Evans, S., Nagourney, R., Cardozo, T., Brown, A. M. C., & DasGupta, R. (2011). An RNAi-based chemical genetic screen identifies three small-molecule inhibitors of the Wnt/ *wingless* signaling pathway. *Proceedings of the National Academy of Sciences*, *108*(15), 5954–5963. https://doi.org/10.1073/pnas.1017496108

Gottardi, C. J., & Gumbiner, B. M. (2004). Role for ICAT in β-catenin-dependent nuclear signaling and cadherin functions. *American Journal of Physiology-Cell Physiology*, *286*(4), C747–C756. https://doi.org/10.1152/ajpcell.00433.2003

Graham, T. A., Clements, W. K., Kimelman, D., & Xu, W. (2002). The Crystal Structure of the β-Catenin/ICAT Complex Reveals the Inhibitory Mechanism of ICAT. *Molecular Cell*, *10*(3), 563–571. https://doi.org/10.1016/S1097-2765(02)00637-8

Graham, T. A., Ferkey, D. M., Mao, F., Kimelman, D., & Xu, W. (2001). Tcf4 can specifically recognize beta-catenin using alternative conformations. *Nature Structural Biology*, *8*(12), 1048–1052. https://doi.org/10.1038/nsb718

Graham, T. A., Weaver, C., Mao, F., Kimelman, D., & Xu, W. (2000). Crystal Structure of a β-Catenin/Tcf Complex. *Cell*, *103*(6), 885–896. https://doi.org/10.1016/S0092-8674(00)00192-6

Gryfe, R., Bapat, B., Gallinger, S., Swallow, C., Redston, M., & Couture, J. (1997). Molecular biology of colorectal cancer. *Current Problems in Cancer*, *21*(5), 233–299. https://doi.org/10.1016/S0147-0272(97)80003-7

Ha, N.-C., Tonozuka, T., Stamos, J. L., Choi, H.-J., & Weis, W. I. (2004). Mechanism of Phosphorylation-Dependent Binding of APC to β-Catenin and Its Role in β-Catenin Degradation. *Molecular Cell*, *15*(4), 511–521. https://doi.org/10.1016/j.molcel.2004.08.010

Hanahan, D., & Weinberg, R. A. (2011). Hallmarks of Cancer: The Next Generation. *Cell*, *144*(5), 646–674. https://doi.org/10.1016/j.cell.2011.02.013

Henen, M. A., Coudevylle, N., Geist, L., & Konrat, R. (2012). Toward Rational Fragment-Based Lead Design without 3D Structures. *Journal of Medicinal Chemistry*, *55*(17), 7909–7919. https://doi.org/10.1021/jm301016m

Hernandez Gifford, J. A. (2015). The role of WNT signaling in adult ovarian folliculogenesis. *Reproduction*, *150*(4), R137–R148. https://doi.org/10.1530/REP-14-0685

Hu, J., Wang, Z., Chen, J., Yu, Z., Zhang, J., Li, W., Lin, M., Yang, X., & Liu, H. (2021). Overexpression of ICAT Inhibits the Progression of Colorectal Cancer by Binding with β-Catenin in the Cytoplasm. *Technology in Cancer Research & Treatment*, *20*. https://doi.org/10.1177/15330338211041253

Huang, S.-M. A., Mishina, Y. M., Liu, S., Cheung, A., Stegmeier, F., Michaud, G. A., Charlat, O., Wiellette, E., Zhang, Y., Wiessner, S., Hild, M., Shi, X., Wilson, C. J., Mickanin, C., Myer, V., Fazal, A., Tomlinson, R., Serluca, F., Shao, W., … Cong, F. (2009a). Tankyrase inhibition stabilizes axin and antagonizes Wnt signalling. *Nature*, *461*(7264), 614–620. https://doi.org/10.1038/nature08356

Huang, S.-M. A., Mishina, Y. M., Liu, S., Cheung, A., Stegmeier, F., Michaud, G. A., Charlat, O., Wiellette, E., Zhang, Y., Wiessner, S., Hild, M., Shi, X., Wilson, C. J., Mickanin, C., Myer, V., Fazal, A., Tomlinson, R., Serluca, F., Shao, W., … Cong, F. (2009b). Tankyrase inhibition stabilizes axin and antagonizes Wnt signalling. *Nature*, *461*(7264), 614–620. https://doi.org/10.1038/nature08356

Huang, Z., Zhang, M., Burton, S. D., Katsakhyan, L. N., & Ji, H. (2014). Targeting the Tcf4 G ^{13} ANDE ^{17} Binding Site To Selectively Disrupt β-Catenin/T-Cell Factor Protein–Protein Interactions. *ACS Chemical Biology*, *9*(1), 193–201. https://doi.org/10.1021/cb400795x

Huber, A. H., Nelson, W. J., & Weis, W. I. (1997). Three-Dimensional Structure of the Armadillo Repeat Region of β-Catenin. *Cell*, *90*(5), 871–882. https://doi.org/10.1016/S0092-8674(00)80352-9

Huber, A. H., & Weis, W. I. (2001). The Structure of the β-Catenin/E-Cadherin Complex and the Molecular Basis of Diverse Ligand Recognition by β-Catenin. *Cell*, *105*(3), 391–402. https://doi.org/10.1016/S0092-8674(01)00330-0

Huelsken, J., Vogel, R., Erdmann, B., Cotsarelis, G., & Birchmeier, W. (2001). β-Catenin Controls Hair Follicle Morphogenesis and Stem Cell Differentiation in the Skin. *Cell*, *105*(4), 533–545. https://doi.org/10.1016/S0092-8674(01)00336-1

Hughes, J., Rees, S., Kalindjian, S., & Philpott, K. (2011). Principles of early drug discovery. *British Journal of Pharmacology*, *162*(6), 1239–1249. https://doi.org/10.1111/j.1476-5381.2010.01127.x

Jelovac, D., & Armstrong, D. K. (2011). Recent progress in the diagnosis and treatment of ovarian cancer. *CA: A Cancer Journal for Clinicians*, *61*(3), 183–203. https://doi.org/10.3322/caac.20113

Johnson, M., & Maggiora, G. M. (1990). *Concepts and applications of molecular similarity*. https://api.semanticscholar.org/CorpusID:117506064

Kalluri, R., & Weinberg, R. A. (2009). The basics of epithelial-mesenchymal transition. *Journal of Clinical Investigation*, *119*(6), 1420–1428. https://doi.org/10.1172/JCI39104

Kim, G., Kurnit, K. C., Djordjevic, B., Singh, C., Munsell, M. F., Wang, W.-L., Lazar, A. J., Zhang, W., & Broaddus, R. (2018). Nuclear β-catenin localization and mutation of the

CTNNB1 gene: a context-dependent association. *Modern Pathology*, *31*(10), 1553–1559. https://doi.org/10.1038/s41379-018-0080-0

Kim, S., & Jeong, S. (2019). Mutation Hotspots in the β-Catenin Gene: Lessons from the Human Cancer Genome Databases. *Molecules and Cells*, *42*(1), 8–16. https://doi.org/10.14348/molcells.2018.0436

Kimura, K., Kanto, T., Shimoda, S., Harada, K., Kimura, M., Nishikawa, K., Imamura, J., Ogawa, E., Saio, M., Ikura, Y., Okusaka, T., Inoue, K., Ishikawa, T., Ieiri, I., Kishimoto, J., Todaka, K., & Kamisawa, T. (2022). Safety, tolerability, and anti-fibrotic efficacy of the CBP/β-catenin inhibitor PRI-724 in patients with hepatitis C and B virus-induced liver cirrhosis: An investigator-initiated, open-label, non-randomised, multicentre, phase 1/2a study. *EBioMedicine*, *80*, 104069. https://doi.org/10.1016/j.ebiom.2022.104069

Klement, K., Brückner, M., & Bernkopf, D. B. (2023). Phosphorylation of axin within biomolecular condensates counteracts its tankyrase-mediated degradation. *Journal of Cell Science*, *136*(20). https://doi.org/10.1242/jcs.261214

Klingensmith, J., Nusse, R., & Perrimon, N. (1994). The Drosophila segment polarity gene dishevelled encodes a novel protein required for response to the wingless signal. *Genes & Development*, *8*(1), 118–130. https://doi.org/10.1101/gad.8.1.118

Komiya, Y., & Habas, R. (2008). Wnt signal transduction pathways. *Organogenesis*, *4*(2), 68–75. https://doi.org/10.4161/org.4.2.5851

Kraus, C., Liehr, T., Hülsken, J., Behrens, J., Birchmeier, W., Grzeschik, K.-H., & Ballhausen, W. G. (1994). Localization of the Human β-Catenin Gene (CTNNB1) to 3p21: A Region Implicated in Tumor Development. *Genomics*, *23*(1), 272–274. https://doi.org/10.1006/geno.1994.1493

Kryczek, I., Liu, S., Roh, M., Vatan, L., Szeliga, W., Wei, S., Banerjee, M., Mao, Y., Kotarski, J., Wicha, M. S., Liu, R., & Zou, W. (2012). Expression of aldehyde dehydrogenase and CD133 defines ovarian cancer stem cells. *International Journal of Cancer*, *130*(1), 29–39. https://doi.org/10.1002/ijc.25967

Lazo, J. S., & Sharlow, E. R. (2016). Drugging Undruggable Molecular Cancer Targets. *Annual Review of Pharmacology and Toxicology*, *56*(1), 23–40. https://doi.org/10.1146/annurev-pharmtox-010715-103440

Ledermann, J. A., Raja, F. A., Fotopoulou, C., Gonzalez-Martin, A., Colombo, N., & Sessa, C. (2013). Newly diagnosed and relapsed epithelial ovarian carcinoma: ESMO Clinical Practice Guidelines for diagnosis, treatment and follow-up. *Annals of Oncology*, *24*, vi24–vi32. https://doi.org/10.1093/annonc/mdt333

Lee, S. B., Gong, Y.-D., Park, Y. I., & Dong, M.-S. (2013). 2,3,6-Trisubstituted quinoxaline derivative, a small molecule inhibitor of the Wnt/beta-catenin signaling pathway, suppresses cell proliferation and enhances radiosensitivity in A549/Wnt2 cells. *Biochemical and Biophysical Research Communications*, *431*(4), 746–752. https://doi.org/10.1016/j.bbrc.2013.01.038

Lee, S.-B., Park, Y. I., Dong, M.-S., & Gong, Y.-D. (2010). Identification of 2,3,6-trisubstituted quinoxaline derivatives as a Wnt2/β-catenin pathway inhibitor in non-small-cell lung cancer cell lines. *Bioorganic & Medicinal Chemistry Letters*, *20*(19), 5900–5904. https://doi.org/10.1016/j.bmcl.2010.07.088

Lepourcelet, M., Chen, Y.-N. P., France, D. S., Wang, H., Crews, P., Petersen, F., Bruseo, C., Wood, A. W., & Shivdasani, R. A. (2004). Small-molecule antagonists of the oncogenic Tcf/β-catenin protein complex. *Cancer Cell*, *5*(1), 91–102. https://doi.org/10.1016/S1535-6108(03)00334-9

Lévy, L., Wei, Y., Labalette, C., Wu, Y., Renard, C.-A., Buendia, M. A., & Neuveut, C. (2004). Acetylation of β-Catenin by p300 Regulates β-Catenin-Tcf4 Interaction. *Molecular and Cellular Biology*, *24*(8), 3404–3414. https://doi.org/10.1128/MCB.24.8.3404-3414.2004

Liao, D., Yang, S., Zhao, L., Ren, W., Liu, S., Yu, H., Chen, Y., Yu, T., Zeng, T., Zhou, L., & Zhang, Y. (2024). ICAT-Mediated Crosstalk Between Cervical Cancer Cells and Macrophages Promotes M2-Like Macrophage Polarization to Reinforce Tumor Malignant Behaviors. *Molecular Carcinogenesis*, *63*(12), 2425–2440. https://doi.org/10.1002/mc.23820

Lipinski, C. A., Lombardo, F., Dominy, B. W., & Feeney, P. J. (2001). Experimental and computational approaches to estimate solubility and permeability in drug discovery and development settings 1PII of original article: S0169-409X(96)00423-1. The article was originally published in Advanced Drug Delivery Reviews 23 (1997) 3–25. 1. *Advanced Drug Delivery Reviews*, *46*(1–3), 3–26. https://doi.org/10.1016/S0169-409X(00)00129-0

Liu, C., Kato, Y., Zhang, Z., Do, V. M., Yankner, B. A., & He, X. (1999). β-Trcp couples β-catenin phosphorylation-degradation and regulates *Xenopus* axis formation. *Proceedings of the National Academy of Sciences*, *96*(11), 6273–6278. https://doi.org/10.1073/pnas.96.11.6273

Liu, C., Li, Y., Semenov, M., Han, C., Baeg, G.-H., Tan, Y., Zhang, Z., Lin, X., & He, X. (2002). Control of β-Catenin Phosphorylation/Degradation by a Dual-Kinase Mechanism. *Cell*, *108*(6), 837–847. https://doi.org/10.1016/S0092-8674(02)00685-2

Liu, J., Pan, S., Hsieh, M. H., Ng, N., Sun, F., Wang, T., Kasibhatla, S., Schuller, A. G., Li, A. G., Cheng, D., Li, J., Tompkins, C., Pferdekamper, A., Steffy, A., Cheng, J., Kowal, C., Phung, V., Guo, G., Wang, Y., … Harris, J. L. (2013). Targeting Wnt-driven cancer through the

inhibition of Porcupine by LGK974. *Proceedings of the National Academy of Sciences*, *110*(50), 20224–20229. https://doi.org/10.1073/pnas.1314239110

Liu, Y., Patel, L., Mills, G. B., Lu, K. H., Sood, A. K., Ding, L., Kucherlapati, R., Mardis, E. R., Levine, D. A., Shmulevich, I., Broaddus, R. R., & Zhang, W. (2014). Clinical Significance of CTNNB1 Mutation and Wnt Pathway Activation in Endometrioid Endometrial Carcinoma. *JNCI: Journal of the National Cancer Institute*, *106*(9). https://doi.org/10.1093/jnci/dju245

Logan, C. Y., & Nusse, R. (2004). THE WNT SIGNALING PATHWAY IN DEVELOPMENT AND DISEASE. *Annual Review of Cell and Developmental Biology*, *20*(1), 781–810. https://doi.org/10.1146/annurev.cellbio.20.010403.113126

Lung, H., Wentworth, K. L., Moody, T., Zamarioli, A., Ram, A., Ganesh, G., Kang, M., Ho, S., & Hsiao, E. C. (2024). Wnt pathway inhibition with the porcupine inhibitor LGK974 decreases trabecular bone but not fibrosis in a murine model with fibrotic bone. *JBMR Plus*, *8*(5). https://doi.org/10.1093/jbmrpl/ziae011

Mabee, C. L., Mabee, S. W., Baker, P. B., Kirkpatrick, R. B., & Levine, E. J. (1995). Fulminant hepatic failure associated with etodolac use. *The American Journal of Gastroenterology*, *90*(4), 659–661.

Mao, Y., Lin, N., Tian, W., Han, X., Han, X., Huang, Z., & An, J. (2012). Design, Synthesis, and Biological Evaluation of New Diaminoquinazolines as β-Catenin/Tcf4 Pathway Inhibitors. *Journal of Medicinal Chemistry*, *55*(3), 1346–1359. https://doi.org/10.1021/jm201494a

McCoy, M. A., Spicer, D., Wells, N., Hoogewijs, K., Fiedler, M., & Baud, M. G. J. (2022). Biophysical Survey of Small-Molecule β-Catenin Inhibitors: A Cautionary Tale. *Journal of Medicinal Chemistry*, *65*(10), 7246–7261. https://doi.org/10.1021/acs.jmedchem.2c00228

Miranda, M., Galli, L. M., Enriquez, M., Szabo, L. A., Gao, X., Hannoush, R. N., & Burrus, L. W. (2014). Identification of the WNT1 residues required for palmitoylation by Porcupine. *FEBS Letters*, *588*(24), 4815–4824. https://doi.org/10.1016/j.febslet.2014.11.016

Miyoshi, K., & Hennighausen, L. (2003). Beta-catenin: a transforming actor on many stages. *Breast Cancer Research*, *5*(2), 63. https://doi.org/10.1186/bcr566

Munemitsu, S., Albert, I., Souza, B., Rubinfeld, B., & Polakis, P. (1995). Regulation of intracellular beta-catenin levels by the adenomatous polyposis coli (APC) tumor-suppressor protein. *Proceedings of the National Academy of Sciences*, *92*(7), 3046–3050. https://doi.org/10.1073/pnas.92.7.3046

Nagaraj, A. B., Joseph, P., Kovalenko, O., Singh, S., Armstrong, A., Redline, R., Resnick, K., Zanotti, K., Waggoner, S., & DiFeo, A. (2015). Critical role of Wnt/β-catenin signaling in

driving epithelial ovarian cancer platinum resistance. *Oncotarget*, *6*(27), 23720–23734. https://doi.org/10.18632/oncotarget.4690

Nalli, M., Di Magno, L., Wen, Y., Liu, X., D'Ambrosio, M., Puxeddu, M., Parisi, A., Sebastiani, J., Sorato, A., Coluccia, A., Ripa, S., Di Pastena, F., Capelli, D., Montanari, R., Masci, D., Urbani, A., Naro, C., Sette, C., Orlando, V., … La Regina, G. (2023). Novel *N* -(Heterocyclylphenyl)benzensulfonamide Sharing an Unreported Binding Site with T-Cell Factor 4 at the β-Catenin Armadillo Repeats Domain as an Anticancer Agent. *ACS Pharmacology & Translational Science*, *6*(7), 1087–1103. https://doi.org/10.1021/acsptsci.3c00092

Nelson, E. (1961). Kinetics of Drug Absorption, Distribution, Metabolism, and Excretion. *Journal of Pharmaceutical Sciences*, *50*(3), 181–192. https://doi.org/10.1002/jps.2600500302

Nguyen, V. H. L., Hough, R., Bernaudo, S., & Peng, C. (2019). Wnt/β-catenin signalling in ovarian cancer: Insights into its hyperactivation and function in tumorigenesis. *Journal of Ovarian Research*, *12*(1), 122. https://doi.org/10.1186/s13048-019-0596-z

Noordermeer, J., Klingensmith, J., Perrimon, N., & Nusse, R. (1994). Dishevelled and armadillo act in the Wingless signalling pathway in Drosophila. *Nature*, *367*(6458), 80–83. https://doi.org/10.1038/367080a0

Nusse, R. (2001). An ancient cluster of Wnt paralogues. *Trends in Genetics*, *17*(8), 443. https://doi.org/10.1016/S0168-9525(01)02349-6

Nusse, R., van Ooyen, A., Cox, D., Fung, Y. K. T., & Varmus, H. (1984). Mode of proviral activation of a putative mammary oncogene (int-1) on mouse chromosome 15. *Nature*, *307*(5947), 131–136. https://doi.org/10.1038/307131a0

Nusse, R., & Varmus, H. E. (1982). Many tumors induced by the mouse mammary tumor virus contain a provirus integrated in the same region of the host genome. *Cell*, *31*(1), 99–109. https://doi.org/10.1016/0092-8674(82)90409-3

Nüsslein-Volhard, C., Wieschaus, E., & Kluding, H. (1984). Mutations affecting the pattern of the larval cuticle inDrosophila melanogaster. *Wilhelm Roux's Archives of Developmental Biology*, *193*(5), 267–282. https://doi.org/10.1007/BF00848156

Omer, C. A., Miller, P. J., Diehl, R. E., & Kral, A. M. (1999). Identification of Tcf4 Residues Involved in High-Affinity β-Catenin Binding. *Biochemical and Biophysical Research Communications*, *256*(3), 584–590. https://doi.org/10.1006/bbrc.1999.0379

Papadopoulos, K. P., Rodon Ahnert, J., Khushman, M. M., Sharma, S., Pelster, M., Cecchini, M., Kummar, S., Choi, M., Akella, L. V, Garofalo, A., Yu, Z., Iyer, V., Nguyen, M. H., Orford, K. W., & Klempner, S. J. (2024). A first-in-human, phase 1/2 trial of FOG-001, a β-

catenin:TCF antagonist, in patients with locally advanced or metastatic solid tumors. *Journal of Clinical Oncology*, *42*(16_suppl), TPS3175–TPS3175. https://doi.org/10.1200/JCO.2024.42.16_suppl.TPS3175

Parkes, E. E., & Kennedy, R. D. (2016). Clinical Application of Poly(ADP-Ribose) Polymerase Inhibitors in High-Grade Serous Ovarian Cancer. *The Oncologist*, *21*(5), 586–593. https://doi.org/10.1634/theoncologist.2015-0438

Pinson, K. I., Brennan, J., Monkley, S., Avery, B. J., & Skarnes, W. C. (2000). An LDL-receptor-related protein mediates Wnt signalling in mice. *Nature*, *407*(6803), 535–538. https://doi.org/10.1038/35035124

Poy, F., Lepourcelet, M., Shivdasani, R. A., & Eck, M. J. (2001). Structure of a human Tcf4-beta-catenin complex. *Nature Structural Biology*, *8*(12), 1053–1057. https://doi.org/10.1038/nsb720

Rafehi, H., Orlowski, C., Georgiadis, G. T., Ververis, K., El-Osta, A., & Karagiannis, T. C. (2011). Clonogenic Assay: Adherent Cells. *Journal of Visualized Experiments*, (49). https://doi.org/10.3791/2573

Raymond, J. W., Watson, I. A., & Mahoui, A. (2009). Rationalizing Lead Optimization by Associating Quantitative Relevance with Molecular Structure Modification. *Journal of Chemical Information and Modeling*, *49*(8), 1952–1962. https://doi.org/10.1021/ci9000426

Reuben, A., Koch, D. G., & Lee, W. M. (2010). Drug-Induced Acute Liver Failure. *Hepatology*, *52*(6), 2065–2076. https://doi.org/10.1002/hep.23937

Riggleman, B., Schedl, P., & Wieschaus, E. (1990). Spatial expression of the Drosophila segment polarity gene armadillo is posttranscriptionally regulated by wingless. *Cell*, *63*(3), 549–560. https://doi.org/10.1016/0092-8674(90)90451-J

Rodon, J., Argilés, G., Connolly, R. M., Vaishampayan, U., de Jonge, M., Garralda, E., Giannakis, M., Smith, D. C., Dobson, J. R., McLaughlin, M. E., Seroutou, A., Ji, Y., Morawiak, J., Moody, S. E., & Janku, F. (2021). Phase 1 study of single-agent WNT974, a first-in-class Porcupine inhibitor, in patients with advanced solid tumours. *British Journal of Cancer*, *125*(1), 28–37. https://doi.org/10.1038/s41416-021-01389-8

Rogers, J. P., Beuscher, Flajolet, M., McAvoy, T., Nairn, A. C., Olson, A. J., & Greengard, P. (2006). Discovery of Protein Phosphatase 2C Inhibitors by Virtual Screening. *Journal of Medicinal Chemistry*, *49*(5), 1658–1667. https://doi.org/10.1021/jm051033y

Roth, B. D. (2002). *The Discovery and Development of Atorvastatin, A Potent Novel Hypolipidemic Agent* (pp. 1–22). https://doi.org/10.1016/S0079-6468(08)70080-8

Rubinfeld, B., Tice, D. A., & Polakis, P. (2001). Axin-dependent Phosphorylation of the Adenomatous Polyposis Coli Protein Mediated by Casein Kinase 1ε. *Journal of Biological Chemistry*, *276*(42), 39037–39045. https://doi.org/10.1074/jbc.M105148200

Sander, T., Freyss, J., von Korff, M., & Rufener, C. (2015). DataWarrior: An Open-Source Program For Chemistry Aware Data Visualization And Analysis. *Journal of Chemical Information and Modeling*, *55*(2), 460–473. https://doi.org/10.1021/ci500588j

Satoh, S., Daigo, Y., Furukawa, Y., Kato, T., Miwa, N., Nishiwaki, T., Kawasoe, T., Ishiguro, H., Fujita, M., Tokino, T., Sasaki, Y., Imaoka, S., Murata, M., Shimano, T., Yamaoka, Y., & Nakamura, Y. (2000). AXIN1 mutations in hepatocellular carcinomas, and growth suppression in cancer cells by virus-mediated transfer of AXIN1. *Nature Genetics*, *24*(3), 245–250. https://doi.org/10.1038/73448

Satpathy, M., Cao, L., Pincheira, R., Emerson, R., Bigsby, R., Nakshatri, H., & Matei, D. (2007). Enhanced peritoneal ovarian tumor dissemination by tissue transglutaminase. *Cancer Research*, *67*(15), 7194–7202. https://doi.org/10.1158/0008-5472.CAN-07-0307

Sawada, K., Mitra, A. K., Radjabi, A. R., Bhaskar, V., Kistner, E. O., Tretiakova, M., Jagadeeswaran, S., Montag, A., Becker, A., Kenny, H. A., Peter, M. E., Ramakrishnan, V., Yamada, S. D., & Lengyel, E. (2008). Loss of E-Cadherin Promotes Ovarian Cancer Metastasis via α5-Integrin, which Is a Therapeutic Target. *Cancer Research*, *68*(7), 2329–2339. https://doi.org/10.1158/0008-5472.CAN-07-5167

Schmeltzer, P. A., Kosinski, A. S., Kleiner, D. E., Hoofnagle, J. H., Stolz, A., Fontana, R. J., & Russo, M. W. (2016). Liver injury from nonsteroidal anti-inflammatory drugs in the United States. *Liver International*, *36*(4), 603–609. https://doi.org/10.1111/liv.13032

Shah, K., & Kazi, J. U. (2022). Phosphorylation-Dependent Regulation of WNT/Beta-Catenin Signaling. *Frontiers in Oncology*, *12*. https://doi.org/10.3389/fonc.2022.858782

Shah, N. B., & Duncan, T. M. (2014). Bio-layer Interferometry for Measuring Kinetics of Protein-protein Interactions and Allosteric Ligand Effects. *Journal of Visualized Experiments*, (84). https://doi.org/10.3791/51383

Shang, S., Hua, F., & Hu, Z.-W. (2017). The regulation of β-catenin activity and function in cancer: therapeutic opportunities. *Oncotarget*, *8*(20), 33972–33989. https://doi.org/10.18632/oncotarget.15687

Shim, J., & MacKerell, Jr. , A. D. (2011). Computational ligand-based rational design: role of conformational sampling and force fields in model development. *MedChemComm*, *2*(5), 356. https://doi.org/10.1039/c1md00044f

Shin, S. H., Lim, D. Y., Reddy, K., Malakhova, M., Liu, F., Wang, T., Song, M., Chen, H., Bae, K. B., Ryu, J., Liu, K., Lee, M.-H., Bode, A. M., & Dong, Z. (2017). A Small Molecule

Inhibitor of the β-Catenin-TCF4 Interaction Suppresses Colorectal Cancer Growth In Vitro and In Vivo. *EBioMedicine*, *25*, 22–31. https://doi.org/10.1016/j.ebiom.2017.09.029

Sorkun, M. C., Khetan, A., & Er, S. (2019). AqSolDB, a curated reference set of aqueous solubility and 2D descriptors for a diverse set of compounds. *Scientific Data*, *6*(1), 143. https://doi.org/10.1038/s41597-019-0151-1

Su, L.-K., Vogelstein, B., & Kinzler, K. W. (1993). Association of the APC Tumor Suppressor Protein with Catenins. *Science*, *262*(5140), 1734–1737. https://doi.org/10.1126/science.8259519

Tago, K., Nakamura, T., Nishita, M., Hyodo, J., Nagai, S., Murata, Y., Adachi, S., Ohwada, S., Morishita, Y., Shibuya, H., & Akiyama, T. (2000). Inhibition of Wnt signaling by ICAT, a novel beta-catenin-interacting protein. *Genes & Development*, *14*(14), 1741–1749.

Tamai, K., Semenov, M., Kato, Y., Spokony, R., Liu, C., Katsuyama, Y., Hess, F., Saint-Jeannet, J.-P., & He, X. (2000). LDL-receptor-related proteins in Wnt signal transduction. *Nature*, *407*(6803), 530–535. https://doi.org/10.1038/35035117

Tauriello, D. V. F., Jordens, I., Kirchner, K., Slootstra, J. W., Kruitwagen, T., Bouwman, B. A. M., Noutsou, M., Rüdiger, S. G. D., Schwamborn, K., Schambony, A., & Maurice, M. M. (2012). Wnt/β-catenin signaling requires interaction of the Dishevelled DEP domain and C terminus with a discontinuous motif in Frizzled. *Proceedings of the National Academy of Sciences*, *109*(14). https://doi.org/10.1073/pnas.1114802109

Tian, W., Han, X., Yan, M., Xu, Y., Duggineni, S., Lin, N., Luo, G., Li, Y. M., Han, X., Huang, Z., & An, J. (2012). Structure-Based Discovery of a Novel Inhibitor Targeting the β-Catenin/Tcf4 Interaction. *Biochemistry*, *51*(2), 724–731. https://doi.org/10.1021/bi201428h

Tian, X., Liu, Z., Niu, B., Zhang, J., Tan, T. K., Lee, S. R., Zhao, Y., Harris, D. C. H., & Zheng, G. (2011). E-Cadherin/ β -Catenin Complex and the Epithelial Barrier. *BioMed Research International*, *2011*(1). https://doi.org/10.1155/2011/567305

Tysnes, B. B. (2010). Tumor-Initiating and -Propagating Cells: Cells That We Would to Identify and Control. *Neoplasia*, *12*(7), 506–515. https://doi.org/10.1593/neo.10290

Valenta, T., Hausmann, G., & Basler, K. (2012). The many faces and functions of β-catenin. *The EMBO Journal*, *31*(12), 2714–2736. https://doi.org/10.1038/emboj.2012.150

Wang, H., Bienz, M., Yan, X.-X., & Xu, W. (2023). Structural basis of the interaction between BCL9-Pygo and LDB-SSBP complexes in assembling the Wnt enhanceosome. *Nature Communications*, *14*(1), 3702. https://doi.org/10.1038/s41467-023-39439-9

Wang, Y., Macke, J. P., Abella, B. S., Andreasson, K., Worley, P., Gilbert, D. J., Copeland, N. G., Jenkins, N. A., & Nathans, J. (1996). A Large Family of Putative Transmembrane Receptors

Homologous to the Product of the Drosophila Tissue Polarity Gene frizzled. *Journal of Biological Chemistry*, *271*(8), 4468–4476. https://doi.org/10.1074/jbc.271.8.4468

Wang, Y.-C., Yo, Y.-T., Lee, H.-Y., Liao, Y.-P., Chao, T.-K., Su, P.-H., & Lai, H.-C. (2012). ALDH1-Bright Epithelial Ovarian Cancer Cells Are Associated with CD44 Expression, Drug Resistance, and Poor Clinical Outcome. *The American Journal of Pathology*, *180*(3), 1159–1169. https://doi.org/10.1016/j.ajpath.2011.11.015

Wang, Z., & Chen, Q. (2016). β-catenin knockdown inhibits the proliferation of human glioma cells in vitro and in vivo. *Experimental and Therapeutic Medicine*, *11*(3), 1059–1064. https://doi.org/10.3892/etm.2016.2998

Webb, P. M., & Jordan, S. J. (2024). Global epidemiology of epithelial ovarian cancer. *Nature Reviews Clinical Oncology*, *21*(5), 389–400. https://doi.org/10.1038/s41571-024-00881-3

Wei, W., Chua, M., Grepper, S., & So, S. (2010). Small molecule antagonists of Tcf4/β-catenin complex inhibit the growth of HCC cells *in vitro* and *in vivo*. *International Journal of Cancer*, *126*(10), 2426–2436. https://doi.org/10.1002/ijc.24810

Wieschaus, E., N□sslein-Volhard, C., & J□rgens, G. (1984). Mutations affecting the pattern of the larval cuticle inDrosophila melanogaster. *Wilhelm Roux's Archives of Developmental Biology*, *193*(5), 296–307. https://doi.org/10.1007/BF00848158

Wu, M.-Y., Wang, C.-C., Chang, Y.-C., Yu, C.-Y., Sung, W.-W., Chen, C.-J., & Tsai, M.-C. (2022). The Therapeutic Role of PNU-74654 in Hepatocellular Carcinoma May Involve Suppression of NF-κB Signaling. *Medicina*, *58*(6), 798. https://doi.org/10.3390/medicina58060798

Wu, R., Zhai, Y., Fearon, E. R., & Cho, K. R. (2001). Diverse mechanisms of beta-catenin deregulation in ovarian endometrioid adenocarcinomas. *Cancer Research*, *61*(22), 8247–8255.

Xing, Y., Clements, W. K., Le Trong, I., Hinds, T. R., Stenkamp, R., Kimelman, D., & Xu, W. (2004). Crystal Structure of a β-Catenin/APC Complex Reveals a Critical Role for APC Phosphorylation in APC Function. *Molecular Cell*, *15*(4), 523–533. https://doi.org/10.1016/j.molcel.2004.08.001

Xing, Y., Takemaru, K.-I., Liu, J., Berndt, J. D., Zheng, J. J., Moon, R. T., & Xu, W. (2008). Crystal Structure of a Full-Length β-Catenin. *Structure*, *16*(3), 478–487. https://doi.org/10.1016/j.str.2007.12.021

Yan, M., Li, G., & An, J. (2017). Discovery of small molecule inhibitors of the Wnt/β-catenin signaling pathway by targeting β-catenin/Tcf4 interactions. *Experimental Biology and Medicine*, *242*(11), 1185–1197. https://doi.org/10.1177/1535370217708198

Yang, D., Singh, A., Wu, H., & Kroe-Barrett, R. (2016). Comparison of biosensor platforms in the evaluation of high affinity antibody-antigen binding kinetics. *Analytical Biochemistry*, *508*, 78–96. https://doi.org/10.1016/j.ab.2016.06.024

Yu, B., Huang, Z., Zhang, M., Dillard, D. R., & Ji, H. (2013). Rational Design of Small-Molecule Inhibitors for β-Catenin/T-Cell Factor Protein–Protein Interactions by Bioisostere Replacement. *ACS Chemical Biology*, *8*(3), 524–529. https://doi.org/10.1021/cb300564v

Yu, F., Yu, C., Li, F., Zuo, Y., Wang, Y., Yao, L., Wu, C., Wang, C., & Ye, L. (2021). Wnt/β-catenin signaling in cancers and targeted therapies. *Signal Transduction and Targeted Therapy*, *6*(1), 307. https://doi.org/10.1038/s41392-021-00701-5

Zechner, D., Fujita, Y., Hülsken, J., Müller, T., Walther, I., Taketo, M. M., Bryan Crenshaw, E., Birchmeier, W., & Birchmeier, C. (2003). β-Catenin signals regulate cell growth and the balance between progenitor cell expansion and differentiation in the nervous system. *Developmental Biology*, *258*(2), 406–418. https://doi.org/10.1016/S0012-1606(03)00123-4

Zhang, H., Jing, X., Wu, X., Hu, J., Zhang, X., Wang, X., Su, P., Li, W., & Zhou, G. (2015). Suppression of multidrug resistance by rosiglitazone treatment in human ovarian cancer cells through downregulation of FZD1 and MDR1 genes. *Anti-Cancer Drugs*, *26*(7), 706–715. https://doi.org/10.1097/CAD.0000000000000236

Zhao, J. (2016). Cancer stem cells and chemoresistance: The smartest survives the raid. *Pharmacology & Therapeutics*, *160*, 145–158. https://doi.org/10.1016/j.pharmthera.2016.02.008

Zhou, P., Byrne, C., Jacobs, J., & Fuchs, E. (1995). Lymphoid enhancer factor 1 directs hair follicle patterning and epithelial cell fate. *Genes & Development*, *9*(6), 700–713. https://doi.org/10.1101/gad.9.6.700

Zou, M., BinEssa, H. A., Al-Malki, Y. H., Al-Yahya, S., Al-Alwan, M., Al-Jammaz, I., Khabar, K. S. A., Almohanna, F., Assiri, A. M., Meyer, B. F., Alzahrani, A. S., Al-Mohanna, F. A., & Shi, Y. (2021). β-Catenin Attenuation Inhibits Tumor Growth and Promotes Differentiation in a BRAFV600E-Driven Thyroid Cancer Animal Model. *Molecular Cancer Therapeutics*, *20*(9), 1603–1613. https://doi.org/10.1158/1535-7163.MCT-21-0037